

Hybrid inorganic-polymer coatings prepared via miniemulsion process

Dissertation

zur Erlangung des Grades
„Doktor der Naturwissenschaften“
im Promotionsfach Chemie

am Fachbereich Chemie, Pharmazie und Geowissenschaften
der Johannes Gutenberg-Universität Mainz

von

Nermeen Nabih
geboren am 24.02.1981 in Kairo, Ägypten

Mainz, September 2011

Die vorliegende Arbeit wurde im Zeitraum von November 2008 bis September 2011 am Max-Planck-Institut für Polymerforschung, Mainz und bei Henkel AG & Co. KGaA, Düsseldorf angefertigt.

Die vorliegende Arbeit wurde in Kooperation mit Henkel AG & Co. KGaA durchgeführt.

Declaration

I hereby declare that the present work is an original work completed independently and has not been presented for a degree in any other university.

Mainz, September 2011

Signature, _____
Nermeen Nabih

Table of contents

1.	Introduction	7
2.	Theoretical background	11
2.1.	Radical polymerization.....	11
2.2.	Stabilization techniques in emulsions	12
2.2.1.	Stabilization using surfactants	13
2.2.1.1.	<i>Ionic surfactants</i>	13
2.2.1.2.	<i>Nonionic surfactants</i>	16
2.2.2.	Stabilization using protective colloids	18
2.2.3.	Stabilization using solid particles.....	18
2.2.4.	Destabilization techniques	18
2.2.5.	Stabilization in miniemulsions	20
2.3.	Automotive coatings and corrosion protection	21
2.3.1.	Corrosion and corrosion protection.....	21
2.3.1.1.	<i>Protection via inorganic pigments and metals</i>	21
2.3.1.2.	<i>Protection via organic coatings</i>	23
2.3.2.	Automotive coatings	24
2.3.2.1.	<i>Pretreatment: inorganic coating layer</i>	25
2.3.2.2.	<i>Primer: organic coating layer</i>	25
2.3.2.3.	<i>Aquence® autodeposition coatings system</i>	27
2.3.3.	Corrosion testing – Salt spray test.....	31
3.	Analytical techniques.....	32
3.1.	Dynamic light scattering	32
3.2.	Elemental analysis	33
3.2.1.	X-ray fluorescence	33
3.2.2.	Inductively coupled plasma–optical emission spectroscopy	34
3.3.	Electron microscopy and related techniques.....	35
3.3.1.	Introduction.....	35
3.3.2.	Transmission electron microscopy	36
3.3.3.	Scanning electron microscopy	37
3.3.4.	Energy dispersive X-ray analysis	39

Table of contents

3.3.5.	Electron diffraction.....	39
4.	Results and discussion	41
4.1.	Synthesis of water-based hybrid inorganic - polymer particles via multiple miniemulsions.....	41
4.1.1.	Objective	41
4.1.2.	Designing the synthetic process	41
4.1.2.1.	<i>Basic idea</i>	41
4.1.2.2.	<i>Proof of concept</i>	45
4.1.2.3.	<i>Choice of organic ingredients</i>	46
4.1.2.4.	<i>Choice of inorganic ingredients</i>	48
4.1.2.5.	<i>Choice of nonionic surfactant for inverse miniemulsions</i>	56
4.1.2.6.	<i>Choice of suitable thermal initiator for the radical polymerization</i>	61
4.1.2.7.	<i>Adjusting droplet size via viscosity adjustments</i>	63
4.1.3.	Variation of Fortegra 100 content	65
4.1.4.	Droplet stability and droplet scenarios.....	66
4.1.5.	Variation of radical polymerization temperature	68
4.1.6.	Variation of zinc phosphate loading.....	69
4.1.7.	Variation of inorganic pigment and its loading.....	71
4.1.8.	Electron microscopy samples' investigation	74
4.2.	Testing of zinc phosphate - polymer miniemulsion as corrosion protection coating.....	84
4.2.1.	Objective	84
4.2.2.	General procedures and guidelines.....	84
4.2.3.	First salt spray testing run.....	89
4.2.4.	Second salt spray testing run	92
4.2.5.	Third salt spray testing run	95
4.2.5.1.	<i>Working on a modified formulation</i>	95
4.2.5.2.	<i>Autodeposition and salt spray test with modified formulation</i>	98
4.2.6.	Proposed corrosion protection mechanism.....	102
4.3.	Synthesis of water-based titanium dioxide - polymer particles via a single miniemulsion	108

Table of contents

4.3.1.	Introduction.....	108
4.3.2.	Designing the synthetic route	108
4.3.3.	Finding a stable precursor / precursor system	109
4.3.3.1.	<i>Alkoxide precursors and their corresponding alcohol – effect of pH changes</i>	109
4.3.3.2.	<i>Carboxylic acids as ligands</i>	111
4.3.3.3.	<i>β-ketoesters and β-diketones as ligands</i>	113
4.3.3.4.	<i>Further ligands</i>	114
4.3.3.5.	<i>General remark on hydrolytic stability</i>	114
4.3.3.6.	<i>Hydrolytic stability within vinylic monomers mixture</i>	115
4.3.4.	Formation of miniemulsions.....	116
4.3.4.1.	<i>Using oleic acid</i>	116
4.3.4.2.	<i>Using oleic acid within vinylic monomers mixture</i>	117
5.	Experimental procedures	122
5.1.	Preparation of water-based hybrid inorganic - polymer particles via multiple miniemulsions.....	122
5.2.	Preparation of zinc phosphate - polymer miniemulsion for corrosion tests....	125
5.3.	Preparation of water-based titanium dioxide - polymer particles via a single miniemulsion	126
5.3.1.	Hydrolytic stability tests	126
5.3.2.	Miniemulsions	127
6.	Conclusion.....	129
7.	Appendix I – Characterization methods	132
8.	Appendix II - Materials.....	134
8.1.	Materials used in inorganic-polymer multiple miniemulsion systems.....	134
8.2.	Materials used in TiO ₂ -polymer single miniemulsion system.....	136
9.	Appendix III – List of abbreviations.....	137
	References.....	138
	List of publications.....	152

1. Introduction

Hybrid mesoscale materials have become one of the most favored research topics lately because they offer novel properties or properties combinations¹. Especially inorganic–organic hybrid nanoparticles and defined pigment-polymer aggregates have gained increased interest due to influential new applications in the fields of optics, electronics, medicine, cosmetics and last but not least in functional coatings². Especially for the latter application, water-based dispersions are preferred or required due to safety, health and environmental (SHE) regulations. In fact the concept of inorganic–organic hybrid particles can be used for advanced water-based dispersions which allow the substitution of traditional solvent-based coating applications without losing performance, e.g. in terms of chemical or mechanical resistance, and is therefore expected to gain further importance and industrial relevance. For this purpose the inorganic components typically have to be homogeneously distributed throughout the coatings film^{3,4}, which is almost impossible to achieve following just mechanical pathways like blending, milling, or mixing. More successfully in this respect are chemical or a physical-chemical synthetic approaches with sol-gel chemistry being the most popular one. For example PPG Industries and BASF have successfully implemented commercial products with increased scratch resistance based on silica-polymer hybrid materials^{5,6}. Many other examples following the sol-gel approach can be found from different companies and for various applications, as reviewed by Sanchez et al.². Another successful, but different physical-chemical concept towards water-based inorganic-polymer coatings was commercialized by Rohm and Haas^{4,7} where an increased attractive interaction between latex particles from emulsion polymerization and preformed inorganic pigments (usually in the micrometer regime) is utilized to obtain functional coatings with high homogeneity and to avoid pigment aggregation.

In general, synthesis through emulsification is among the most important synthesis routes for water-based hybrid materials. In this relationship the miniemulsion process gained significant importance in the past decade. In a miniemulsion system the individual droplets can be considered as so-called “nanoreactors”. The nanoreactor concept allows new reactions and material combinations in quasi-aqueous media which cannot be

achieved by traditional methods. Typical of emulsion systems, miniemulsions are made up of a water continuous phase and oil dispersed phase (oil-in-water, o/w, direct miniemulsions) or vice versa (water-in-oil, w/o, inverse miniemulsions). For the formation of miniemulsions, a high shear force is required. On a laboratory scale, ultrasonication is used most often, while on industrial scale, high pressure homogenizers are applied⁸. As a result of the high shear, fission and fusion of the droplets occur till a steady state is reached. The special features of miniemulsions lie in the mode used to stabilize the droplets against collision, as well as to suppress Ostwald ripening of the droplets. The amount of surfactant used for stabilizing miniemulsions against collision is efficiently used resulting in an incomplete coverage of the droplets⁸ and are thus dubbed critically stabilized systems⁹. Moreover, in a miniemulsion system, no free micelles exist⁹. To synthesize hybrid inorganic-organic particles in miniemulsion, there are mainly two paths, with respect to the inorganic material, that can be carried out: either to use preformed inorganic materials or to synthesize them in-situ. In contrast to the standard macroemulsion polymerization preformed, inorganic pigments can become encapsulated inside of individual miniemulsion droplets provided they are small enough in size. For this purpose a compatibilization step can be required between the inorganic and the organic constituents of the emulsion^{3, 6, 8}. This can be done via hydrophobization^{6, 10}, treatment with surfactant⁶, creation of an electrostatic attraction between both components^{3, 6} or even through hydrogen bonding interactions³. If the compatibilizer is not to take part in the polymerization, the disadvantage of this system, besides having to find a suitable compatibilization method, is that with higher loadings of the inorganic material, problems with homogeneity can arise¹⁰.

Alternatively, inorganic materials can be synthesized in-situ. An extensive amount of work has been published involving precursors with polymerizable groups, mainly involving synthesis via sol-gel process².

However, the focus of our contribution is based on a versatile in-situ pigment preparation process which was extended to prepare water-based inorganic-polymer hybrid particles. At first the co-homogenization of inverse precursor miniemulsions is used for the preparation of inorganic pigments within a polymerizable continuous phase. Afterwards the system is converted to a direct miniemulsion by addition of an aqueous surfactant

solution followed by homogenization. Subsequent polymerization of the polymerizable phase, which is now in the dispersed droplet state and still contains the inorganic material from the previous in-situ synthesis, leads to the desired water-based inorganic-polymer hybrid material dispersion. Functional coatings were the focus of the application of this system. For this reason, three pigments were synthesized via this process: zinc phosphate, calcium carbonate, and barium sulfate, all of which are widely used in coatings. As for the polymer matrix, a rather complex epoxy-acrylic-styrene polymer composition was chosen to demonstrate the great versatility of the concept.

The water-based zinc phosphate / polymer miniemulsion was then tested for corrosion protection, via autodeposition – a process used in the automotive industry. So, why specifically focus on corrosion and particularly in automotive industry?

On one hand, corrosion has a great impact on our history, economy, and our every day life. In history, for example, the downfall of the Roman Empire was said to be partially due to corrosion reasons. In modern history there are also catastrophic events that have occurred due to corrosion reasons such as the downfall of the Silver Bridge in Ohio in 1967¹¹. On the economy, the impact, thus, cannot be undervalued. On the other hand, the attention given to corrosion in the automotive industry is justified: cars are required to perform well under different environments. In the same location, there is minimal temperature difference of 20 °C between the different seasons. That is besides extreme temperature regions, such as near-polar regions, desert areas, or humid areas and coastal locations¹². Car owners' expectations have also increased, which pressures the automotive manufacturers to meet their expectations technologically and financially. It is said, for example, that corrosion protection and durability of a car's color and gloss have doubled in comparison to how it was 25 years ago¹². Clearly any possibility to cut costs while keeping the system environmentally friendly, with no toxic components as well as reduced or no VOC (volatile organic compounds) components, as well as superior performance, is highly valued.

Therefore, the zinc phosphate / polymer hybrid water-based miniemulsion, synthesized in this work was used to prepare coated steel panels via autodeposition. Their corrosion resistance is investigated in comparison to a current corrosion resistance system as well as to a blank sample.

In a further extension of this work, an attempt was made to synthesize water-based titanium dioxide / polymer hybrid particles via a single miniemulsion process, with a target of combining white pigment and polymer in one pot-synthesis.

Although, this work focused on automotive coatings with respect to the choice of inorganic and polymer nature, as well as application, the synthesis route is not limited to this application and can be extended to other functional coatings, barrier coatings or even electrodeposition coatings, as well as other industrial applications.

2. Theoretical background

2.1. *Radical polymerization*

In 1929, Carothers had classified polymerization reactions to addition and condensation reactions. Alternatively, another classification divides the reaction to chain and step growth polymerizations. Chain growth polymerizations are characterized by high degree of polymerization already at an early stage of the reaction¹³. This polymerization proceeds through reactive centers, which further categorize the polymerization reactions into: radical, cationic, anionic and coordination^{13, 14}. Radical polymerization was used in this work and would thus be described here, especially in heterophase, emulsion systems. Radical initiators are used to generate radicals, either thermally, via exposure to light or high energy or via redox reactions. Polymerization reactions then proceed through the well established initiation, propagation and termination steps^{13, 14}.

Radical polymerizations can be carried out via several processes, such as bulk, solution, as well as various heterogeneous methods^{13, 15}. Heterogeneous systems have the advantage of producing high polymer content, in combination with high molecular weights, at lower viscosities⁹. Examples for heterogeneous systems include: suspension, dispersion, precipitation and last but not least – emulsion polymerization¹⁵. Elaboration will be made hereunder on the surfactant stabilized methods, namely: emulsion, microemulsion and miniemulsion polymerizations¹⁶.

The main difference in those polymerization techniques lies mainly on the nucleation mechanism, on which the properties of the resulting dispersion depend. Assuming an aqueous continuous phase and a water soluble surfactant, in emulsion polymerization, micellar nucleation dominates, when the surfactant concentration is above the critical micelle concentration (cmc) level. Droplet nucleation is insignificant due to the relatively large size of the monomer droplet (1 – 10 μm), which leads to a relatively small surface area making them hard to compete with the monomer swollen micelles (5 – 10 nm) for radical capture¹⁷. In microemulsions, no monomer droplets exist, but rather monomer swollen micelles, as well as free micelles. Therefore, the nucleation mechanism is also that of micellar nucleation¹⁶, where continuous particle nucleation takes place due to the

diffusion of the monomers and surfactant¹⁸. This results in the existence of polymer particles coexisting with free micelles in the resultant polymerized microemulsion¹⁸. Miniemulsions, in contrast to microemulsions and (macro)emulsions, possess no free micelles or monomer swollen micelles, but rather monomer droplets stabilized by surfactants (50 – 500 nm) and are thus capable to capture radicals, as opposed to monomer droplets in (macro)emulsions. Thus, in miniemulsions, droplet nucleation takes place, simultaneously in the monomer droplet, resulting in a polymer particle that corresponds to the initial monomer droplet^{9, 16, 17}.

Figure 1 illustrates schematically the nucleation differences between the above-mentioned techniques.

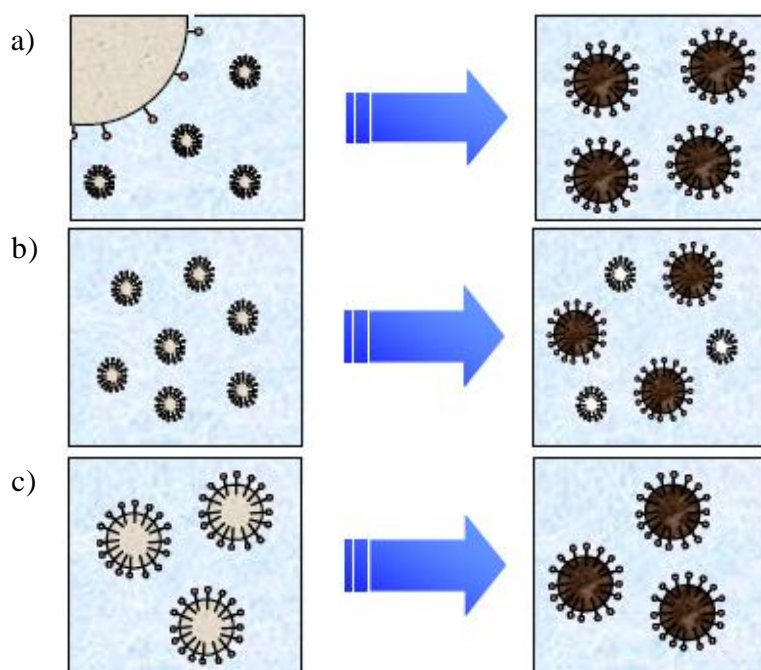


Figure 1 Schematic diagram representing the different nucleation mechanisms and the resulting polymer particles for: a) emulsion polymerization, b) microemulsion polymerization and c) miniemulsion polymerization¹⁹.

2.2. Stabilization techniques in emulsions

There are various stabilization techniques in emulsions that take advantage of electrostatic interactions, steric interactions, surface adsorption or wetting properties of species at the dispersed / continuous interface. In the next sections, the different

interactions will be elaborated with a focus on the first two interactions – electrostatic and steric. Those interactions were an integral part of this work, both for synthesis, i.e. stabilization of miniemulsions, and coating application process, namely autodeposition coatings.

2.2.1. Stabilization using surfactants

2.2.1.1. Ionic surfactants

Derjaguin and Landau in 1941, as well as, Vervey and Overbeek in 1948, have arrived independently to the same theory for the stabilization of colloidal droplets. In their theory, later named as DLVO theory, attractive forces and repulsive forces compete against one another, resulting either in the stabilization or the destabilization of the system. In this case, the total interaction is nothing but the summation of both the attractive and repulsive energy:

$$V_T = V_A + V_R$$

where V_T represents the total potential energy of interaction, V_A that of attraction, while V_R represents that of repulsive energy²⁰.

Van der Waals forces create the attractive interaction between the droplets and are given by:

$$V_A = \frac{-Aa}{12H}$$

where A is the Hamaker constant, a is the particle radius and H is the shortest interparticle distance²⁰.

As for the repulsive forces, they arise due to the charged particle surface and the unequal counterion distribution. This is given by:

$$V_R = \frac{\varepsilon_r a^2 \psi^2 \exp(-\kappa H)}{2a + H}$$

where ε_r is the dielectric constant of the medium, ψ is the surface potential of the charged particle, a is particle radius, H is the shortest interparticle distance, while κ is the inverse of the Debye length²⁰. The Debye length corresponds to the distance to which the surface potential of the charged particle falls to its $1/\exp$ value²¹.

Figure 2 shows a schematic diagram of two positively charged droplets, and their respective counterions. The potential energy diagram illustrates the changes in the attractive and repulsive potential as a function of their interparticle distance. The total potential energy curve displays an energy barrier. This barrier represents the repulsive forces that have to be overcome for the system to destabilize and reach the primary energy minimum, or irreversible destabilization, at a very close distance. In this case, attractive van der Waals forces control the system and are responsible for the system collapse.

It was found that for droplets that are relatively large with a somehow small Debye length, i.e. when $\kappa a \gg 1$ (ratio of particle size to double layer thickness is very large), a secondary shallow minimum appears at a distance from particle surface. This shallow minimum represents reversible flocculation of the system²⁰.

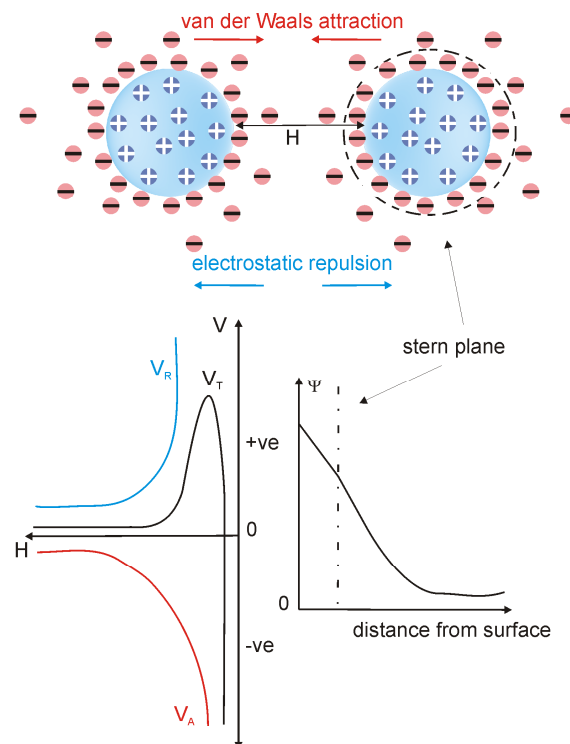


Figure 2 Schematic diagram illustrating ionically stabilized droplets, DLVO theory and electric double layer model, where V = potential energy, V_A = attractive potential, V_R = repulsive potential, V_T = total potential, H = shortest interparticle distance and ψ = electric potential. V_T represents the case when $\kappa a \ll 1$. Please refer to text for details. Adapted from^{20, 22}.

So how does the unequal charge distribution of the counterion induce a strong electrostatic repulsion to overcome the attractive Van der Waals forces? Historically, the first model set to answer this was represented by the Helmholtz model in 1879 followed by that of Guoy and Chapman between 1910 and 1917. The contemporary model was that of Stern, introduced in 1924, which basically combines both preceding models. In this model, the counterion distribution is divided into two layer: the Stern layer and the diffuse layer²². In the Stern layer the counterions are in contact with the charged surface followed by a diffuse layer where the counterions diffuse further from the charged droplets²³. A schematic diagram of both distributions is shown in Figure 2. Throughout both layers, the electric potential also shows distinct features. In the Stern layer, the electric potential falls rapidly till it reaches the Stern plane, where it then, in the diffuse layer, falls gradually to zero as the distance from the surface increases²². The relation between the electric potential vs. distance from the charge particle's surface is also shown in Figure 2.

The width of both layers, the electric double layer, is represented by the Debye length, $1/\kappa$, which is given by:

$$\frac{1}{\kappa} = \sqrt{\frac{\epsilon_r \epsilon_o RT}{4\pi F^2 \sum_i c_i Z_i^2}}$$

where ϵ_r is the dielectric constant of the medium, ϵ_o is the permittivity of vacuum, R is the gas constant, T is the absolute temperature, F is Faraday's constant, c_i is the molar concentration of ions while Z_i is the valency of the ions in solution. In other words, the debye length, which describe how far the counter ions have diffused within the continuous phase, is thus a measure of how far the repulsive forces extend. It is proportional to square root of absolute temperature and the dielectric constant of the medium. This signifies why the debye length is larger in polar solvents but is very small in organic solvents. Moreover, the debye length is inversely proportional to ion valency and the square root of ion concentration²².

Ionic stabilization in terms of the debye length is important not only for the understanding of miniemulsion stabilization using ionic surfactants, but also how to induce destabilization in ionically stabilized systems, as is the case with autodeposition coatings. This is of high relevance for this work and the destabilization / autodeposition

mechanism which will be described in detail in section 2.3.2.3 “ *Aquence® autodeposition coatings system*”.

2.2.1.2. Nonionic surfactants

Nonionic stabilization is essential for stabilizing non-polar systems but also for systems that are required to be stable in salt containing environments. In this work, since inorganic salt precursors were used, a stabilization using nonionic surfactants was necessary.

Nonionic surfactants are amphiphilic molecules, but could also be amphiphilic polymers such as block or graft copolymers, where in a water-based system, the hydrophobic part gets adsorbed to the emulsion droplets, while the hydrophilic parts protrudes in the aqueous phase.

Assuming a protrusion of a length of δ and a shortest interparticle distance of H , as schematically shown in Figure 3, both attractive and repulsive forces analysis is carried out, as was done in the case of DLVO theory.

The attractive forces acting on the droplets in this case are still that of the van der Waals forces, G_A .

The repulsive forces in this case are apparent once the distance between the droplets, H , falls to lower than 2δ , i.e. once the protruding surfactant part start approaching each other. Assuming that the continuous phase is a good solvent for the extended surfactant parts, there are two main parameters that contribute to the repulsion between the droplets: the entropic interaction – G_S – and the mixing interaction – G_{mix} .

The entropic interaction arises due to the approaching or the overlapping of the extended surfactant parts. This approach dictates lower possible configurations for the extensions, i.e. a reduction of the system entropy would result – an unfavorable situation, which therefore leads to the repulsion between the droplets.

The mixing interaction, sometimes also referred to as osmotic repulsion, arises due to decrease of the solvent molecules in the region where the surfactant protrusions approach each other, resulting in an increase in the osmotic pressure. As a result, the solvent molecules will diffuse from the bulk to this region in order to reduce the osmotic pressure, leading to repulsion between the droplets.

The mixing interaction thus represents a repulsive force as long the solvent – surfactant extension interaction is favorable, i.e. in good solvents. In poor solvent conditions, the mixing interaction will cause attraction between droplets to occur.

Figure 3 shows the free energy of each of the above interactions as a function of the interparticle distance, H , as well as the total free energy of interaction of the system, G_T . G_T shows a minimum whose depth is a function of the particle radius - a , Hamaker constant - A , (van der Waals forces) and protrusion length²⁴ - δ .

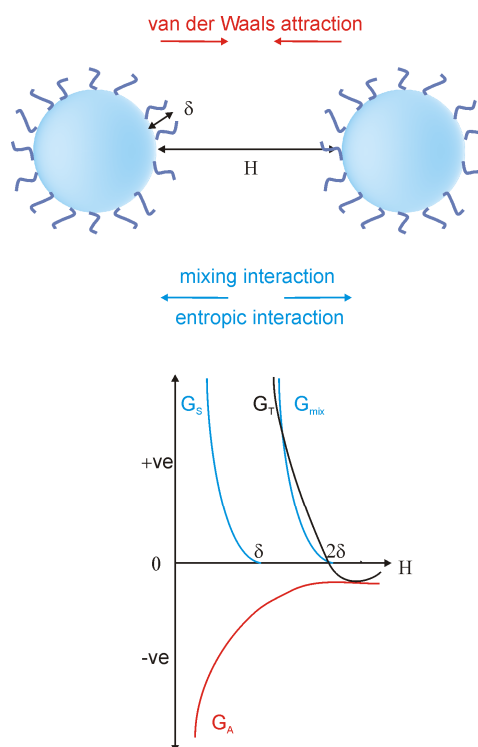


Figure 3 Schematic diagram showing two sterically stabilized droplets and the corresponding energy diagram showing attractive and repulsive interactions in case the protruding surfactant part extends in a good solvent. Adapted from²⁴.

Moreover, further interactions can also impart additional stabilization to the emulsion system. One established example is that of polyethylene oxide (PEO) chains which create hydrogen bonding with the water molecules of the continuous phase²⁰. The presence of the hydrogen bonding between the PEO chains and the water molecules restrict the latter's free motion, i.e. the hydration shells formed exert what is referred to as hydration pressure, which results in additional repulsion between the emulsion droplets²⁵.

2.2.2. Stabilization using protective colloids

Assuming a water-based emulsion, protective colloids refers to when a dispersion of hydrophilic species is added to a dispersion of hydrophobic species, with resulting increase in the latter's stability²⁶. Those hydrophilic species are mainly polymers, which could be natural, such as starch, or synthetic, such as polyvinyl alcohol. They could also be ionic, e.g. sodium carboxymethyl cellulose, or nonionic, e.g. dextrin. According to Bechhold, the added hydrophilic species are adsorbed on the hydrophobic droplets, forming a coating²⁷ – hence the name “protective colloids”.

2.2.3. Stabilization using solid particles

Stabilization using solid particles, also known as Pickering stabilization, constitute particles that lie on the water / oil interface in an emulsion and thus preventing dispersed droplets from coalescence²⁸. Those solid particles, which can be nano- or micron-sized²⁹, should be partially wettable by both the oil and the water phase²⁸. When the particles have a contact angle with the aqueous phase lower than 90°, they are said to be hydrophilic particles and thus stabilize o/w emulsions, e.g.: metal oxides. Conversely, if the particles have a contact angle with water more than 90°, the particles are then hydrophobic and are suitable for stabilizing w/o emulsions, e.g.: hydrophobized silica particles²⁹.

2.2.4. Destabilization techniques

In light of the aforementioned stabilization techniques, few factors can be controlled to induce destabilization of emulsions. Here are some main factors:

- **Electrolyte concentration:**

An increase in the concentration of the free ions in solution is equivalent to an increase in the ionic strength, which is given by:

$$I = \frac{1}{2} \sum_i c_i Z_i^2$$

where I is the ionic strength, c_i is the molar concentration of ions and Z_i is the valency of the ions²². By investigation of the Debye length expression, it is deduced that an increase

in the ionic strength leads to a decrease in the Debye length, i.e. a decrease in the energy barrier created by repulsive forces. With a further increase in the ionic strength, attractive forces prevail over the repulsive forces leading to destabilization. The concentration at which the electrostatic forces are neutralized is referred to as “critical coagulation concentration”²⁵. This is the destabilization mechanism used in autodeposition, as will be discussed in section 2.3.2.3 “*Aquence® autodeposition coatings system*”.

- **Temperature:**

A substantial effect could be seen in case that the stabilization is based on hydrogen bonding as in the case of PEO chains. An increase in temperature would provide enough energy to reduce the energy barrier produced by hydrogen bonding, leading to flocculation of the droplets, which can be reversed by cooling the emulsion down²². Alternatively expressed, the dehydration of the PEO chains leads to changing the situation from a good solvent to a poor solvent conditions, i.e. G_{mix} becomes attractive rather than repulsive.

- **pH changes:**

Changes in the pH have an effect on the Debye length also due to changes in the ionic strength of the medium. Furthermore, pH changes may lead to an alteration in the protonation or deprotonation state of some surfactants, for example, for surfactants containing carboxylate groups or ammonium groups, which may affect their stability²². A further example is that of proteins, that are used as protective colloids. At their isoelectric point, it was found that they lose their protective ability, since under this condition, their precipitation occur; though they still remain attached to the droplets²⁷.

- **Bridging:**

Bridging can occur by the binding of surfactant or polymeric stabilizer chains, which are extended in the solvent, to each other. This is triggered or favored by these factors: either there is not a high coverage of the particle surface. This leads to the possibility of the protrusions to bind to more than one particle. Or, if the protrusions are long, this increases the possibility of chain interactions. This is more enhanced if the chain-chain interactions are more favorable than solvent-chain interactions²⁰.

- **Depletion flocculation:**

The addition of non-adsorbing polymers to a dispersion would lead to a depletion region, in which the free polymers are not approaching the dispersed droplets. This forces the dispersed droplets to approach each other which result in their flocculation²⁴.

2.2.5. Stabilization in miniemulsions

The above stabilization mechanisms have all been employed to stabilize miniemulsions. But this stabilization is effective against collision of the droplets. A further stabilization mechanism is still required to avoid a net diffusion of droplet constituents from one droplet to the other.

The driving force for this additional destabilization is due to Laplace pressure, expressed as follows:

$$P_{Laplace} = \frac{2\gamma_{LL}}{a}$$

where γ_{LL} is the oil-water interfacial tension and a is the droplet radius⁹. This expression indicates that the Laplace pressure for smaller droplets is higher than that for larger ones. In order to balance out this pressure difference, constituents from the smaller droplets would diffuse through the continuous phase to the larger droplets till the smaller droplets would disappear altogether.

To balance out the Laplace pressure in a different way other than spontaneous diffusion of droplets' constituents, an osmotic pressure agent is added: a material that is soluble in the dispersed phase but is (almost) insoluble in the continuous phase (a hydrophobe in direct miniemulsions and a lipophobe in the inverse miniemulsions). This agent would build osmotic pressure inside the droplets:

$$\Pi_{Osmotic} = RTc$$

where R is the gas constant, T is the temperature, c is the molar concentration of the solute³⁰, which is in the case of a direct miniemulsion, the concentration of the hydrophobe in the dispersed phase. The presence of the osmotic pressure counteracts the effect of the Laplace pressure, and thus control to a certain extent the growth of the droplets.

2.3. Automotive coatings and corrosion protection

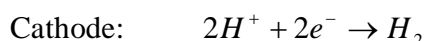
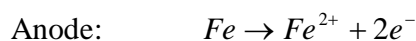
In the next sections, an introduction will be provided for corrosion protection mechanisms, corrosion protection means and materials, as well as established methods in the automotive industry in this regard.

2.3.1. Corrosion and corrosion protection

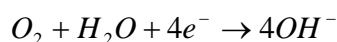
Corrosion is defined as “a chemical or electrochemical reaction between a material, usually a metal, and its environment that produces deterioration of the material and its properties”¹¹. Since it is said that the main economic losses caused by corrosion is that of steel³¹, steel corrosion will be taken as a focus to describe the involved electrochemical reactions.

Steel is an alloy of iron, carbon and further other metals to lower extent. Due to the different constituents and their distribution, anodic and cathodic areas arise. The adsorption of water takes place on the substrate followed by dissolution of salts which leads to the formation of an electrolyte – the last missing ingredient for an electrolytic cell. Next oxidation and reduction reactions can take place at the anode and cathode, depending on whether oxygen is present. The following reactions occur³¹:

If oxygen is absent:



But in the presence of oxygen, the cathodic reaction changes to:



In light of the above, it is clear that certain factors facilitate the occurrence of corrosion: the contact of water and oxygen with the substrate and the presence and dissolution of salts.

2.3.1.1. Protection via inorganic pigments and metals

Inorganic pigments and metals can be used to protect the substrate from corrosion by four main mechanisms: either through a barrier effect, anodic protection, cathodic protection or oxidative passivation. All of which will be explained briefly hereunder, as well as the

mechanisms responsible for the corrosion protection of zinc phosphate – the inorganic pigment of choice in this work.

- **Barrier effect:**

The barrier effect refers to inorganic pigments that are used as a shield to protect the metal substrate from the direct contact with water.

Figure 4 shows an illustration of a coating on a metal substrate that constitutes barrier pigments, in comparison with one that does not. This illustration clarifies how those pigments perform: they force the water to take a much longer path to reach the metal surface. For this criterion to be fulfilled, the water permeability through those pigments should be minimal. Examples of such pigments include: aluminum flakes and micaceous (plate-like) iron oxide³².

Figure 4 Illustration showing the barrier effect using lamellar particles (left), where water is forced to follow longer path in order to reach the substrate, compared to coating film containing no lamellar particles³².

- **Anodic protection:**

The idea is preventing the reaction at the anode to take place and thus prevent the corrosion from occurring. This may also be referred to as passivation, or anodic passivation, since the pigments used renders the anode passive³².

The origin of the anodic passivation is as follows: it was found that beyond a certain oxygen concentration, the corrosion was retarded. One explanation was that Fe^{3+} is generated instead of Fe^{2+} at the anode, whose hydroxide is less water soluble than that of Fe^{2+} . Following the same manner, oxidizing agents or pigments are used to passivate the anode, such as: chromates, nitrites, molybdate, plumbate and tungstate salts³¹.

- **Cathodic protection:**

If iron becomes the cathode, rather than the anode, corrosion of steel does not take place. This is termed cathodic protection. To accomplish this, a metal higher in the electromotive series is added that will act as a sacrificial anode and thus protect the

cathode (iron in this case) from undergoing the oxidation reaction. An example is using zinc as in galvanized steel³¹.

- **Oxidative passivation:**

As in the case of aluminum, it undergoes oxidation forming an aluminum oxide film on top of aluminum substrate, preventing further corrosion³².

- **Zinc phosphate for corrosion protection:**

The choice of zinc phosphate as the anticorrosive pigment for this work was based on it being one of the most widely used phosphate-containing anticorrosive pigment³³. The main mechanism by which zinc phosphate seems to work is that by anodic protection: zinc phosphate will hydrolyze to form zinc hydroxide and phosphate ions³³, where the latter may then react with ferric or ferrous ions and precipitate due to their very low solubility creating a barrier at the anode³¹.

2.3.1.2. Protection via organic coatings

Earlier than the 1950s organic coatings were thought to provide good barrier properties to protect the substrate from corrosion. Later, experimental results actually showed that this cannot be the barrier mechanism that is responsible for corrosion protection since the permeability of the organic coatings allowed the passage of water and oxygen. Two main factors were found to be determinant: the conductivity of the organic layer, and most importantly, wet adhesion. It was found out that conductive organic coatings always gave poor corrosion protection, while vice versa is not always the case, therefore, it was still not the prime factor for protection. The condition of wet adhesion was a crucial factor. Wet adhesion refers to the adhesion of the organic film to the substrate, even after water permeation to the interface region. If no sufficient wet adhesion is available, the organic coating will suffer delamination and formation of blisters. These would occur due to the corrosion process, which would lead to the formation of iron ions and hydroxyl ions, thus increasing the osmotic pressure under the film, which if strong enough would break the surface – coating adhesion. Another reason for the formation of blisters and delamination is the water at the surface / coating interface which creates compressive stress in the coating³¹. In other words, if poor wet adhesion occurs, then corrosion, delamination and blisters would result.

The most widely used organic primer is that made of epoxy (a primer is the first organic layer coating on the substrate, as will be explained hereunder). The high performance provided by cured epoxy systems depends entirely on their structure and their crosslinked networks: the moiety of bisphenol A, for example, provides high thermal resistance and rigidity, the ether linkages provide good chemical resistance, while the hydroxyl groups and the epoxide groups provide good adhesion and crosslinking possibility with various curing agents. This combination of properties is hardly met by other materials³⁴.

2.3.2. Automotive coatings

In a multilayer automotive coating, there are five coating layers applied on the substrate, each of which has a specific role in delivering the final appearance, performance and durability of the coating. Figure 5 illustrates the different layers and their corresponding thicknesses. Starting from the top layers, both the clear coat and the base coat comprise the top coat. The former is responsible for prolonged durability, as it includes, for example, UV (ultraviolet) absorbers and radical scavengers. The latter is responsible for color and further special effects, such as metallic finishes. Next follows the primer surfacer, which provides chip resistance of the coating. Finally, the primer and pretreatment are the ones applied directly on the substrate and are responsible for the corrosion protection of the car¹². Those two layers will be discussed in details in the next sections, where the traditional technologies for both layers as well as an equivalent modern system provided by Henkel will be elaborated upon.

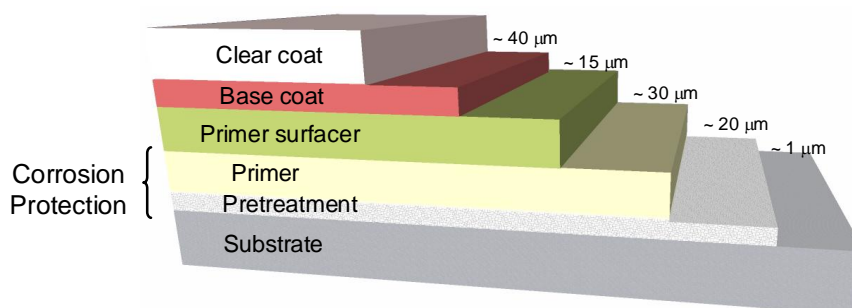


Figure 5 Illustration showing the multilayers composing automotive coatings, their typical thickness, as well as the ones responsible for corrosion protection. Shown information obtained from¹².

2.3.2.1. Pretreatment: inorganic coating layer

The goal of pretreatment is to create an inorganic layer directly on the substrate surface, also referred to as conversion coating.

One of the basic and very effective pretreatment methods in the automotive industry was chromate conversion coatings. The success of corrosion protection through chromate conversion coatings relied on its effective mechanism. Cr(III) formed a hydroxide on the metal surface, acting as barrier for corrosion. Also, Cr(VI) diffused to defect areas, where it would be reduced to Cr(III), thus healing any defect in the hydroxide barrier layer, in addition to inhibiting anodic and cathodic reactions³⁵. Due to its carcinogenic component³⁵, this technology came to an end by restricting its use in vehicles in 2000 according to a European directive. Other regions followed suit.

As a replacement to the chromate conversion coating, zinc phosphate is used, typically a low zinc phosphate coating is needed, i.e. where the zinc to phosphate ratio in the solution is said to be between 1 : 20 to 1 : 100. In any case, what is vital for the mechanism of the corrosion protection is the formation of a thin, dense coating layer (15 g/m² for cold rolled steel) of hopeite or phosphophyllite – the two crystal structures that are formed on the steel surface from the solution constituents, as well as interaction with the substrate³⁶.

Besides the standard cleaning, degreasing and rinsing processes for the substrate, two additional steps are used specific to the conversion step: an activation step before phosphating and a passivation step after phosphating. The activation step aims at increasing crystallization sites on the substrate, while the passivation step is aimed at increasing the anticorrosion property of the coating, via addition of further salts that are believed to reduce the pore size of the phosphate layer – though the exact mechanism is not fully understood. This complex pretreatment process can be composed of up to fourteen steps, including cleaning and surface preparation steps³⁶.

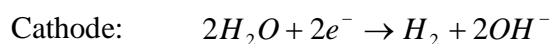
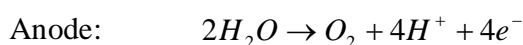
2.3.2.2. Primer: organic coating layer

The primer is the first organic layer to be applied on the substrate. Typically, after pretreatment of the substrate, this organic layer is applied by electrodeposition, which

was first introduced to the automotive industry in the 1960s as a result of support mainly by Ford³⁷. In electrodeposition, the coating is applied to the substrate electrophoretically; by the aid of an electric field³⁸.

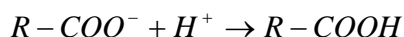
To apply electrodeposition, the substrate is immersed in a bath, containing a dispersion, along with a counter electrode, while being connected to an electric source; whether the substrate is set as the anode or cathode, depends on the type of dispersed polymer particles, whether anionic or cationic, respectively.

The first reaction that takes place is hydrolysis of water:

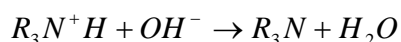


Most importantly from the above equations is the generation of positively charged hydrogen ions at the anode as well as, negatively charged hydroxyl ions at the cathode, with the respective pH changes. This occurs in close proximity to the electrodes. All dispersed polymers are functionalized in order to become ionic: for anionic polymers, carboxylic acids are the functional groups with amines acting as the corresponding neutralizers, or for cationic polymers, amines are used for functionalization, neutralized by low molecular weight carboxylic acids, such as formic, acetic or lactic acid^{37, 38}.

If negatively charged polymers are dispersed in the bath, then coagulation at anode takes place by:



If positively charged polymers are dispersed in the bath, then coagulation at cathode takes place by:



Historically, when the electrodeposition system was introduced in the 1960s, only anodic electrodeposition was known. Not until end of the 1970s was the cathodic electrodeposition established³⁷ at PPG³⁴. The latter is the one commonly used nowadays, as it provided higher performance than anodic systems for several reasons: 1) carboxylic acids in the anodic systems were easily hydrolyzed in alkaline conditions of the bath³⁷; 2) when the substrate is the anode, hydrogen ions are produced that may lead to the liberation of Fe(II) and Fe(III), where the latter can form insoluble salts with the

carboxylic acid. Most importantly, hydrogen ions can also lead to partial dissolution of the zinc phosphate pretreatment layer³⁸; 3) last but not least, coatings applied via cathodic electrodeposition lead to a much higher performance against corrosion versus anodic electrodeposited coatings³⁷, most probably because of the better wet adhesion achieved with epoxy resins to substrates³⁸.

2.3.2.3. Aquence® autodeposition coatings system

Aquence® is a registered trade name for the anti-corrosion system from Henkel. Aquence® provides an alternative to the combination of a pretreatment and an electrodeposition coating. In this system, the metal parts do not require any pretreatment by conversion coatings. The substrates are immersed in several baths step-wise. There are several cleaning and rinsing steps, followed by immersion in an autodeposition bath (also known as autophoretic bath), where the organic layer as well as the color pigment are deposited. Next, the substrate with the wet organic film is rinsed and immersed in a last bath: the reaction rinse – where the inorganic anticorrosive pigments are taken up by the wet coating layer. Finally, curing takes place in an oven at a suitable temperature^{39, 40}. The different steps are illustrated in Figure 6.

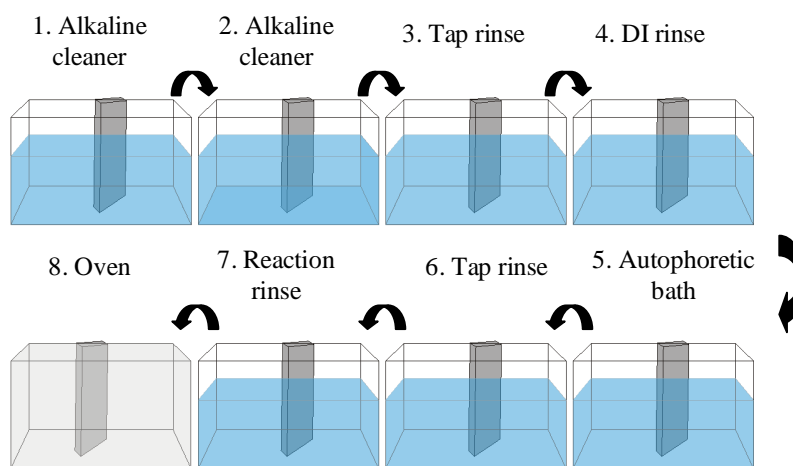


Figure 6 Set up for the steps carried out typically for Aquence® coatings. Organic coatings carried out in the autophoretic bath step, while inorganic treatment in the reaction rinse step.

The system as such has eliminated the need for a pretreatment step³⁹, with the related stages of activation and passivation, though cleaning and rinsing is still necessary to ensure a good adhesion to the surface. It has also managed to overcome electric power

costs as opposed to electrodeposition³⁷ and to provide good coverage even for complex geometries due to the elimination of any Faraday cage effect⁴¹.

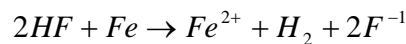
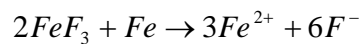
In the next two sections, the main reactions and mechanisms of the organic coating in the autodeposition bath, as well as the inorganic treatment in the reaction rinse, will be explained.

▪ **Organic coating layer – autodeposition bath:**

In this coatings process, the deposition relies on a chemical reaction to deposit the organic layer³⁹, rather than an electrochemical one as in the case of electrodeposition.

The autodeposition bath is a slightly acidic, aqueous bath containing anionically stabilized dispersions. Moreover, the bath also contains hydrofluoric acid and iron fluoride. Typically, the solid content lies between 3 – 7 wt%. The bath can also include carbon blacks as color pigments, if required^{39, 40}.

Once a steel panel is inserted in the bath, the following reactions take place^{39, 40}:



In other words, once the steel panel is inserted in the bath, Fe^{2+} ions are liberated increasing the ionic strength of the bath. As mentioned earlier, the ionic strength is proportional to the ion concentration but more importantly also to the square of the ion valency, i.e. the ionic strength would quadruple only considering liberated iron ions valency. Once the ionic strength exceeds that for critical coagulation concentration, attractive forces take over the system and consequently destabilization takes place (Schulze-Hardy rule^{23, 42}):



But since the high concentration of iron ions is in the vicinity of the steel substrate, the destabilization process takes place also in the vicinity of the substrate leading to deposition on the steel panel.

This process continues to take place as long as iron ions are liberated and can diffuse through the growing film. With time and consequently with an increase in the film thickness, this process eventually slows down. Hence, the system is said to be “self-limiting”^{39, 40}. An illustration of the coatings process is shown in Figure 7.

Other metal substrates can also be coated via the above described process, such as zinc or aluminium⁴³. Various examples on coating formulation and coating process can be found in the US Patents 5,646,211 and 7,138,444 B2^{43, 44}.

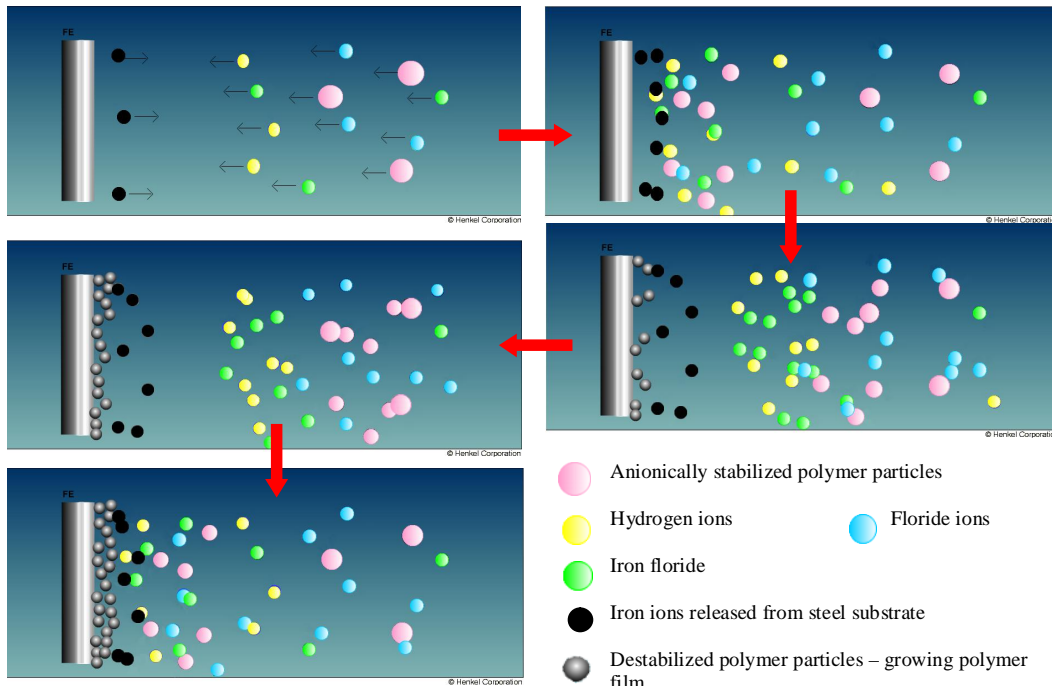


Figure 7 Illustration representing the coating of a steel panel dipped in an autodeposition bath. Starting from upper left hand corner and following the arrows: stimulated release of iron ions from steel substrate → destabilization of anionically stabilized polymer particles in the vicinity of the substrate → coagulation and deposition on the steel panel, start of film growth → further release of iron ions by diffusion through growing film → further destabilization, deposition and film growth. [Source: adapted from a video available on⁴⁵].

One critical issue required for the coatings to be deposited as such is that the destabilization of the anionically stabilized polymer particles should only be triggered by the immersion of the substrate in the bath and a subsequent release of metal ions, but otherwise, the dispersion must remain stable under the slightly acidic pH and in the presence of the hydrofluoric acid and iron fluoride. To check for dispersion stability at such conditions a quick test is carried out using a Lineguard 101 Meter (product by Henkel Technologies), shown in Figure 8. This meter measures the fluoride activity by measuring the current passing between two electrodes (a p-type silicone at anode and a platinum electrode at the cathode) which are placed in a solution containing the fluoride (and eventually the sample to be tested for stability in an HF solution) and which are

connected to a voltage. The presence of fluoride ions causes the etching of the p-type silicone electrode. With a given area of the silicone electrode and a given applied voltage, it was found that the fluoride activity is proportional to the measured current in a dilute fluoride solution, regardless of the presence of other ions in solution. This is described in details in a patent by Steinbrecher et al. from the year 1967⁴⁶. A solution of HF (concentration of 500 ppm) results in a current of $\sim 200 \mu\text{A}$. In other words, a stable dispersion containing 500 ppm HF should not cause the deflection of the Lineguard 101 meter and a constant reading of $\sim 200 \mu\text{A}$ should be shown.



Figure 8 Lineguard 101 Meter for measuring the fluoride activity, and thus determining whether a dispersion is stable against autodeposition bath constituents.

Typically, miniemulsions are used nowadays as the dispersions for this coating procedure, as it was realized that using miniemulsions for autodeposition coatings improved the coating's coverage and corrosion resistance at substrates' edges⁴⁰. Another important characteristic of miniemulsions is that their stabilization against collision is carried out with a low amount of surfactants, leading to an incomplete surface coverage of the dispersed droplets and yet a stable miniemulsion⁹. This so-called critical stabilization is crucial for the destabilization of miniemulsion during autodeposition because only weak ionic attractive forces are employed, in contrast to electrodeposition, where strong attractive forces exist between the polymers and the target substrate.

- **Inorganic treatment – reaction rinse:**

A reaction rinse typically contains an acidic solution of a group IIA or group IIB metal cation salt (e.g. calcium, barium, magnesium, zinc), as well as a phosphate source or phosphoric acid⁴⁷. The wet coat deposited on the metal substrate by the previous step is porous³⁹, and by immersion of the substrate in the reaction rinse, the latter constituents

are allowed to diffuse. It is believed that the inorganic anticorrosive pigments reach the metal substrate^{42, 47}, but the exact mechanism of protection is not well understood⁴⁷. Therefore, in the Aquence® system, even though the order of layer application is reversed compared to a pretreatment / electrodeposition (organic layer by autodeposition, followed by inorganic layer by reaction rinse), the order of layers on substrate is essentially the same, considering diffusion of inorganic pigments to the substrate surface. In other words, in all cases, a direct contact of pigments with the substrate surface is established.

2.3.3. Corrosion testing – Salt spray test

In this work, a neutral salt spray (NSS) test has been carried out. In a typical process, according to ASTM B117, which is equivalent to ISO 9227 - NSS, coated panels are scribed, thus exposing the metal. They are then placed in a chamber or a cabinet where they are sprayed continuously with a neutral (pH = 6.5 to 7.2) 5 wt% NaCl solution, at a temperature of 35 °C, at 100% relative humidity^{31, 48, 49}. The idea is to test the coating at extreme conditions and to check the corrosion propagation along the scribe. Panels are also then examined for delamination, as well as blistering. This test is categorized as an accelerated corrosion test, where it was found that most results show that there are little agreement with actual weather tests, since in reality no such harsh conditions exist and also, changes in conditions also occur, for example: drying and cooling. Still this test is the most widely used accelerated test³¹.

3. Analytical techniques

3.1. *Dynamic light scattering*

Dynamic light scattering (DLS) measurements rely on measuring the light scattered fluctuations over time⁵⁰, caused by Brownian motion of particles, as a result of thermal fluctuations of the solvent molecules⁵¹. According to the approximations in Rayleigh scattering, the intensity of the scattering light is proportional to d^6 (particle diameter) and inversely proportional to λ^4 (wavelength of incident light)⁵². Fluctuations in the scattered light frequency may be seen as a result of the Doppler Effect whether the moving particle is approaching or receding from the detector⁵³. Alternatively, fluctuations can be viewed as the result of constructive and destructive interference of scattered light, as the particles move over time⁵⁴. An autocorrelation function is then used to analyze the intensity fluctuations over short time intervals and determine the translational diffusion coefficient, D ⁵⁰.

This autocorrelation function is given by:

$$G(\tau) = \langle I(t) \bullet I(t + \tau) \rangle;$$

where τ represents the correlator time⁵². The autocorrelation function decays exponentially with time. The exponential decay time constant can be related to the diffusion coefficient⁵⁴, which leads to the determination of the particle's hydrodynamic radius through the Stokes-Einstein equation:

$$R_H = \frac{k_B T}{6\pi\eta D}$$

where k_B is the Boltzmann constant, T is the temperature and η is viscosity of the solvent^{50, 51}. Figure 9 represents a schematic diagram of DLS main components, illustrating their main roles and the corresponding obtained information.

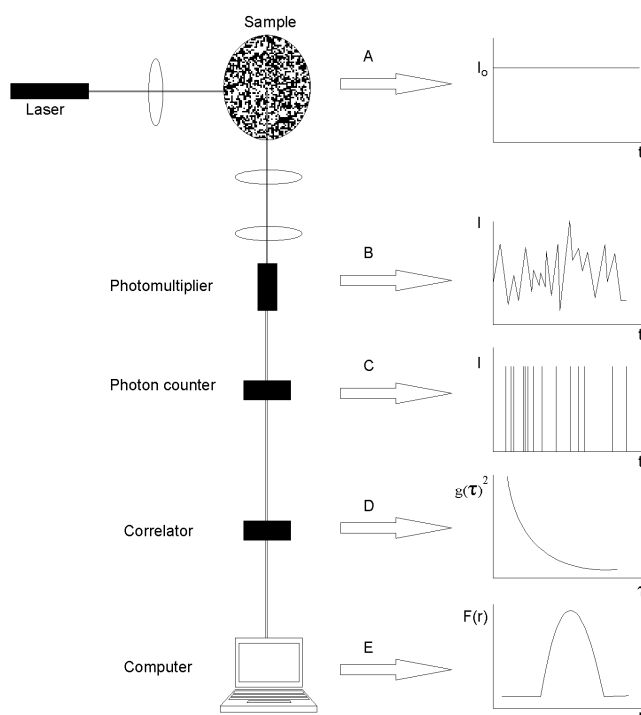


Figure 9 Schematic diagram of the main components of a dynamic light scattering apparatus and the corresponding information obtained from each⁵⁵.

3.2. Elemental analysis

Two techniques have been used in this work to investigate the inorganic elements content, namely X-ray fluorescence and inductively coupled plasma – optical emission spectroscopy. Both will be discussed briefly hereunder.

3.2.1. X-ray fluorescence

The generation of X-ray occurs when an incoming photon expels an inner shell electron, creating a hole, followed by filling of this hole by an outer shell electron with subsequent emission of the difference in energy as X-rays. With the formation of several holes in an element and the subsequent emission of several X-ray lines, this serves as a fingerprint to identify the element^{56, 57}.

The wavelength of the emitted characteristic X-ray varies with the element's atomic number, Z , according to Moseley's law:

$$1/\lambda = K(Z - \sigma)^2$$

in which K is a constant dependent on each spectral series and σ is a shielding constant⁵⁷. Once the element is identified from the set of characteristic X-ray emission, the intensities of the peaks are used to determine the available concentration of the known element by comparison to a calibration line of the same element at different concentrations^{56,57}.

The fluorescent yield varies with Z^4 , as given by the relation:

$$w = Z^4 / (Z^4 + c);$$

where w is the x-ray fluorescent yield, Z is the atomic number and c is a constant, dependent on whether the expelled electron originated from K, L or M shell⁵⁸. This is the main reason why the sensitivity of this analysis method is low with low atomic number elements.

3.2.2. Inductively coupled plasma–optical emission spectroscopy

Inductively coupled plasma–optical emission spectroscopy (ICP-OES) was independently established by Fassel in the US and Greenfield in the UK in the 1970s⁵⁹. The method relies on the excitation of atoms and ions and the identification of the subsequently emitted characteristic radiation in the UV and visible range, upon restoration of the atom or ion to their ground state.

An argon plasma is generated by an electromagnetic field within an inductive coil via a radio frequency generator. The liquid sample is turned into an aerosol by the aid of a nebulizer and passed through the plasma. Once in this high temperature region (5,300 K – 10,000 K), the sample is vaporized, atomized, ionized, partially or fully ionized depending on ionization energy. Table 1 lists selected elements, their ionization energies and their degree of ionization. The energy surplus is used for atom or ion excitation. The emitted radiation upon return to ground state is then resolved via diffraction grating. Quantitative determination is carried out by comparison of the analyte intensity signal to that of standard calibration lines^{59, 60}.

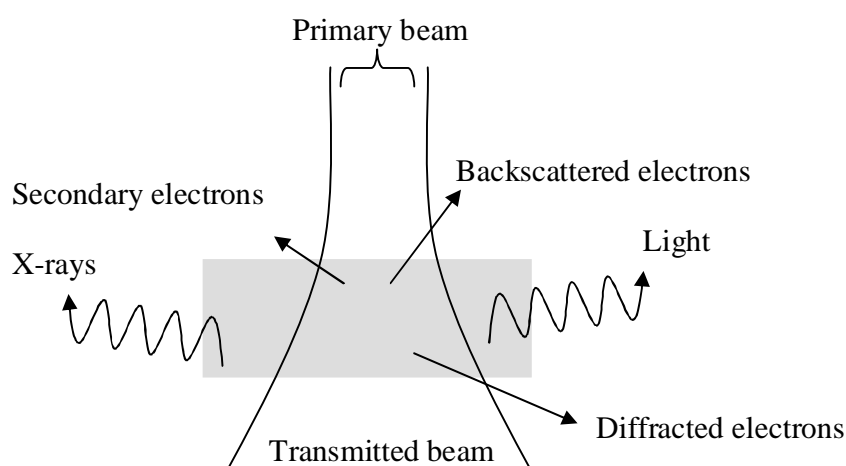
Table 1 Selected elements with their respective first ionization energies and their degree of ionization⁶⁰.

Element	1 st Ionization energy [eV]	Degree of ionization (%)
Zn	9.39	75
P	10.49	33
Ca	6.11	99
Ba	5.21	91

3.3. Electron microscopy and related techniques

3.3.1. Introduction

When an electron beam strikes a specimen, several interactions result, as illustrated in Figure 10. Secondary and backscattered electrons are utilized in scanning electron microscopy (SEM), transmitted electrons in transmission electron microscopy (TEM), X-rays in energy dispersive x-ray analysis (EDX), diffracted electrons in diffraction patterns, both diffracted electrons and transmitted electrons are used for obtaining high resolution transmission electron microscopy images (HR-TEM) and light emitted can be used for cathodoluminescence microscopy. Except for the latter interaction, the various interactions have been employed in this work for sample characterization and would therefore be briefly explained hereunder.

**Figure 10** Schematic diagram showing the main interactions of a primary electron beam with a specimen (gray)⁵⁸.

3.3.2. Transmission electron microscopy

In transmission electron microscopy (TEM), electrons are emitted via an electron source, typically an electron gun or a field emission gun. The emitted electrons are then accelerated down the microscope column in vacuum. Figure 11 shows the main components of a TEM column. The wavelength of the emitted electrons is given by:

$$\lambda = \frac{h}{\sqrt{2m_e eV(1 + \frac{eV}{2m_e c^2})}};$$

where h is Planck's constant, e is the electron charge, m_e is electron mass at rest and c is the speed of light. Substituting those constants in the expression, leaves the wavelength as a function of V , the accelerating voltage^{58, 61}.

The samples need to be thin to allow the electron beam to pass through unscattered. With increasing sample thickness, more electrons will be scattered which renders the image dark, in bright field mode. This same effect can also be observed with a difference of element's atomic number. As the atomic number increases, scattering power also increases. This contrast is an effect known as mass-thickness contrast^{61, 62}.

In HR-TEM, a large objective aperture is used so that both the transmitted and diffracted beam is allowed to interfere. This interference allows the imaging of columns of atoms of crystallographic planes^{62, 63}.

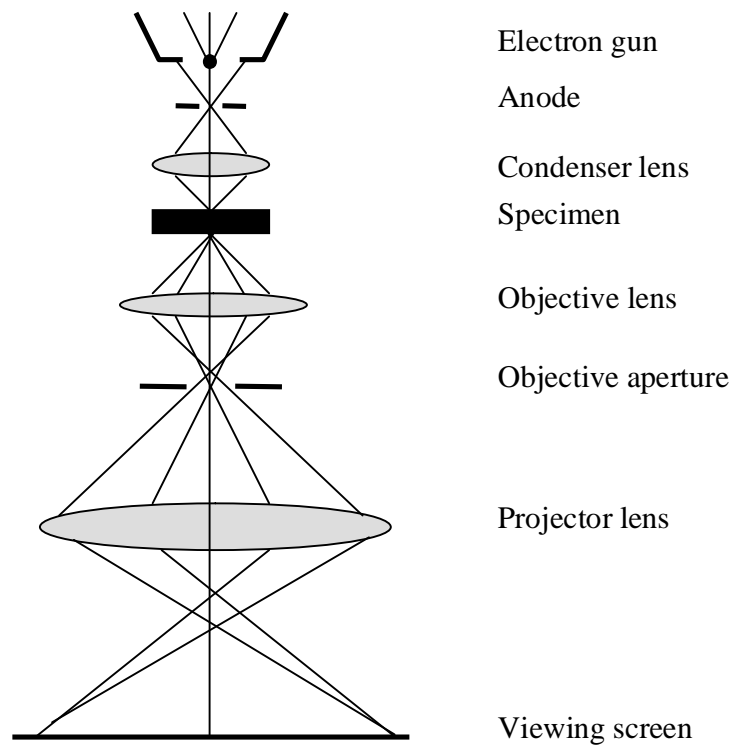


Figure 11 TEM ray diagram illustrating typical TEM main components⁶¹.

3.3.3. Scanning electron microscopy

As mentioned above, two other results from the electron beam interaction with the specimen are secondary electrons and backscattered electrons. Those are the electrons that are used for image formation in SEM. The main SEM components are shown in ray diagram, Figure 12.

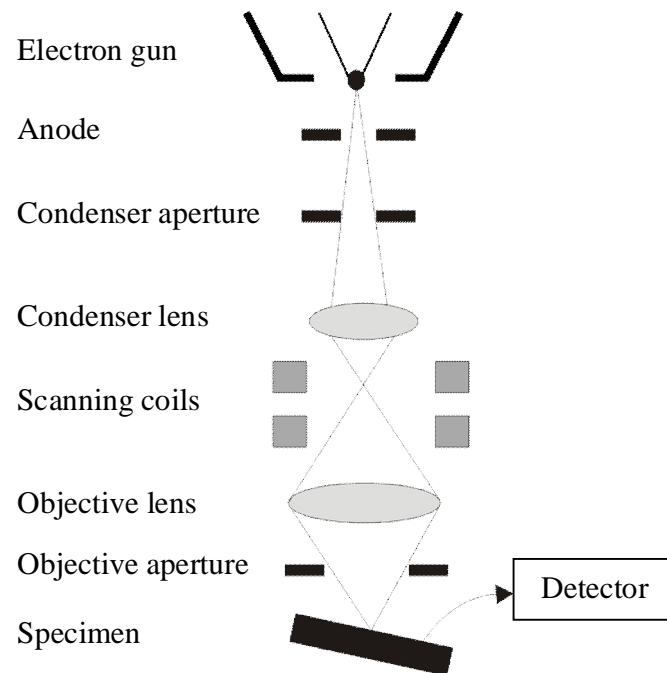


Figure 12 Ray diagram illustrating typical SEM components. Adopted from^{64, 65}.

Secondary electrons are electrons emitted as a result of inelastic scattering interactions between the primary beam and the specimen. They are normally emitted from near surface region and with energies up to 50 eV^{65, 66}.

Backscattered electrons are a result of elastic Rutherford scattering. When the primary beam approaches the atom's nucleus, it gets deflected by the atom's electron cloud⁶⁶.

There are two main contrast modes obtained in SEM imaging: topographic and material contrast. Topographic contrast makes use of the "edge effect" and relies mainly on detection of secondary electrons – a local edge or elevation at the specimen results in an increased emission of secondary electrons due to an increased specimen's interaction volume with primary electron beam⁶⁶. As for the material contrast, backscattered electrons are employed since the backscattered electrons are dependent on the element's atomic number, while the secondary electrons are not⁶⁵.

3.3.4. Energy dispersive X-ray analysis

In simple terms, energy dispersive X-ray (EDX) analysis is a method that uses the characteristic X-rays emitted from the sample in an electron microscope as a result of the inelastic interaction between the primary electron beam and the specimen. X-rays detection allows the determination of the elements at the primary electron beam's position.

X-rays are emitted when an inner shell electron is excited followed by a higher shell electron moving into the created vacancy. The difference in energy between each level can be emitted as X-ray radiation^{66, 67}.

EDX can be carried out as single-point analysis (as was used in this work to confirm element's presence in TEM), 2 dimensional spectrum image (as line scans performed in this work) or as 3 dimensional spectrum images (which have not been explored here)⁶⁷. Even though that EDX can be used as well for quantitative analysis, this feature has also not been explored, since results would not have been representative of overall sample constituents. Detection limit of EDX analysis is approximately 0.1 at.% which may increase in case of light elements⁶⁷.

In our work, EDX was used primarily in the cross-section investigation of the coatings film, where an EDX line scan was used in combination with SEM. The line scan lateral resolution is said to be highly dependable on size of the SEM probe, thickness of the film and the composition of the film, i.e. element's atomic number⁶⁸.

3.3.5. Electron diffraction

Diffraction is the result of elastic scattering between incoming beam and the crystal atoms. According to Bragg's law, the condition to obtain constructive interference is given by:

$$n\lambda = 2d \sin \theta$$

where n is the order of diffraction, λ is the incoming beam's wavelength, d is the interplanar distance and θ is scattering angle. When the incoming beam is a beam of electrons whose wavelength is much smaller than a typical X-ray (e.g. 0.0037 nm for

100 kV accelerated electron beam compared to 0.154 nm for $\text{Cu}_{\text{K}\alpha}$ X-rays), then Bragg's law for first order diffractions can be approximated to:

$$\lambda = 2d\theta$$

According to this approximation, and since the angle of scattering is equal to the angle of incidence, this leads to the condition that the incoming electron beam should be almost parallel to the planes of atoms for a strong diffraction to take place⁵⁸.

In TEM, there are two modes: image mode and diffraction mode. In the latter, the projector lens is focused on the back focal plane of the objective lens – where the diffraction occurs⁶².

Typical diffraction patterns for crystalline material are show in Figure 13.

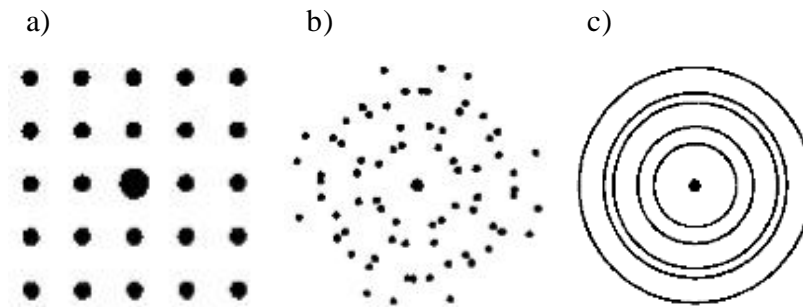


Figure 13 typical diffraction patterns for a) perfect single crystal, b) small number of grains and c) polycrystalline material. Images taken from⁵⁸.

In this work, crystallinity of the inorganic materials was determined locally through electron diffraction in TEM, rather than X-ray diffraction due to the amorphous nature of the polymer matrix.

4. Results and discussion

4.1. Synthesis of water-based hybrid inorganic - polymer particles via multiple miniemulsions

4.1.1. Objective

In this chapter, a versatile synthetic route was devised with the target of preparing water-based hybrid inorganic - polymer particles, suitable to be used as a functional coating. The synthetic route was also designed to contain no organic solvents throughout the complete process. To show the versatility of this synthetic route, a rather sophisticated and complex polymerizable composition containing (meth)acrylic monomers, styrene, epoxy resin and a suitable latent epoxy curing agent was chosen as a present example for an advanced coatings systems. Likewise, the inorganic pigments can be varied in their chemical composition on a very broad basis. As an example, zinc phosphate, calcium carbonate and barium sulfate were used – being most commonly used in coating applications.

4.1.2. Designing the synthetic process

4.1.2.1. Basic idea

Figure 14 shows a schematic illustration of the devised synthetic route. The process starts with the formation of two separate inverse miniemulsions, both possessing the same continuous phase composition, which constitutes a mixture of vinylic monomers, an epoxy resin as well as a suitable curing agent. This mixture composition will be referred to hereafter as “polymerizable phase” or “polymerizable composition”. Each of the inverse miniemulsions holds as its dispersed phase an aqueous solution of one of the precursors required for inorganic pigment formation. For example, for the preparation of calcium carbonate, one inverse miniemulsion contains a solution of calcium acetate as dispersed phase, while the other contains a solution of sodium carbonate.

In a second step, those two inverse miniemulsions are added together and homogenized using ultrasound, resulting in an inverse miniemulsion, whose dispersed phase contains both the precursors, forcing them to react and create the desired inorganic pigment.

Still in a third step, this inverse miniemulsion would be added to a solution of a suitable o/w surfactant, followed by homogenization. The result is a water-based miniemulsion containing as a dispersed phase the polymerizable phase, which in turn holds the in-situ synthesized inorganic pigment.

As a last step, miniemulsion free radical polymerization is carried out via thermal initiation. Other initiation techniques are also possible.

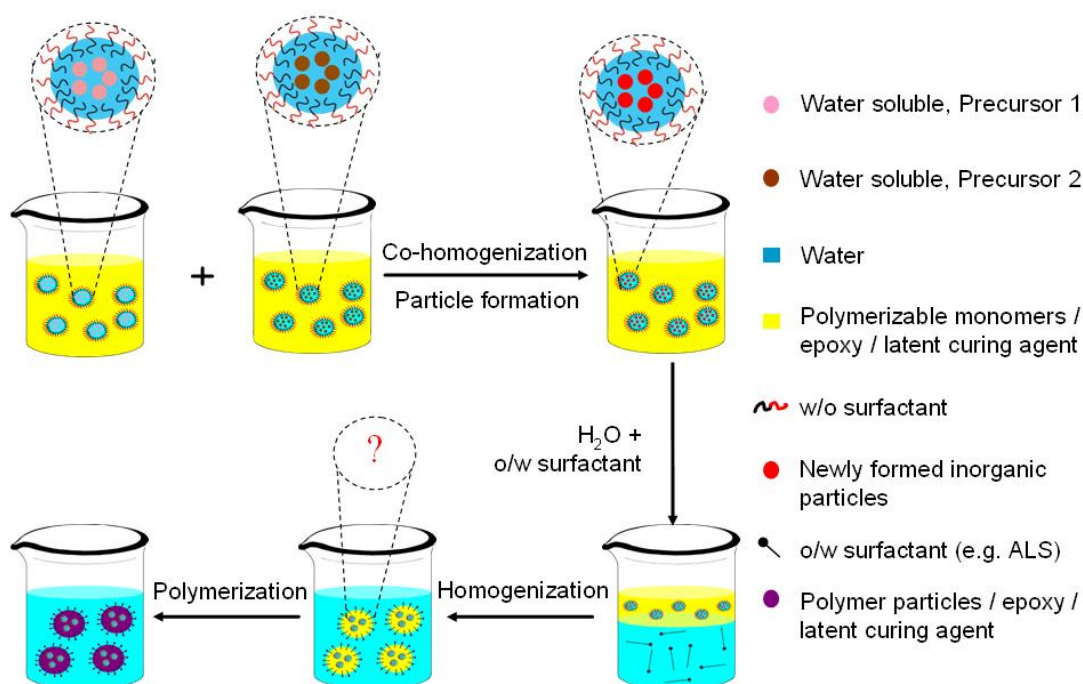


Figure 14 Synthesis process, starting from top left corner: formation of two inverse miniemulsions with inorganic precursors as the dispersed phase followed by co-homogenization. Next, transfer to a direct miniemulsion via addition of o/w surfactant solution followed by homogenization and polymerization.

This synthetic route is made up of a few concepts:

- 1) Co-homogenization of two inverse miniemulsions, each containing a precursor for the in-situ synthesis of an inorganic pigment:

As above-mentioned, two precursor-containing inverse miniemulsions are prepared first which consist of identical continuous phases, but have droplet ingredients which would undergo spontaneous reaction in a homogeneous system. This idea is based on one of the

earliest experiments carried out in miniemulsions to prove the suppressed diffusion between the dispersed droplets. Those first experiments of co-mini-emulsification were carried out for synthesizing colored pigments starting from inverse systems, namely nickel murexide (red) and iron(III) hexacyanoferrate(II) (Prussian blue), which made it easier to follow the development before and during ultrasonication^{69, 70}. Upon combining the precursor miniemulsions, no reaction is observed at first, which perfectly supports the validity of the already mentioned miniemulsion nanoreactor concept and the interparticle diffusion suppression. Upon co-homogenization, the shear forces imparted on the individual droplets of both precursors does force them to undergo fission and fusion, leading to an immediate reaction between the precursors. Not only was the synthesis route successful in preparation of the pigments, but it also proved the stability of the miniemulsion and the suppression of diffusion between the droplets: when the two miniemulsions were mixed containing the two different precursors, the color did not develop to red, for the former, or blue for the latter. Only after ultrasonication did color changes start to occur. Since then, this method was used frequently in a versatile manner as a synthetic procedure to prepare, besides others, inorganic-organic hybrids as in the work of Ramírez et al.⁷¹ and Tiarks et al.⁷².

2) Formation of inverse miniemulsions with a continuous phase of polymerizable monomers:

The idea of utilizing a polymerizable continuous phase to circumvent the tedious use of auxiliary solvents was reported before. The first work dealing with monomers as the continuous phase of emulsions was published in 1983 by Gan and Chew^{73, 74}. Since then, further research has been carried out where polymerization was always performed with the monomers in the continuous phase, leading to the synthesis of foams⁷⁵⁻⁷⁷, porous hydrogels⁷⁸ or simply porous polymers⁷⁹, as well as the incorporation of inorganic materials inside the dispersed phase^{74, 75, 77}. In all cases, the results in those works were polymers in a solid form. To our knowledge, this is the first work done where a polymerizable continuous phase has been used in an inverse (mini)emulsion formation followed by transfer to a direct miniemulsion, followed by polymerization, so that the result is a water-based dispersion.

3) Transfer of inverse miniemulsion into a direct miniemulsion:

The idea of transferring an inverse emulsion into a direct one (water-in-oil-in-water, w/o/w) or vice versa (oil-in-water-in-oil, o/w/o) was first investigated in 1925^{80, 81} and was termed as multiple or double emulsions. The concept was established in the fields of conventional macroemulsions^{81, 82} and microemulsions⁸¹. However, for such systems, there is a serious stability limitation related to diffusion of the constituents as described by Garti⁸¹. There was only one work that could be found from 2005 by Boutti et al.⁸³, in which a miniemulsion was partly involved. In their work, silica particles were synthesized in cyclohexane via a microemulsion process followed by grafting of 3-aminopropyl triethoxysilane to the silica particles and transfer to a direct miniemulsion, with subsequent interfacial polycondensation to form polyamides. Please note, that microemulsions and miniemulsions share drastic different features in terms of size and size distribution, droplet formation, surfactant and co-surfactant concentrations, interdiffusion processes, etc. Furthermore this work did not mention any information on long-term stability of the emulsion, as the resultant miniemulsion after polymerization was directly centrifuged. To the best of our knowledge our studies describes for the first time the conversion of an inverse miniemulsion into a direct miniemulsion.

4) Miniemulsion free radical polymerization:

Miniemulsion polymerization is used since through this polymerization path, the polymer particles after polymerization correspond to the initial monomer droplets, i.e. the nanoreactor concept⁹ - one of the main miniemulsion characteristics. This is as a result of the suppressed diffusion between the miniemulsion droplets, which make them ideal for the synthesis of hybrid materials¹⁰, as well as radical copolymerization where monomers possess different water solubilities⁹.

In our formulation, the Ostwald ripening is suppressed in the final water-based miniemulsion by the epoxy resin and the latent curing agent, both of which are highly water insoluble.

Another application related reason why miniemulsions were most suitable for functional coatings is the amount of surfactants used. In miniemulsions, the droplet surface is not fully covered with surfactant⁸⁴. This indicates that the surfactant amount used is minimal, which is an important criterion for coatings, as will be explained later when discussing

choice of surfactants. Furthermore, it was also mentioned earlier (Section: 2.3.2.3. “*Aquence® autodeposition coatings system*”) that this incomplete coverage characteristic in miniemulsions was also important for autodeposition processes.

4.1.2.2. Proof of concept

It was necessary to show the above-designed process is doable with simple components. To do this, the following components were selected: as a vinylic monomer, styrene was used, while an amphiphilic block copolymer was used as the w/o surfactant, namely poly(ethylene-co-butylene)-*b*-poly(ethylene oxide), which will be referred to as PE/B-*b*-PEO. Zinc acetate and phosphoric acid were used as the precursors for the formation of zinc phosphate, with a zinc phosphate loading of ca. 3 wt% to styrene.

The inverse miniemulsions prepared with a continuous phase of styrene were not long-lived. Only about one day of stability was achieved, which was not critical since it provided enough stability for the entire process to be carried out. Worth mentioning that afterwards long-term stable o/w hybrid miniemulsions were achieved after multiple miniemulsification and polymerization.

For the formation of the direct miniemulsion, ALS-33 (ammonium lauryl sulfate, 33 wt% solution) and Lutensol AT50 were used as the o/w surfactants, while for the polymerization, AIBN, KPS as well as redox initiation were used, for each o/w surfactant used.

Both o/w surfactants were successful in forming the direct miniemulsions. In the final formulation, the use of ALS-33 would be preferential to allow autodeposition to take place during coating formation. The polymerization was incomplete with the redox system, while complete polymerization took place with both AIBN and KPS, but with slight creaming of the miniemulsion. XRD (X-ray diffraction) shows that the resulting polystyrene-zinc phosphate is amorphous, which is explained by the presence of the amorphous polystyrene and the relatively low zinc phosphate concentration.

Despite non-ideal results in terms of polymerization and also broad droplet size distributions, the results show feasibility of the process.

4.1.2.3. Choice of organic ingredients

▪ Epoxy resin

As previously mentioned, cured epoxy is the choice of resin for primers because of their mechanical strength, chemical and corrosion resistance, as well as good adhesion properties³⁴. Typically, the use of epoxy requires the use of an organic solvent either as a viscosity modifier or solvent in case of solid epoxies, for example, which then requires in the synthetic process an additional step for distillation to extract the solvent – the so called stripping process³⁷. In our process, in order to avoid the use of any organic solvent, the epoxy resin, together with the latent curing agent, both in solid form, were left to dissolve in a mixture of vinylic monomers.

In all the experiments, epoxy resins based on the reaction of bisphenol A and epichlorohydrin – BADGE, bisphenol A diglycidylether - was used, as shown in Figure 15. Epoxy resins based on BADGE are the most widely used epoxy resins in the coatings industry because of its adhesion properties and anti-corrosion properties⁸⁵. Typically, the properties are highly dependent on the value of “n” in the structure. The $n = 0$ is a crystalline solid. The available commercial grades though for the coatings industry are liquid resins, whose n value lies between 0.11 and 0.15, while with $n > 1$, the epoxy resin becomes an amorphous solid⁸⁵. Other consequences dependent on the n value include an increase in molecular weight, but most importantly an increase in EEW – epoxy equivalent weight; the weight of resin required to obtain one equivalent of epoxy functional group³⁴. In this work only solid epoxy resins were used with n values of ~ 2 and ~ 5 for D.E.R. 671 and D.E.R. 664, respectively.

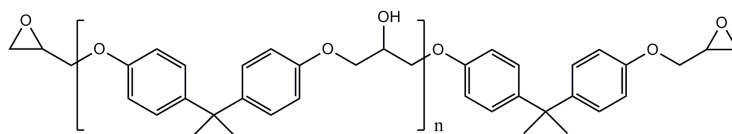


Figure 15 BADGE - resultant of the reaction of bisphenol A and epichlorohydrin.

▪ Vinylic monomers

The use of vinylic monomer mixtures did not only act as reactive diluent for the epoxy resin but the resulting polymers had also an effect on the organic coating properties.

An acrylic-epoxy system shows a better durability than only epoxy systems⁸⁶. Furthermore, the addition of vinyl ester functionality to the epoxy resin improves its hydrolysis and chemical resistance properties³⁴, this is done through the use of methacrylic acid to enable grafting onto the epoxy resin via radical polymerization⁴⁴ and at higher temperatures. The addition of styrene to the mixture was also justified: styrene acrylics are lower in cost than a pure acrylic mixture, and additionally, the presence of styrene increases the hydrophobicity of the acrylics and thus increase the water resistance of the coating²¹. The UV instability of styrene- and bisphenol A-based epoxy resin in this case is not an issue as this organic coating should be applied as a primer and direct exposure to UV light was not a concern.

Likewise, the concentrations were adjusted to serve the purpose: the epoxy resin has to be used at the highest possible concentration (solubility and viscosity limited), while hydrophilic monomers, namely methacrylic acid and 2-hydroxyethyl methacrylate, were reduced to minimize unwanted secondary nucleation during radical miniemulsion polymerization⁸⁷. Moreover, a suitable latent curing agent, with an unblocking temperature of over 170 °C was added to induce crosslinking at a curing stage after the film formation on the substrate by heating in an oven. The final composition of the polymerizable phase is summarized in Table 2. To reach this composition, many steps were taken, which will be explained step-by-step in the next sections.

The formulation as such represents a typical coatings composition^{44, 88, 89}. This provided also a proof for the flexibility and diversity of the synthetic route. Changes in the polymerizable phase composition and concentration was also possible as will be shown.

Table 2 Main composition of polymerizable phase. A suitable latent epoxy resin is still added to the mixture.

Epoxy resin or monomer	Weight percent w.r. to total epoxy / monomer
D.E.R. 664*	35.0
Butyl acrylate	19.369
Methyl methacrylate	20.682
Styrene	21.448
2-Hydroxyethyl methacrylate	2.444
Methacrylic acid	1.058

* D.E.R. 664 is a medium molecular weight solid bisphenol-A diglycidyl ether epoxy resin based with an EEW value of 875 – 955 g/eq.

4.1.2.4. Choice of inorganic ingredients

Zinc phosphate was the choice of pigment for corrosion testing, for reasons explained earlier. To prove that the synthetic method can still be applied for the synthesis of other pigments, two other pigments also widely used in coatings application were chosen, namely calcium carbonate and barium sulfate, both of which are used as extenders in the coating industry^{3,90} (extenders are pigments whose main function is to occupy volume in a coatings film and reduce coating cost, but also help to adjust coating properties⁹¹). In addition to being an extender, barium sulfate can also be used as a white pigment⁹². Moreover, it is even said that calcite, one of the calcium carbonate crystal structures may possess anticorrosion properties⁹³. All three pigments are strictly water insoluble at neutral pH (solubility product constant: 9.12×10^{-33} at 20 °C, 9.3×10^{-9} at 20 °C and 1.07×10^{-10} at 25 °C, respectively)⁹⁴. Therefore, suitable water soluble precursors were necessary. Synthetically, the choice of precursors is only limited by the solubility in water. But since the functional coating application was the target, chlorides for example were not advisable, in order to avoid promotion of corrosion⁹⁵. For that reason, the cation precursors were chosen to be acetates, since being organic they should not disrupt or alter the functional coating performance. The anion precursor was chosen to be phosphoric acid for the preparation of zinc phosphate, while for the preparation of calcium carbonate and barium sulfate, a sodium precursor for the anion was used.

The stoichiometry of both precursors is also important. In the case of the zinc phosphate synthesis, a molar ratio of $\text{Zn}^{2+} : \text{PO}_4^{3-} = 1 : 1.05$, according to Herschke et al. was chosen⁹⁶. For the syntheses of calcium carbonate and barium sulfate, a molar ratio of 1 : 1 for the cation : anion precursors was used. Additionally, an attempt was made to synthesize hydrated zinc iron phosphate in the crystal phase known as phosphophyllite, but the synthesis was unfortunately limited by the precursors' solubility.

Also here, the versatility of the process is proven via synthesis of various inorganic pigments which can also be extended to others, as long as the precursors are water soluble. In the following details will be given on preliminary tests made in order to arrive at the above-mentioned precursors' suitability.

▪ Zinc phosphate

In the literature, several precursors have been used as a Zn source: zinc chloride⁹⁷⁻⁹⁹, zinc oxide⁹⁷, zinc nitrate^{98, 100}, zinc sulphate^{98, 101}, and zinc acetate^{96, 102-104}. For the phosphate precursor, either phosphoric acid^{96, 97, 101} was used or one of its sodium⁹⁷⁻⁹⁹, potassium⁹⁹ or ammonium^{100, 102, 103} salts. Marella et al.⁹⁷ and Sziklai et al.¹⁰¹ explain that using the combination of zinc oxide and phosphoric acid is favorable to avoid the formation of a by-product, which for an anticorrosion application is highly unfavorable. Unfortunately, the solubility of zinc oxide in water limits its use in miniemulsion. Al-Maydama et al.¹⁰⁵ have used a zinc oxide slurry, which would not be useful in a miniemulsion system. Likewise, Marella et al.⁹⁷ in their work to synthesize zinc phosphate in microemulsions used zinc oxide, though how they managed to have it incorporated in the dispersed phase is not explained. Therefore, a zinc salt and phosphoric acid have been used for the trials.

In such a system, there are many parameters that should be optimized, not only the type of zinc salt, but also the stoichiometric ratio of zinc to phosphate.

Zinc phosphate has four polymorphs¹⁰⁶, namely hopeite and parahopeite ($\text{Zn}_3(\text{PO}_4)_2 \cdot 4 \text{H}_2\text{O}$), tarbuttite ($\text{Zn}_2\text{PO}_4(\text{OH})$) and spencerite ($\text{Zn}_2\text{PO}_4(\text{OH}) \cdot 1.5 \text{H}_2\text{O}$). The difference between hopeite and parahopeite lies in the structure, hopeite has an orthorhombic^{103, 106} structure while parahopeite has a triclinic structure. Moreover, the hopeite structure has two main modifications to the orthorhombic structure, α - and β -hopeite^{99, 103-105}, even a γ hopeite modification has been identified^{99, 104, 105}. The differences lie only in the hydrogen bonding¹⁰³. Not only does the stoichiometry affect

the crystal structure obtained but also the temperature of the synthesis. Herschke et al.^{96, 103} synthesized α -hopeite at 90 °C while β -hopeite was synthesized at only 20 °C, while Pawlig et al.¹⁰⁴ have synthesized α -hopeite at only 50 °C. Castellano et al.⁹⁸ carried out the synthesis at 90 °C and obtained either parahopeite or a mixture of parahopeite and spencerite. Zinc phosphate in the hopeite structure is used in the phosphate pretreatment step¹⁰⁷, mainly that with α -hopeite modification¹⁰⁴. Therefore, temperature is also an important factor.

In order to establish a zinc precursor, three samples were prepared, with one of two precursors, either zinc nitrate hexahydrate or zinc acetate dihydrate, also with one of two zinc to phosphate molar ratios, either 1 : 1.05 or 1.5 : 1. A summary of the samples prepared is shown in Table 3. For all samples, the w/o surfactant used was the block copolymer PE/B-*b*-PEO in a continuous phase of cyclohexane.

Table 3 Prepared samples showing the precursors used and the molar ratio of $\text{Zn}^{2+} : \text{PO}_4^{3-}$.

Sample	Zn precursor	$\text{Zn}^{2+} : \text{PO}_4^{3-}$ (molar)
A	$\text{Zn}(\text{NO}_3)_2 \cdot 6 \text{H}_2\text{O}$	1 : 1.05
B	$\text{Zn}(\text{NO}_3)_2 \cdot 6 \text{H}_2\text{O}$	1.5 : 1
C	$\text{Zn}(\text{CH}_3\text{COO})_2 \cdot 2\text{H}_2\text{O}$	1 : 1.05

All samples were analyzed using X-ray diffraction. Comparing sample A and sample B (as they differ only in the molar ratio of $\text{Zn}^{2+} : \text{PO}_4^{3-}$), both samples show three possible matches for the different zinc phosphate phases: hopeite, parahopeite, and zinc hydrogen phosphate hydrate. The XRD pattern for sample A is shown in Figure 16, while the XRD pattern for sample B is not shown here.

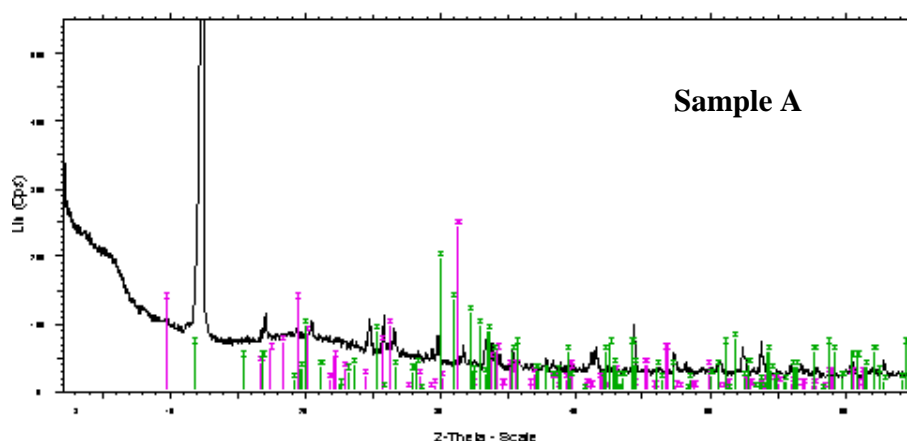


Figure 16 X-ray diffraction pattern of sample A (black), as well as characteristic peaks of hopeite (purple) and parahopeite (green). XRD pattern of sample A also matched with zinc hydrogen phosphate hydrate (characteristic peaks not shown here).

When comparing XRD patterns of sample A and sample C (as they differ only in the precursor used) shown in Figure 16 and Figure 17, respectively, sample C shows more reflexes that are also more well-defined than those of sample A. In sample C, only two matches are possible (hopeite and zinc hydrogen phosphate hydrate), instead of three matches in sample A (parahopeite, hopeite, and zinc hydrogen phosphate hydrate). This result is, to a certain extent, in consistence with that in the literature. For example, Herschke et al.^{96, 103} have used the same acetate precursor and obtained only the hopeite structure – either α or β depending on the temperature. Moreover, Pawling et al.¹⁰⁴ state clearly having tried a number of zinc precursors (namely, carbonate hydroxide, chloride, citrate, nitrate and acetate) and had obtained best results, in terms of purity and crystallinity, when using the acetate precursor. They succeeded in synthesizing only α -hopeite structure at only 50 °C. On the other hand, in sample C, zinc hydrogen phosphate hydrate has also been produced in the process, even though our synthesis was carried out using the same molar ratios used by Herschke et al.^{96, 103} who had produced only one phase (hopeite).

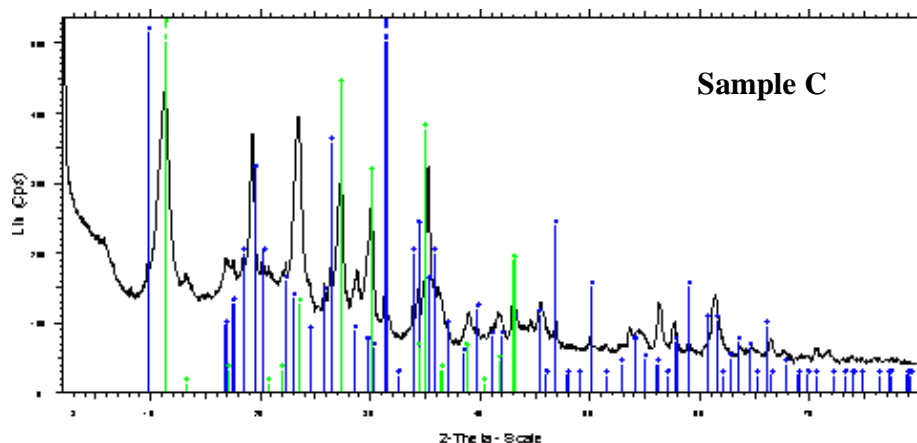


Figure 17 X-ray diffraction pattern of sample C (black), as well as characteristic peaks of hopeite (blue) and zinc hydrogen phosphate hydrate – $(\text{ZnHPO}_4)_2 \cdot 3 \text{H}_2\text{O}$ (green).

As mentioned above, the temperature seems to be an essential factor especially in the synthesis of α -hopeite and therefore, sample C was repeated by replacing cyclohexane with Isopar M (isoparaffin fluid) as the continuous phase to be able to heat up the miniemulsion to high temperatures (boiling point range of Isopar M is 206 - 255 °C). The miniemulsion sample was then left overnight in an oil bath at 90 °C. This sample will be referred to as sample D.

Heating the miniemulsion in the oil bath at 90 °C has led to phase separation. Still the precipitate was analyzed using XRD, as shown in Figure 18. The XRD pattern shows clearly that the hopeite structure is prevailing and the possibility of presence of other phosphates is minimal. Those precursors and molar ratios were then chosen for zinc phosphate synthesis, where the hopeite structure could possibly be formed during polymerization (at high temperature) or even during curing at a later stage.

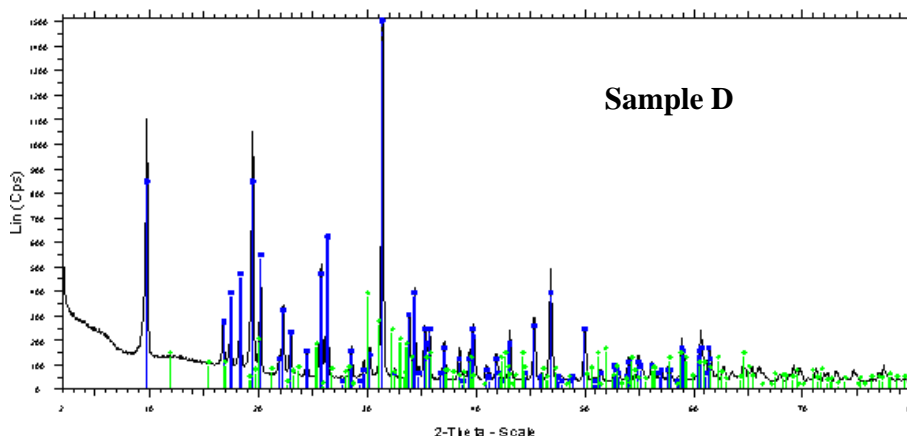


Figure 18 X-ray diffraction pattern of sample D (black), as well as characteristic peaks of hopeite (blue) and parahopeite (green).

▪ **Calcium carbonate**

Preliminary experiments were also carried out here to investigate the best precursor combination for the synthesis of calcium carbonate. Inverse miniemulsions were carried out in a continuous phase of cyclohexane, using Fortegra 100 (chemical structure shown in Table 5) as the w/o surfactant. The combination of cyclohexane and Fortegra 100 did not result in a stable miniemulsion, as gelling took place to a certain extent during ultrasonication. Nevertheless, the analysis was carried out to investigate the crystal phases obtained. Three different routes were employed, as summarized in Table 4.

Table 4 Summary of trials for synthesis of calcium carbonate.

	Precursor 1	Precursor 2
Route 1	Ca(OH) ₂	CO ₂
Route 2	CaCl ₂	Na ₂ CO ₃
Route 3	CaAc ₂ · H ₂ O	Na ₂ CO ₃

In route 1, calcium hydroxide and carbon dioxide gas were intended to be tried out after Willert et al.¹⁰⁸ where it was mentioned that a liquid starting point was obtained by a mixture of Ca(OH)₂ and H₂O in a ratio of 1 : 2. Unfortunately, the solubility of Ca(OH)₂ in water is very poor and even with an excess of water what is obtained is a suspension which separates on rest. Another precursor which has also been mentioned in this paper was CaCl₂. This precursor has not been tried out since the by-product would result in formation of HCl which would not be system friendly to our epoxy containing samples.

The second route tried out was after Pai and Pillai¹⁰⁹, where they have synthesized amorphous calcium carbonate particles via co-ultrasonication of the two precursor-containing inverse miniemulsions, namely calcium chloride and sodium carbonate. In their work, they used cyclohexane as the continuous phase and Lubrizol U (chemical structure shown in Table 5) as the surfactant. The same was tried out, only using Fortegra 100 as the surfactant. The resulting precipitate was investigated by XRD which resulted in clear NaCl reflexes, confirming that the produced calcium carbonate was also in this case amorphous, in agreement with the work of Pai and Pillai. XRD pattern is not shown here. Due to the presence of chloride ion, an alternative route was then sought.

In route 3, the CaCl_2 of route 2 was replaced by the acetate monohydrate – $\text{CaAc}_2 \cdot \text{H}_2\text{O}$. XRD pattern for the prepared sample is shown in Figure 19. The shown peaks can be assigned to sodium acetate as well as calcium carbonate in the vaterite phase, though the weak calcium carbonate signals does not rule out the presence of amorphous calcium carbonate as well. This route was then chosen for the calcium carbonate synthesis.

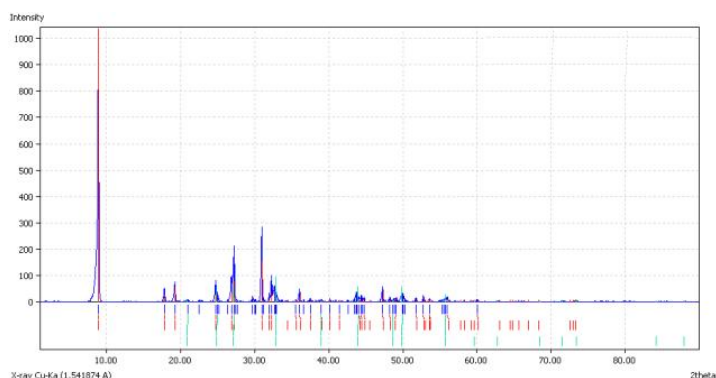


Figure 19 XRD pattern for the sample prepared via route 3 (blue) showing clear sodium acetate peaks (red) and weak calcium carbonate peaks in vaterite crystal structure (green).

▪ Barium sulfate

Preliminary tests for barium sulfate were simple since barium sulfate is available in one polymorph – the barite structure. Tests were also carried out in cyclohexane using Fortegra 100 as the w/o surfactant. Barium nitrate and barium hydroxide monohydrate had poor solubility, so again the acetate precursor was used as the barium precursor while the sodium sulfate was used as the sulfate source. XRD investigation (not shown here)

confirmed the formation of barite. Moreover, in hybrid miniemulsions, the proof of crystallinity will be shown.

▪ Zinc iron phosphate – phosphophyllite

Phosphophyllite is equivalent to hopeite only with one iron(II) ion replacing one of the zinc(II) ions¹¹⁰. Both hopeite and phosphophyllite are the main phases responsible for corrosion resistance in metal treatment^{36, 110}, where phosphophyllite is formed for example during phosphate conversion coating when steel is the substrate³⁶.

The problem was to find the same anion-based precursor for Fe^{2+} and Zn^{2+} where both are soluble in water.

- carbonates: zinc carbonate is commercially available as basic zinc carbonate, i.e. a mixture of zinc carbonate and zinc hydroxide and is water insoluble.
- oxides: both are insoluble.
- nitrates: iron(II) nitrate is commercially not available.
- acetates: iron(II) acetate is insoluble.

There was only one paper found discussing the synthesis and the structure of phosphophyllite¹¹⁰. In this work, $(\text{NH}_4)_2\text{HPO}_4$ was used as the phosphate source while either the chlorides or the sulfates were used as the Fe^{2+} and Zn^{2+} precursors. Since the chlorides for our purpose of corrosion resistance are not suitable, the sulfates were therefore preferred.

As for the molar ratios used, Thomas et al.¹¹⁰ report that only with 40% or more Fe^{2+} content, phosphophyllite was produced. With less than 40% content, a mixture of hopeite and phosphophyllite were obtained. Therefore, in our synthesis, the Fe^{2+} content used was 50%, so that the molar ratios of the used ions would be $\text{Fe}^{2+} : \text{Zn}^{2+} : \text{PO}_4^{3-} = 1 : 1 : 2$. The precursors used were the heptahydrates: $\text{ZnSO}_4 \cdot 7 \text{H}_2\text{O}$ and $\text{FeSO}_4 \cdot 7 \text{H}_2\text{O}$.

Unfortunately, in order to prepare a 2.5 wt% or 5 wt% loading to polymer phase, the amount needed from the zinc or iron precursor had a limited solubility in the dispersed phase. Conceptually, the synthesis of phosphophyllite presented a good example where the synthetic route can be extended to include three precursor inverse miniemulsions that can then be homogenized together. No further experiments were carried out with this inorganic pigment.

4.1.2.5. Choice of nonionic surfactant for inverse miniemulsions

A very challenging task was the choice of a nonionic surfactant that would be able to perform well in forming a w/o miniemulsion in a continuous phase of this very unusual nature. A survey of possible nonionic surfactants was carried out. To evaluate the different surfactants, a simplified formulation was used: the continuous phase was composed of a mixture of butyl acrylate, methyl methacrylate and styrene. The choice was made as such in order to check the miniemulsification possibility, as well as the polymerization with the three main vinylic monomers. Another reason was that the addition of epoxy resin would increase the viscosity of the polymerizable phase – a parameter that still needed to be optimized.

As for the dispersed phase, phosphoric acid was chosen in order to monitor the stability of the emulsion formation even at a low pH. The amount of surfactant was arbitrarily chosen to be 2.5 wt% to the dispersed phase.

A total of sixteen surfactants were evaluated. Two criteria were used to judge the success of miniemulsification: dynamic light scattering (DLS) measurements of this inverse miniemulsion, as well as visual inspection in order to evaluate how long it remains stable. In order to perform DLS measurements, dynamic viscosity of monomer mixture as well as its refractive index were required. Both were determined experimentally, resulting in $\eta = 0.9$ mPa.s and $n = 1.4659$, respectively; the measurements were carried out at 20 °C. To make sure that the experimentally determined values are close to the expected (theoretical) values, calculations were made via appropriate mixing rules. For the refractive index, the theoretical value was found to be $n = 1.4604$, calculated from a mixing rule based on Lorentz-Lorentz refractive index function¹¹¹. The mixing rule is given by:

$$\left(\frac{1}{\rho}\right)f(n_D) = \left(\frac{w_1}{\rho_1}\right)f(n_{D,1}) + \left(\frac{w_2}{\rho_2}\right)f(n_{D,2}) + \left(\frac{w_3}{\rho_3}\right)f(n_{D,3})$$

where ρ is the density of the pure monomer at 20 °C, n_D is the refractive index of a given monomer, w is the weight fraction of a given monomer. f is the function of the refractive index, which is in this case the Lorentz-Lorentz refractive index function given by:

$$f(n_D) = \frac{n_D^2 - 1}{n_D^2 + 2}$$

A suitable mixing rule to calculate the dynamic viscosity could not be found. The experimental values were used for the DLS measurements.

The results of this investigation are summarized in Table 5. Only four surfactants were successful in the miniemulsion formation, namely Grindsted PGPR 90, Isolan PDI, Isolan GPS and Fortegra 100. Their chemical structures are also shown in Table 5.

Grindsted PGPR 90 is a surfactant typically used for chocolates and confectionary applications¹¹². Isolan GPS was developed for the purpose of being a surfactant in oil-based lotions and other personal care products. In the lotions prepared with Isolan GPS, it was found that the presence of isostearate groups increased the stability of the emulsion while the polyhydroxystearate groups helped to reduce the emulsion viscosity¹¹³.

Last but not least, Fortegra 100 - a block copolymer, commercially available as an epoxy toughening agent – was also successful in the preparation of a miniemulsion. Despite the fact that the exact chemical structure of Fortegra 100 is not revealed by Dow, the Dow patency clearly describes Fortegra 100 as an amphiphilic block copolymer¹¹⁴. In this patent, the amphiphilic block copolymer is described as one that has the ability to self assemble and form structures similar to that of surfactants but with epoxy/curing agent mixture: one block must be epoxy/curing agent miscible while the other is immiscible. One possible structure for Fortegra 100 could be poly(ethylene-*alt*-propylene)-*b*-poly(ethylene oxide), which is the one given in Table 5.

Therefore, Fortegra 100 was an attractive option, since the target formulation did contain epoxy to a large extent. This was expected to give an additional stability to the system and/or even a toughening property for the coating. In other words, using Fortegra 100 provided a dual functionality to the system: once as a w/o surfactant, while the other was toughening properties. The other three surfactants possess also dual properties: besides acting as w/o surfactants, they all possess OH groups which could take part in polymerization or in crosslinking. This dual functionality is also important when it comes to coatings formulation, since surfactants in general affect the permeability of the coatings film¹¹⁵, as well as its adhesion, water resistance and may thus affect also corrosion properties.

As can be seen from Table 5, most of the surfactants evaluated resulted in a phase separation upon ultrasonication, except for the above mentioned ones. Grindsted

PGPR 90 and both Isolan grades were visually stable for about 1 day before phase separation could be observed. For the Fortegra 100, 2 days of stability were observed. Despite the mediocre stability shown, at that point there were two important achievements: 1) an inverse miniemulsion having a monomer mix as its continuous phase was possible and 2) this stability was long enough in order to continue the process of miniemulsification. After all, the phosphoric acid miniemulsion is not the goal but only a starting point for the further formation of the zinc phosphate.

Not only because Fortegra 100 showed the longest stability in comparison to the other surfactants, but also because Fortegra 100 is an epoxy toughener, which may impart additional toughening properties for the coating, it was decided that further tests would be carried out with Fortegra 100. In the next step, the whole process will first be carried out using the simplified monomer mix, i.e. zinc phosphate formation followed by transfer to direct miniemulsion and polymerization. Once the whole process is proven doable, the further polymerizable phase ingredients (shown in Table 2) will be incorporated in the system.

Results and discussion

Table 5 Overview of surfactants' testing results for the inverse miniemulsion prepared by the simplified formulation as well as the surfactants' chemical structure. (-) represents phase separation upon ultrasonication, (+) represents miniemulsion formation of a certain period of time. Duration given indicated stability based on visual inspection till phase separation.

Surfactant	Chemical structure	Result
PE/B-b-PEO		-
Lubrizol U		-
Grindsted PGPR 90		+ (1 day)
Tween 20		-
Span 80		-
Fortegra 100		+ (2 days)
Hostacerin DGI		-

Results and discussion

Surfactant	Chemical structure	Result
Hostacerin DGMS		-
Genapol UD 030		-
Hostaphat KL 340D		-
Hostaphat KW 340D		-
Isolan PDI		+ (1 day)
Isolan IS		-
Isolan GI 34		-
Isolan GO 33		-
Isolan GPS		+ (1 day)

PHS = polyhydroxystearic acid and IS = isostearic acid

4.1.2.6. Choice of suitable thermal initiator for the radical polymerization

Fortegra 100 was used to prepare two inverse miniemulsions, one containing phosphoric acid solution as the dispersed phase, while the other containing zinc acetate solution in its dispersed phase, both having as a continuous phase the simplified monomer mixture of butyl acrylate, methyl methacrylate and styrene, along with n-hexadecane as an Ostwald ripening agent for the still-to-be-formed direct miniemulsion. After their co-homogenization and subsequent formation of zinc phosphate in the aqueous droplets, an aqueous solution of ALS-33 was added. The choice of ALS-33 as the o/w surfactant was only based on its nature being an anionic surfactant and thus allows destabilization and autodeposition coating application as explained in theoretical background. After homogenization, a direct miniemulsion was formed whose droplets carry the monomer mixture, which in turn carried the zinc phosphate particles.

The above process was carried out three times in order to test three different thermal initiators, two oil soluble ones, V-70 and AIBN (with a ten hour half-life time in toluene of 30°C and 65 °C, respectively), and the water soluble KPS (with a ten hour half-life time in water at a temperature of 60 °C). In case of the oil soluble initiators, they were dissolved in the simplified monomer mixture from the very beginning, before the formation of zinc acetate and phosphoric acid containing miniemulsions. For KPS initialized polymerization, KPS solution was added directly after the direct miniemulsion formation.

The three polymerizations were carried out for about eighteen hours at the ten hour half-life time temperature. Only the miniemulsion polymerized with KPS had polymerized to completion with a solid content of ~ 18 wt%. The miniemulsion polymerized with V-70 showed slight phase separation, while the sample polymerized with AIBN showed high coagulation, first observed 4-5 h after the start of the polymerization. Therefore, KPS was set as the choice for all further polymerizations.

This whole procedure was monitored at each step using DLS measurements. Figure 20 shows the droplet size distribution for the inverse miniemulsions containing phosphoric acid (miniemulsion 1), zinc acetate (miniemulsion 2), and zinc phosphate (miniemulsion 3), formed by co-homogenization of miniemulsion 1 + 2. The mean

droplet diameters are 304 nm, 380 nm and 325 nm, respectively – all in the typical miniemulsion range.

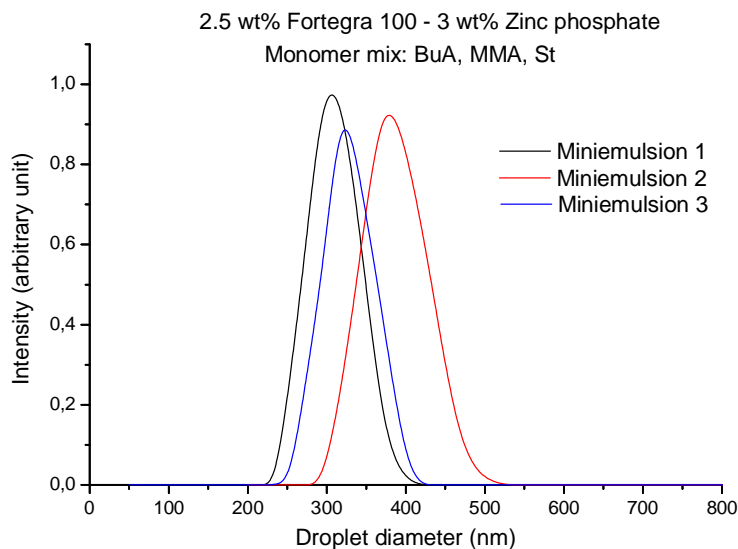


Figure 20 Droplet size distribution as given by DLS measurements taken for inverse miniemulsions in St-MMA-BuA using 2.5 wt% Fortegra 100 (to the dispersed phase) and 3 wt% zinc phosphate (to the organic content). Volume weighted droplet size distributions are based on NICOMP analysis for: miniemulsion 1 (phosphoric acid inverse miniemulsion), miniemulsion 2 (zinc acetate inverse miniemulsion) and miniemulsion 3 (after co-homogenization of both and subsequent formation of zinc phosphate in droplets).

Figure 21 shows the droplet distribution for the direct miniemulsion before polymerization (miniemulsions 4) and particle size distribution after polymerization (miniemulsion 5). The mean diameters are 585 nm and 519 nm, respectively – a rather large dispersed phase diameter. The smaller mean diameter shown after polymerization is typical due to the increased density of the particles as the polymer particles replace the monomers, as well as to corresponding changes in the refractive index. This miniemulsion was stable for about 3 weeks, then started to phase separate. The droplet size will be adjusted in the next section by increasing the ALS-33 content as well as the Fortegra 100 content.

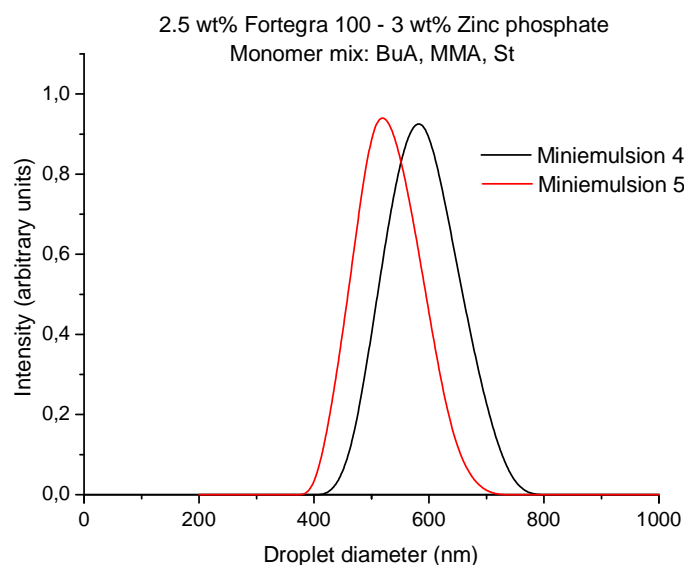


Figure 21 DLS measurements taken for direct miniemulsions, before polymerization (miniemulsion 4) and after polymerization using KPS (miniemulsion 5). Samples were prepared using 2.5 wt% Fotegra 100 (to the aqueous dispersed phase), 0.7 wt% ALS-33 (to the oil dispersed phase, containing zinc phosphate) and 3 wt% zinc phosphate (to the organic content). Volume weighted droplet size distributions are based on NICOMP analysis.

4.1.2.7. Adjusting droplet size via viscosity adjustments

In this section, the polymerizable phase gets more sophisticated by the addition of its further targeted constituents, namely epoxy resin along with latent curing agent, methacrylic acid and 2-hydroxyethyl methacrylate.

As mentioned earlier, both the epoxy resin used and the latent curing agent are in a solid form. Thus, by dissolution of both in the vinylic monomers, a high increase in viscosity occurs. As mentioned earlier, the target was to have the highest epoxy content possible, but at the same time, a particle size in the typical miniemulsion range. To achieve this, starting from an epoxy resin content of 50 wt%, the content was adjusted in steps with a decrement of 5 wt%. The droplet size of the direct miniemulsion showed a high dependency on the viscosity of the polymerizable phase. Table 6 shows the viscosities of the polymerizable phase with different epoxy resin contents, in comparison to the previously used simplified monomer mixture composed of butyl acrylate, methyl methacrylate and styrene.

Results and discussion

Table 6 Viscosity measurements of polymerizable phase show a dependency on the epoxy resin content, in comparison to the simplified monomer mixture employed earlier.

D.E.R. 664 content (wt% to total organic content)*	Viscosity of polymerizable phase (20 °C, mPa's)
50 wt%	1350
45 wt%	740
40 wt%	579
35 wt%	210
0 wt% (mixture of butyl acrylate, methyl methacrylate and styrene)	0.9

* total organic content without considering latent curing agent, whose ratio to epoxy resin was kept constant throughout the experiments.

Due to the high viscosity of the polymerizable phase, which is the continuous phase for the inverse miniemulsion, DLS measurements for the inverse miniemulsions were not feasible. Therefore, samples prepared with the different content of epoxy resin were monitored using DLS measurements only for the direct miniemulsions before polymerization. Figure 22 shows the DLS results. With a content of 50 wt% of epoxy, the inverse miniemulsion showed a phase separation right after ultrasonication; the continuous phase's viscosity was too high to enable a stable miniemulsion formation. Samples containing 45 and 40 wt% epoxy resin showed a broad droplet size distribution, extending to the micron sized range. With 35 wt% epoxy content a sudden shift in the particle distribution occurred, to significantly lower diameters with a mean diameter of 238 nm. Therefore, this was the epoxy content of choice in the polymerizable phase. Worth mentioning is that miniemulsification of high viscous phases is possible by increasing the temperature during homogenization. In our case, this technique was not feasible due to the presence of vinylic monomers, which may undergo evaporation or polymerization.

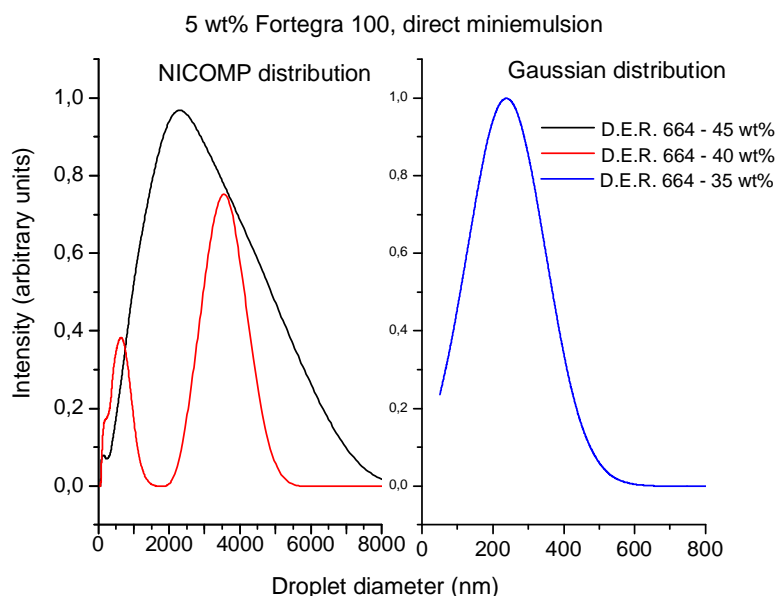


Figure 22 DLS measurements taken for direct miniemulsions, before polymerization for samples prepared using 5 wt% Fortegra 100 (to the aqueous dispersed phase), 4.43 wt% ALS-33 (to the oil dispersed phase, containing zinc phosphate), and a zinc phosphate loading of 1 wt% to the organic content. Samples were prepared with different D.E.R. 664 content. Measurements are based on volume weight droplet diameter distribution, either depending on NICOMP analysis (D.E.R. 664, 45 and 40 wt%) and Gaussian (D.E.R. 664, 35 wt%), depending on the χ^2 value.

4.1.3. Variation of Fortegra 100 content

The first variation done on the formulation was to test the effect of variation of Fortegra 100 with respect to the droplet size in the direct miniemulsion before polymerization. Typically in single miniemulsion systems, when the concentration of surfactant available at the oil/water interface in a direct miniemulsion is increased, the droplet size decreases due to an increased coverage at the interface¹¹⁶. Also, when two surfactants are present in single miniemulsion systems, one at the interface and one dissolved in the dispersed phase, as a template, for example, the latter was found to diffuse, being amphiphilic, and contribute to the droplet coverage, resulting also in a decrease in the droplet size¹¹⁷. Therefore, it was interesting to find out how would the change in the Fortegra 100 concentration change the droplet size in this unusual system. To find this out, five different concentrations were tried: 1.25, 2.5, 5, 7.5 and 10 wt% of Fortegra 100 with respect to dispersed phase. Unexpectedly, the droplet sizes of the direct miniemulsions

before polymerization showed an increase with an increase of the Fortegra 100 concentration, as shown in Figure 23.

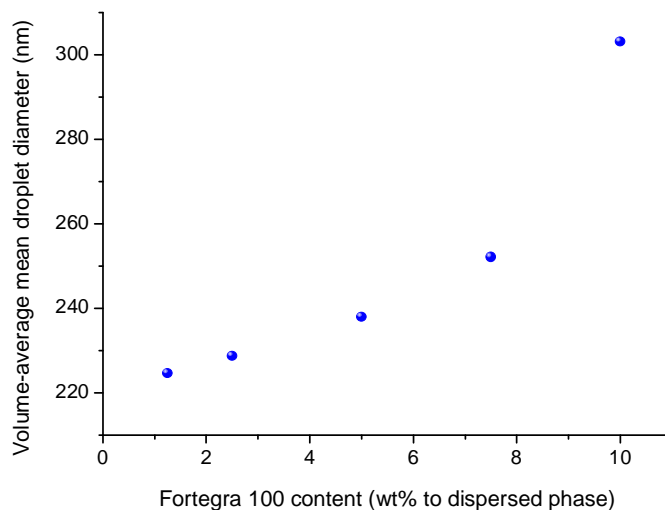


Figure 23 Effect of variation of Fortegra 100 in terms of the mean diameters of direct miniemulsions before polymerization, based on a volume weighted, Gaussian distribution. All samples were prepared with a 1 wt% zinc phosphate loading to the organic content.

4.1.4. Droplet stability and droplet scenarios

What does this imply about the system / Fortegra 100 preference? To be able to answer this, another substantial question arises: after the multiple miniemulsions, how does the droplet in the direct miniemulsion before polymerization look like? In a gedanken experiment, three possible scenarios are presented, as shown in Figure 24. Scenario A represents a w/o/w miniemulsion, where an inner water pool is retained within the monomer droplet, even after the formation of the second miniemulsification. There are two main reasons to deem this scenario highly improbable. The first reason is related to the high shear imposed on the system through ultrasonication. This high shear means that all droplets have undergone a second fission and fusion till steady state is reached. As such, it is highly unlikely that the “inner” water pools have remained intact throughout this process, but rather have reunited with the water in the continuous phase. Another reason why this scenario is improbable is related to the surfactant loading. As explained earlier, the surfactant levels in miniemulsions are generally much lower than those in microemulsions, leading to incomplete droplet coverage and significantly higher surface

tension values. This incomplete coverage therefore leads to the situation that the w/o/w system is also thermodynamically highly unfavorable due to the extra surface area that needs to be stabilized. In any case, for our synthetic purpose, the need for an inner water compartment is unnecessary once the target inorganic material has been formed (zinc phosphate, calcium carbonate or barium sulfate).

Now that the droplet contains no inner pool but has as constituents, zinc phosphate, Fortegra 100 and the polymerizable phase, two scenarios related to the w/o surfactant are left, either Fortegra 100 would diffuse to the oil/water interface (scenario B) or it would “interact” with the other droplet constituents and would situate itself inside the droplets primarily rather than being predominantly situated at the interface (scenario C). If scenario B did take place, then Fortegra 100 would increase the surfactant coverage of the droplet, and contribute besides ALS-33 to the droplet stabilization, which would lead to a decrease in droplet size of the dispersed phase. But in fact, the opposite did take place as shown by varying the Fortegra 100 concentration, illustrated by DLS measurement results in Figure 23. This signifies that Fortegra 100 is treated as a droplet constituent, favoring scenario C. One possible reason for this feature could be due to Fortegra 100 being an amphiphile block copolymer and an epoxy toughener, which contains one block as epoxy miscible while the other as epoxy immiscible, with an ability to self assemble in epoxy resins on the nanoscale¹¹⁴. It is not clear though if there are interactions between Fortegra 100 and the inorganic materials. This would highly depend on the inorganic material itself, its wetting properties, and its crystal structure.

Whether Fortegra 100 is solely inside the droplet or only predominantly inside the droplet with partial availability at the interface is at this point not clear. During coating applications via autodeposition, it will be affirmed that to a certain extent, Fortegra 100 is also available at the interface. Details on this result will be presented in the chapter dealing with zinc phosphate in corrosion testing.

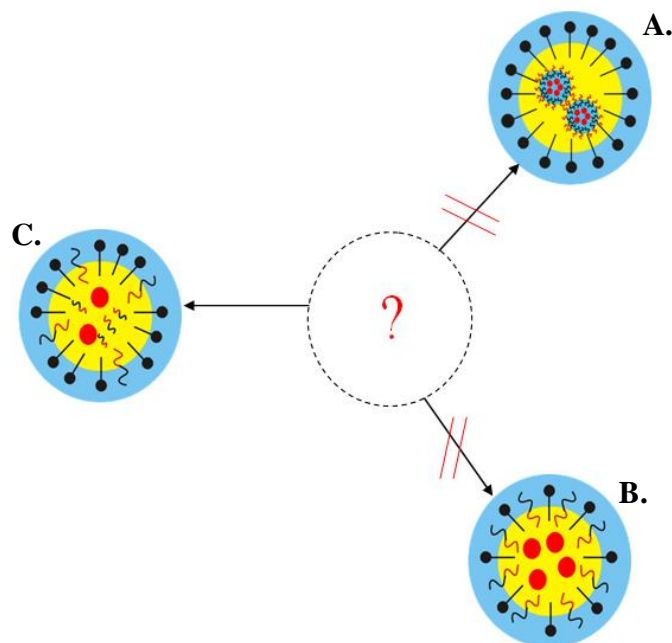


Figure 24 Possible scenarios of how the droplet of miniemulsion looks after transfer to a direct miniemulsion before polymerization. For discussion of the different scenarios, please refer to text.

4.1.5. Variation of radical polymerization temperature

To investigate if the polymerization can simply be carried out at a higher temperature and at relatively short time, which could also be favorable to induce hopeite formation, as previously shown, an experiment was carried out where two samples were prepared with 1 wt% zinc phosphate loading to the organic content and with a Fortegra 100 concentration of 5 and 10 wt%. The polymerization in this case was carried out for 3 h only at a temperature of 80 °C instead of 60 °C for about eighteen hours.

The DLS investigation of those samples showed a difference in the polydispersity of the miniemulsion. With the polymerization carried out at 60 °C for 18 h, a monomodal, somehow narrow droplet distribution was obtained, with mean droplet diameters of ~ 192 and 199 nm for the samples prepared with 5 and 10 wt%, respectively. The Gaussian distribution of χ^2 value was relatively small. In contrast, when polymerization was carried out at 80 °C for a duration of only 3 h, a broader distribution was obtained with higher χ^2 values. In this case, mean diameters of 103 nm and χ^2 of 25 were obtained for the sample prepared with 5 wt% Fortegra 100, while mean diameters of 88 nm and

$\sim 2 \mu\text{m}$ with a χ^2 value of 37 were obtained with that prepared with 10 wt%. The particle size distributions are shown in Figure 25. Therefore, for further samples, the polymerization conditions will be fixed at 60 °C during overnight.

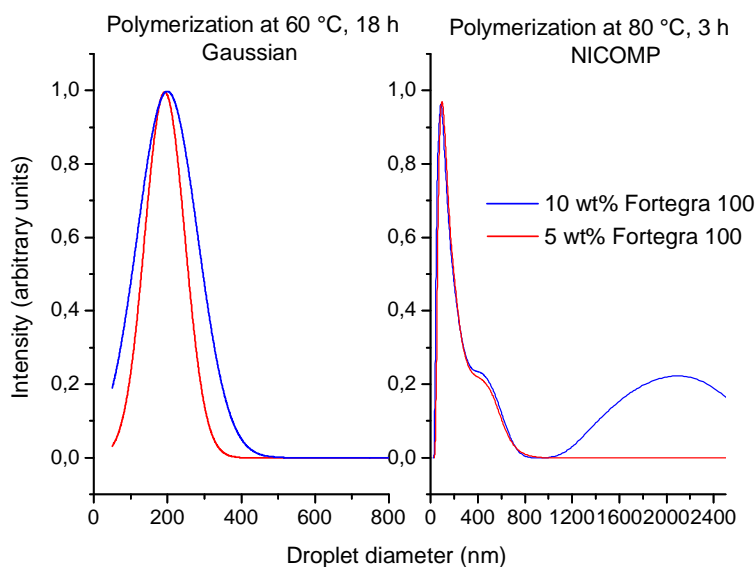


Figure 25 Volume weighted droplet diameters for the system containing 5 and 10 wt% Fortegra 100 polymerized at either 60 °C for 18 h or at 80 °C for 3 h. Left shows volume weighted Gaussian distribution. Right shows volume weighted NICOMP distribution, depending on the χ^2 value.

4.1.6. Variation of zinc phosphate loading

So far, only zinc phosphate has been tried out with a loading of 1 wt% to the organic content. In this section, samples with higher zinc phosphate loading, namely 2.5 and 5 wt% loading are prepared.

The two highest concentrations of Fortegra 100 were of interest, since their concentration in relation to the epoxy content lies in the recommended range for imparting toughening properties¹¹⁸. In other words, 7.5 wt% Fortegra 100 in ratio to the dispersed phase is equivalent to about 6.5 wt% to the epoxy content, while 10 wt% Fortegra 100 to the dispersed phase is equivalent to about 8.7 wt% to the epoxy content. On account of toughening properties, 10 wt% Fortegra 100 to the dispersed phase was used to prepare the samples with increased zinc phosphate loading.

DLS was used to investigate the samples in direct miniemulsion, before and after polymerization. The results show a monomodal distribution, relatively small χ^2 , except

for the sample prepared with 5 wt%, before polymerization. This sample shows a broad distribution, where the NICOMP distribution is a bimodal one. After polymerization, the system shows again the usual monomodality and a relatively acceptable χ^2 value. It has to be mentioned though, that during polymerization coagulation occurred. Excluding the values of the latter sample, the mean diameters for the samples before polymerization lie between 303 and 372 nm, while after polymerization, the mean diameters lie between 199 and 280 nm. The droplet diameters clearly increase with increasing zinc phosphate loading.

An elemental analysis for the samples was carried out using X-ray fluorescence (XRF). The results show that the higher the zinc phosphate loading, the more the loss in the zinc and phosphorous content (though more the former than the latter). For a loading of ~ 1 wt%, the XRF confirmed the presence of 100% of the zinc and phosphorous compared to the theoretical values. Also with a loading of 2.5 wt%, 100% of phosphorous was again achieved compared to theoretical value while only 75% of zinc was achieved. With increasing the loading to 5 wt%, more loss occurs in both phosphorus and zinc, only 75% and 53% are achieved, respectively. To confirm that this large deviation of the zinc values are not due a re-dispersible sedimentation, the miniemulsion was stirred for 2 days, freeze dried and re-analyzed. Results were same, in agreement also with the measured low content, which then confirms loss of zinc and phosphorus during polymerization in the form of slight coagulation.

DLS and XRF results are summarized in Table 7.

Results and discussion

Table 7 Result summary for the samples prepared with 10 wt% Fortegra 100 with zinc phosphate loading of 1 wt%, 2.5 wt% and 5 wt%. Results represent those obtained from DLS for direct miniemulsion before polymerization (AM) and after polymerization (AP). Elemental analysis was carried out using XRF for direct miniemulsions after polymerization.

	1 wt%	2.5 wt%	5 wt%
AM (mean droplet diameter, nm)	303 nm	372 nm	185 nm* 444 nm*
AP (mean droplet diameter, nm)	199 nm	240 nm	280 nm
Theoretical Zn content	0.2 wt%	0.4 wt%	0.75 wt%
Experimental Zn content (XRF)	0.2 wt%	0.3 wt%	0.4 wt%
% achieved	100%	75%	53%
Theoretical P content	0.1 wt%	0.2 wt%	0.4 wt%
Experimental P content (XRF)	0.1 wt%	0.2 wt%	0.3 wt%
% achieved	100%	100%	75%

* mean droplet diameters based on a NICOMP distribution

4.1.7. Variation of inorganic pigment and its loading

In the previous section, some stability problems occurred with higher loading of zinc phosphate. Therefore, it was decided to evaluate if this trend would occur also with 7.5 wt% Fortegra 100, which, as mentioned earlier, still is high enough to impart toughening properties to the epoxy system.

At this concentration of Fortegra 100, zinc phosphate samples were prepared at a loading of 2.5 wt% and 5 wt%. Additionally, at those same two loadings, calcium carbonate and barium sulfate were prepared to demonstrate the versatility of the synthetic process.

All direct miniemulsions were investigated by a DLS, both after miniemulsion formation by ultrasonication before polymerization and after polymerization. Results are summarized in Table 8. All mean droplet diameters lie between 280 and 390 nm for miniemulsion samples after ultrasonication, while for the samples after polymerization, mean particle diameters lay between 120 nm and 200 nm in the typical miniemulsion range. Comparing the DLS results for zinc phosphate with those prepared with 10 wt% Fortegra 100, it can be observed that even with a 5 wt% loading of zinc phosphate, a monomodal distribution of droplets were obtained (before polymerization) and

coagulation during polymerization was greatly reduced. This was a significant stability improvement, which was only possible with lowering Fortegra 100 content. Additionally, from DLS results, it is clear that all droplets shrink after polymerization due to the polymer formation and consequent increase in their density. However, it is unlikely that shrinking alone is responsible for these drastic particle size differences. Furthermore a clear trend between mean particle diameter and the pigment loading was not observed. Additional to the TEM (transmission electron microscopy) results described below these observations may indicate that interactions within these hybrid systems before, after and during polymerization are highly complex.

Table 8 Mean droplet diameters for the miniemulsions prepared with zinc phosphate (ZP), calcium carbonate (CC) and barium sulfate (BS), each with 2.5 wt% and 5 wt% loading (to organic content), before and after polymerization. Mean droplet diameters are given based on a volume weighted Gaussian distribution.

Sample	Mean droplet diameter, volume weighted (nm) AM*	Mean particle diameter, volume weighted (nm) AP**
ZP-5	370	203
ZP-2.5	393	161
CC-5	348	123
CC-2.5	352	124
BS-5	303	157
BS-2.5	282	175

*AM: after miniemulsion formation and before polymerization, **AP: after polymerization.

Elemental analysis was used to investigate the samples and was performed through both XRF and inductively coupled plasma-optical emission spectroscopy (ICP-OES) measurements. Table 9 displays the obtained results for the different nanopigment loadings from both methods. Oxygen (in phosphate, carbonate and sulfate), carbon (in carbonate), and sulfur (in sulfate) were not measured. In the case of the former two elements, it would have been hard to differentiate them from the organic O and C, while in the case of sulfur, sulfur content from the surfactant ALS-33 and from the initiator

KPS, outweigh the sulfur from barium sulfate. Additionally, SDS (sodium dodecyl sulfate) was used in sample preparation of the ICP-OES experiments.

The first observation to be made is that the zinc and phosphorus content was increased compared to the samples prepared earlier with 10 wt% Fortegra 100. This was another indication of the increased stability obtained in the system with a decrease in the Fortegra 100 content. There are mainly two trends throughout the results. One trend can be seen by comparing the values obtained through the different method for the same sample. In all samples, the values obtained via XRF analysis are higher than those obtained by ICP-OES analysis, for a given sample. This can be assigned to the mechanism of analysis of each method. In XRF, the samples analyzed are submitted in a freeze-dried form and would represent an average of the element in question available in the analyzed fraction of the sample. In ICP-OES, dilution of the sample takes place, which may affect the stability of the miniemulsion. Moreover, in ICP-OES, the elements detected are only those that reach the plasma flame. In other words, any sediment particles or heavy particles may not altogether reach the plasma flame to be analyzed. The other trend that can be observed in Table 9 is that with increasing the loading of a given inorganic material, the percentage achieved from the theoretical value decreases. This may be assigned to stability of the miniemulsion, where stability of the system seems to be affected with higher loadings and where a small amount of coagulum was found after polymerization. One more observation from the table is that different inorganic materials lead to different values remaining in the system, i.e. different stabilities of the miniemulsion. This can be considered as another indication that the interactions within the described hybrid systems are very complex.

Results and discussion

Table 9 Summary of elemental analysis results for the various samples. Analyses were carried out via XRF and ICP-OES measurements.

ZINC PHOSPHATE, 2.5%						
	Zn theoretical	Zn experimental	% achieved	P theoretical	P experimental	% achieved
XRF	0.4%	0.4%	100%	0.2%	0.2%	100%
ICP	19.3 mg/l	11.6 mg/l	60%	9.55 mg/l	7.2 mg/l	75.4%
ZINC PHOSPHATE, 5%						
	Zn theoretical	Zn experimental	% achieved	P theoretical	P experimental	% achieved
XRF	0.8%	0.5%	62.5%	0.5%	0.4%	80%
ICP	37.45 mg/l	13.2 mg/l	35.2%	18.75 mg/l	9.84 mg/l	52.5%
CALCIUM CARBONATE, 2.5%						
	Ca theoretical	Ca experimental	% achieved	-	-	-
XRF	0.45%	0.3%	66.7%	-	-	-
ICP	22.8 mg/l	13.0 mg/l	57%	-	-	-
CALCIUM CARBONATE, 5%						
	Ca theoretical	Ca experimental	% achieved	-	-	-
XRF	0.9%	0.3%	33.3%	-	-	-
ICP	44.7 mg/l	10.4 mg/l	23.2%	-	-	-
BARIUM SULFATE, 2.5%						
	Ba theoretical	Ba experimental	% achieved	-	-	-
XRF	0.7%	0.6%	85.7%	-	-	-
ICP	33.8 mg/l	21.9 mg/l	65.9%	-	-	-
BARIUM SULFATE, 5%						
	Ba theoretical	Ba experimental	% achieved	-	-	-
XRF	1.35%	0.9%	66.7%	-	-	-
ICP	67.75 mg/l	33.6 mg/l	49.6 %	-	-	-

4.1.8. Electron microscopy samples' investigation

Transmission electron microscopy (TEM) and scanning electron microscopy (SEM) were used to investigate different samples, but also in-situ energy dispersive X-ray (EDX) analysis was carried out to confirm the presence of the target elements. Moreover, electron diffraction in TEM was also used to confirm the crystallinity of the inorganic particles.

One of the earliest investigations carried out was for the inverse miniemulsion containing zinc phosphate in the dispersed phase and polymerizable phase as the continuous phase,

in an attempt to understand the structures already at an early step of particle formation. The investigation was carried out using SEM for a sample containing 5 wt% of Fortegra 100 with respect to the dispersed phase and a zinc phosphate loading of 1 wt% to the organic content, as shown in Figure 26 a), b) and c). The images show an interesting coral-like structure with a random grouping of white particulates. In-situ inspection of the white particulates using EDX (energy dispersive X-ray analysis) confirm the presence of zinc and phosphorous in those areas and the absence of zinc and phosphorus elsewhere through out the coral-like structure.

How can this coral-like structure be explained? First, we need to consider what components of the system are available here. For sure, zinc and phosphorus have been proven by EDX. But for the polymerizable continuous phase, it is expected that all the monomers have been evaporated during the sample preparation and also due to the high vacuum of the microscope. Thus what is left are Fortegra 100 and epoxy resin (both being polymers), as well as latent epoxy curing agent. In the work done by Thompson et al.¹¹⁹ a similar textured epoxy was also reported and imaged by SEM (image shown in Figure 26 d)). This work also belongs to the group of work done by Bates in toughening epoxy resins using block copolymers, the same group that patented the use of amphiphilic copolymer toughened epoxy resins with Dow¹¹⁴, the producer of Fortegra 100. In this work done by Thompson et al., the block copolymer used is poly(ethylene oxide)-*b*-poly(ethylene-*alt*-propylene), i.e. the most probable structure belonging to Fortegra 100, as shown in Table 5 in section 4.1.2.5 “*Choice of nonionic surfactant for inverse miniemulsions*”. In their work, the epoxy resin used, though, is D.E.R. 332, still based on BADGE, but a liquid one, with a lower EEW value (171 – 175 g/eq.). The loading used in their study was 5 wt% of block copolymer w.r.to epoxy resin. This is also similar to our sample here, since 5 wt% Fortegra 100 to dispersed phase = ~ 4.1 wt% to D.E.R. 664. Thompson et al.¹¹⁹ explain that these structures are possible due to self assembly of the block copolymers: one block being epoxy miscible (referred to as “epoxy-philic” block), namely the poly(ethylene oxide) block, while the other block is epoxy immiscible (referred to as “epoxy-phobic” block), namely the poly(ethylene-*alt*-propylene) block. Consequently, the block copolymer self assembles in the epoxy matrix forming structures. Though, in our system, a different relation of “epoxy-philic” and “epoxy-phobic” could

be obtained since in the presence of water, the PEO block may “prefer” to be in the water rather than the epoxy continuous phase, therefore, sterically stabilizing the inverse miniemulsion against collision.

Some important observations can be made from the images shown in Figure 26 a) to c): 1) the zinc phosphate particulates are gathered in bundles. This could be a representation of the aqueous droplets in the inverse miniemulsion; 2) those dried “droplets” seem to have a dimension of about 50 μm , which is much larger than typical miniemulsion droplet sizes and can be assigned to drying effects.

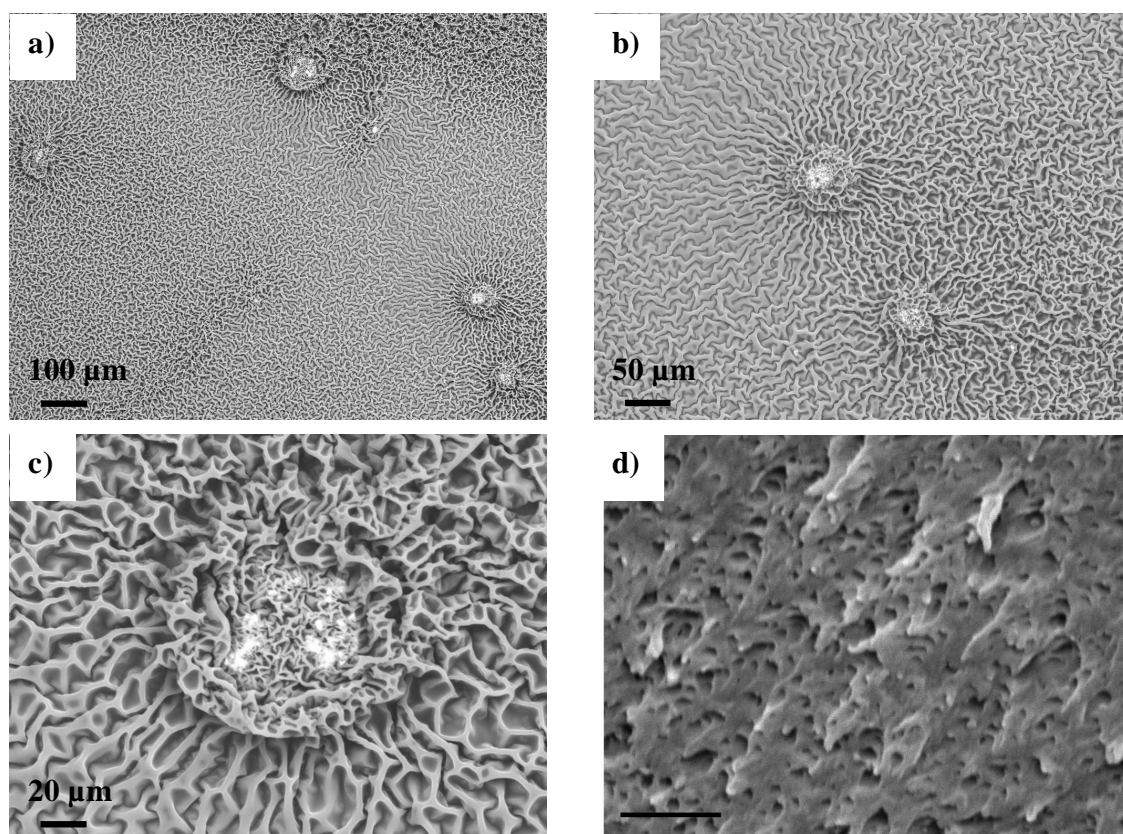


Figure 26 a) to c)ⁱ SEM images for zinc phosphate inverse miniemulsion prepared with 5wt% Fortegra 100 (to the dispersed phase, equivalent to 4.1 wt% to epoxy resin) and a zinc phosphate loading of 1 wt% (to the organic content). d) SEM image of epoxy resin modified with 5 wt% of (PE-*alt*-P)-*b*-PEO, in ratio to epoxy resin. Micrograph taken from Thompson et al.¹¹⁹. Scale of the given bar is 500 nm.

ⁱ SEM images taken with Philips XL30 with an acceleration voltage of 20 kV. Samples were sputtered with gold before imaging and were investigated undiluted.

Samples were also investigated after polymerization using TEM. As mentioned earlier, the samples were preferably prepared with a high concentration of Fortegra 100 in order to provide toughening properties to the epoxy resin. In an initial investigation, TEM was used to inspect the samples prepared with 10 wt% Fortegra 100.

The examination of the TEM sample prepared with 1 wt% zinc phosphate almost showed no presence of zinc phosphate. This was assigned to the very low zinc phosphate concentration which made it difficult to locate them. Samples prepared with higher zinc phosphate concentrations showed zinc phosphate particulates, as shown in Figure 27 a) and b) for 2.5 wt% zinc phosphate loading, and c) and d) for 5 wt% zinc phosphate loading. In all samples, zinc phosphate particulates (dark regions) are shown to be covering or lying on the polymeric particles (brighter, bigger particles). It is worth noting that some particles also did not contain any zinc phosphate particles.

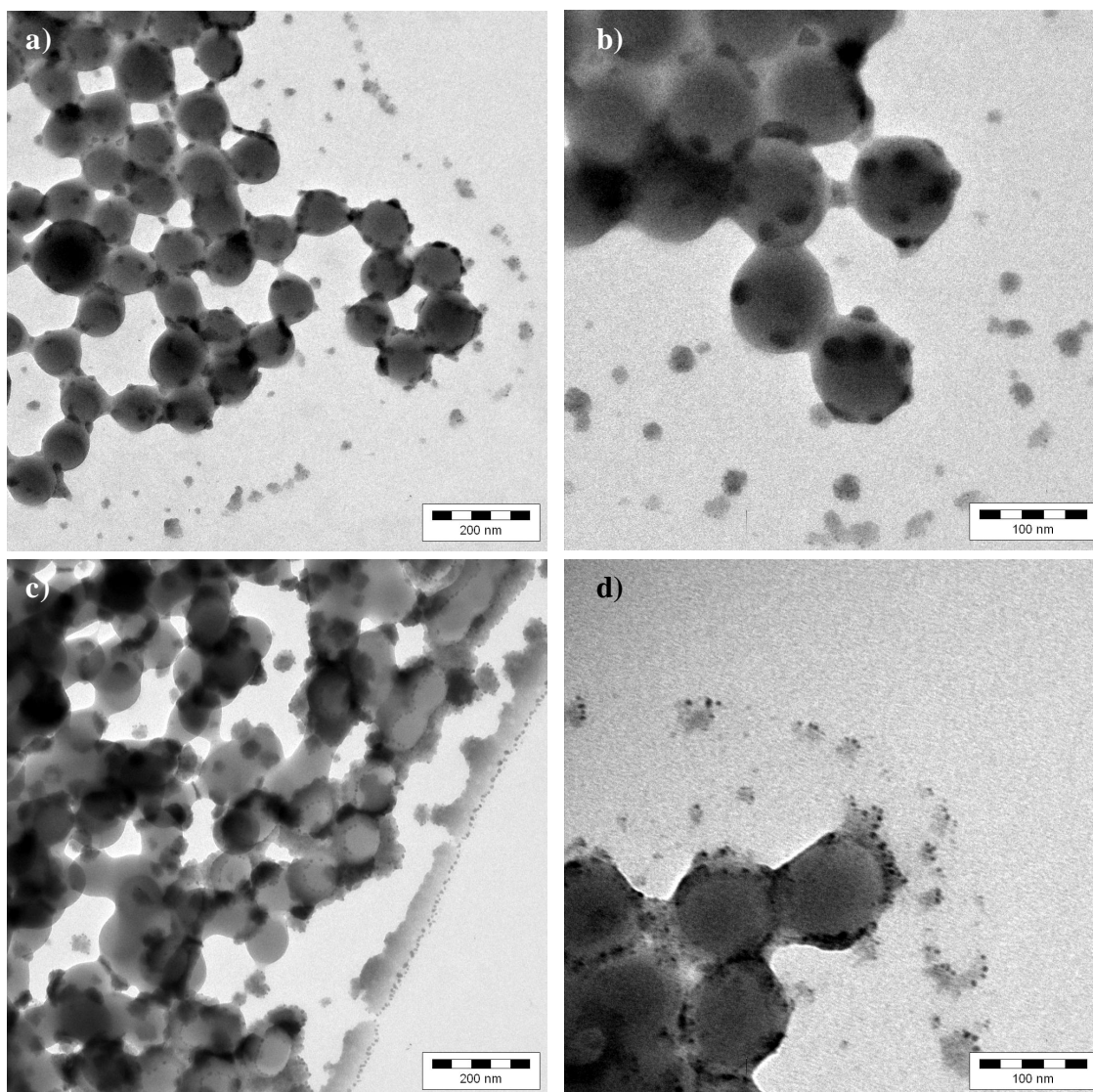


Figure 27 TEMⁱⁱ images taken for the sample prepared with 10 wt% Fortegra 100 and a zinc phosphate loading of: a) and b) 2.5 wt% to organic content; c) and d) 5 wt% to organic content. Images are taken for the sample as a direct miniemulsion after polymerization.

As aforesaid, using 10 wt% of Fortegra 100 was not ideal in terms of stability, especially with a zinc phosphate loading of 5 wt%. Further samples were prepared using 7.5 wt% Fortegra 100: zinc phosphate, calcium carbonate, or barium sulfate, each with a loading of 2.5 wt% and 5 wt%. TEM images for those samples are shown in Figure 28.

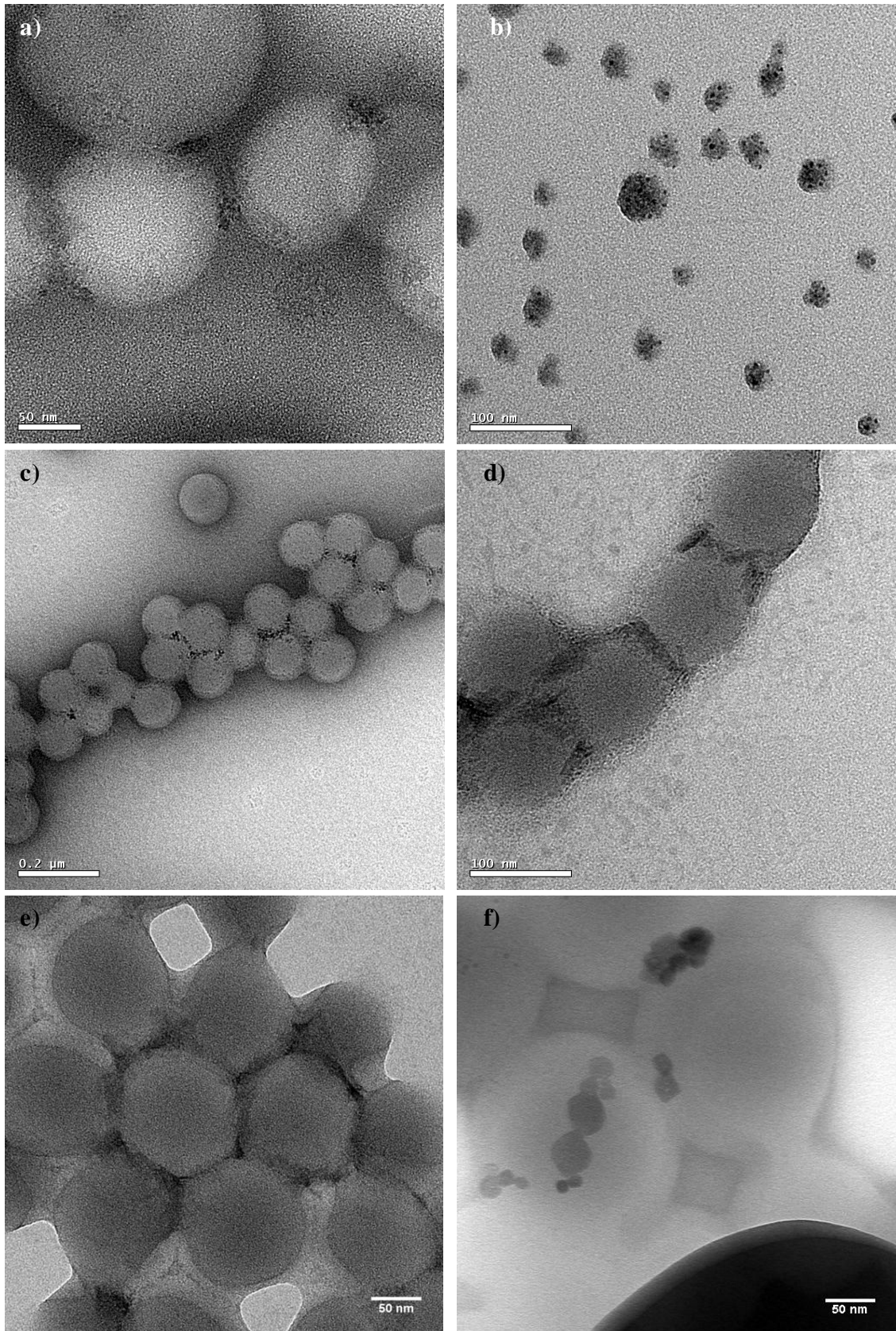
ⁱⁱ TEM images taken using Philips CM12, with an accelerating voltage of 120 kV. Samples were diluted and placed on a Formvar coated copper grids.

For zinc phosphate, the morphology shown is same as that for samples prepared with 10 wt% Fortegra 100: zinc phosphate particulates onto polymeric particles (Figure 28 a) and b) for 2.5 wt% and 5 wt% loading, respectively.

For calcium carbonate, the morphology looks slightly different: the polymeric particles are still spherical, but the calcium carbonate particles seem to have a preference to interparticle interface. Another observation is related to crystallinity. Figure 28 c) and d) are two images taken from the same sample, that with 2.5 wt% calcium carbonate. Image d) show a rather anisotropic shape, which is not the case in image c). This was the first indication that calcium carbonate could be present in both crystalline and amorphous phase. Image Figure 28 e) illustrates an example of particles prepared with 5 wt% calcium carbonate.

Figure 28 f) and g) show images for barium sulfate samples with a loading of 2.5 wt% and 5 wt%, respectively. Again, a different morphology of the inorganic particulates is shown here. The barium sulfate particulates seem to form an aggregate at only one area of the polymeric particles, even more clearly with the higher loading, image g). Image h) is an HR-TEM (high resolution TEM) that shows the crystal planes of barium sulfate, thus proving its crystallinity.

One important observation from comparing all images shown in Figure 28, is that each inorganic pigment adopts a different morphology with respect to the polymeric particle. This could again be another indication of the different and complex interactions between the inorganic pigments and the polymeric particles, which may include, for example, wetting properties. Also it is worth mentioning that in all samples bare polymeric particles could be found.



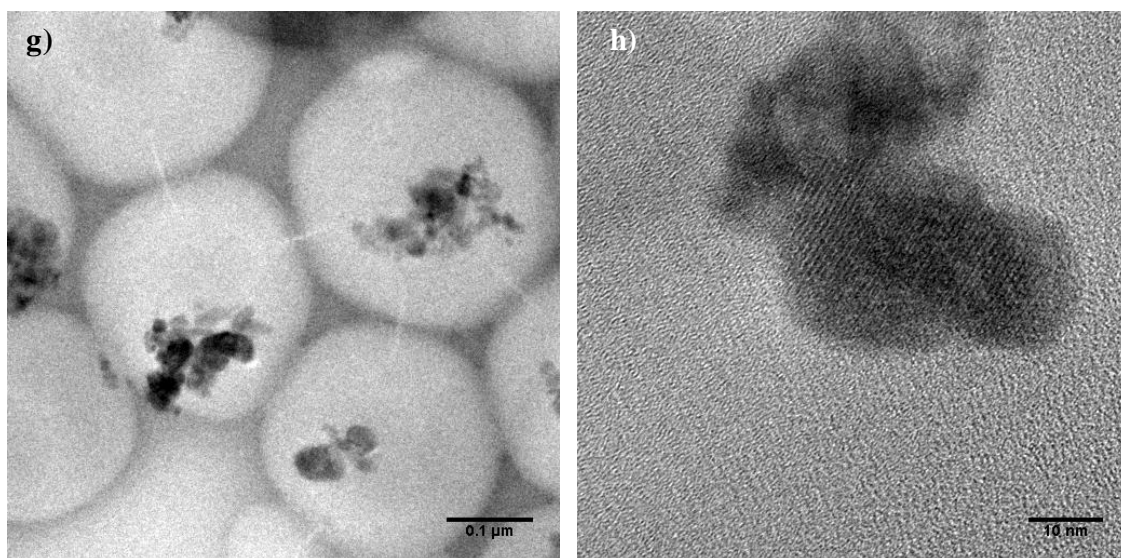


Figure 28 TEM imagesⁱⁱⁱ taken for samples prepared with: a) 2.5 wt% zinc phosphate, b) 5 wt% zinc phosphate, c) and d) 2.5 wt% calcium carbonate, e) 5 wt% calcium carbonate, f) 2.5 wt% barium sulfate and g) and h) 5 wt% barium sulfate. All samples were prepared with 7.5 wt% Fortegra 100 and investigated after polymerization.

It was clear already from the TEM images of barium sulfate that it was crystalline – barite phase, the only crystal structure of barium sulfate⁹². In case of zinc phosphate and calcium carbonate, electron diffraction was carried out in-situ during TEM investigation to determine their crystallinity. Electron diffraction patterns and their corresponding intensity profiles for both pigments are shown in Figure 29. For zinc phosphate, the electron diffraction pattern exhibits spots, which signify that it is crystalline or at least that crystalline regions are present. This can also be inferred from the corresponding intensity profile that shows few peaks (Figure 29 a) and c)). Unfortunately, due to the relatively low loading compared to the available organic material, a very low signal was obtained and therefore made it hard to determine a crystal structure from the few peaks shown in the intensity profile.

Calcium carbonate, besides its amorphous form, has three anhydrous polymorphs: calcite, aragonite and vaterite. The latter polymorph is metastable and would transform to calcite and aragonite in aqueous medium¹²⁰. Electron diffraction pattern show few faint spots, which may indicate a predominantly amorphous structure. This also fits the

ⁱⁱⁱ TEM images taken using Tecnai F20 (Fei) with an accelerating voltage of 200 kV. Samples were diluted and added to carbon coated copper grid.

corresponding intensity profile which shows no peaks (Figure 29 b) and d)) but observations made earlier from TEM showed crystalline and amorphous structures.

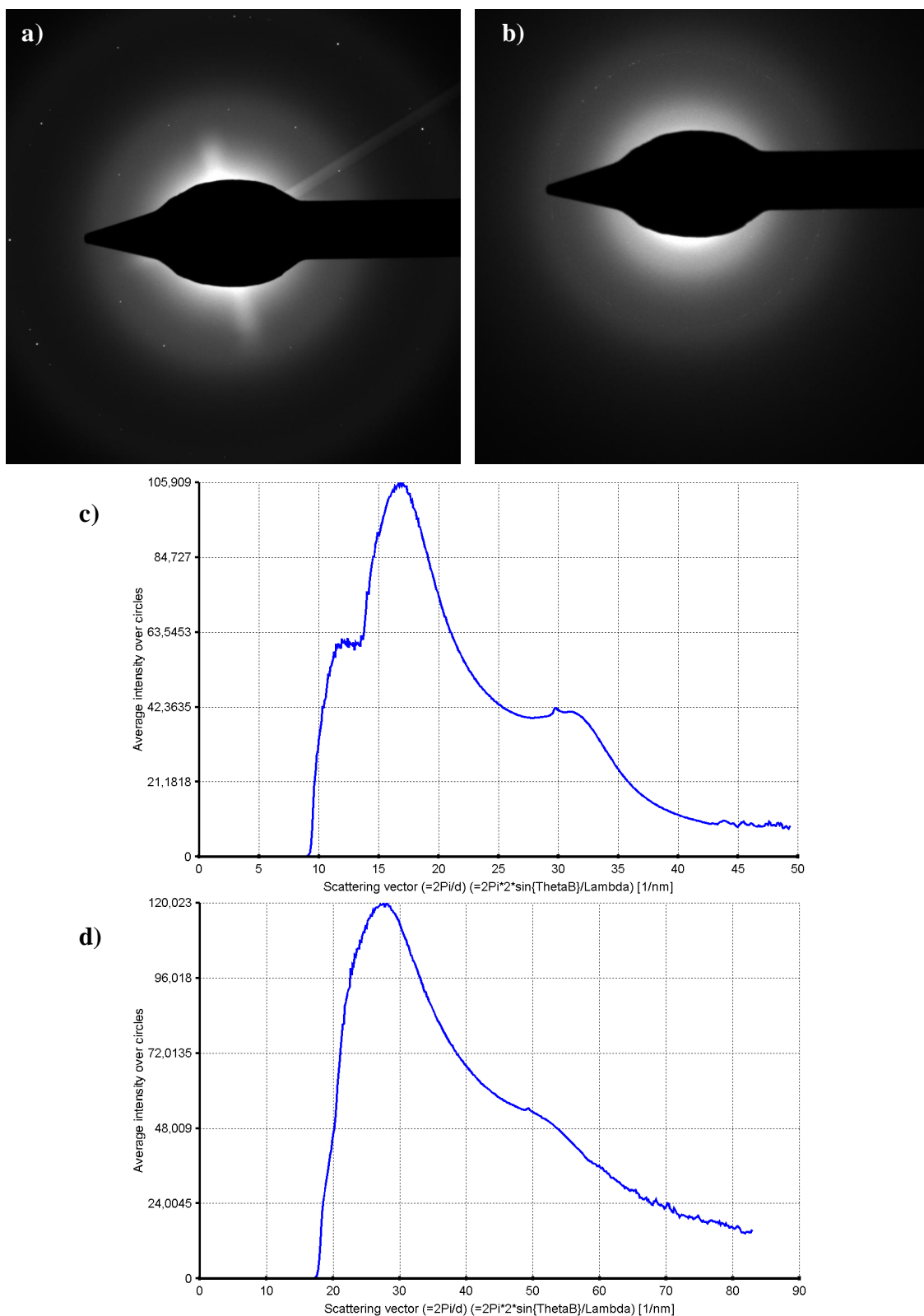


Figure 29 Electron diffraction patterns for samples prepared with: a) 5 wt% zinc phosphate loading and b) 5 wt% calcium carbonate and their corresponding intensity profiles in c) and d), respectively.

4.2. Testing of zinc phosphate - polymer miniemulsion as corrosion protection coating

4.2.1. Objective

In this chapter, the direct miniemulsions prepared earlier containing zinc phosphate were used to coat steel panels via the autodeposition process and tested against corrosion using neutral salt spray tests for 21 days. In total, three salt spray tests were carried out, each time with a formulation modification. Formulation adjustments would only be mentioned briefly, highlighting the main changes and their aim.

4.2.2. General procedures and guidelines

For all three tests carried out, there was a unified testing method used, which will be outlined here.

- **Choice of substrate:**

In our work, cold rolled steel was used as the substrate for all corrosion testing. One reason is that cold rolled steel is mainly used for the car body, typically with a thickness of 0.5 to 1.5 mm¹²¹. Another reason related to the corrosion is that cold rolled steel suffers more internal stresses than hot rolled steel, and is therefore more vulnerable to corrosion³¹.

- **HF Stability test:**

As mentioned earlier in the theoretical background section, HF is used as one of the main autodeposition bath constituents that would lead to the release of iron ions from steel substrate. Generally, the presence of H⁺ ions may affect the stability of the anionically stabilized miniemulsions. Therefore, under those conditions, the used miniemulsion should be stable so that coating would only be triggered upon the insertion of the substrate. The stability of the miniemulsion was determined with a Lineguard 101 meter. More details on measurements can be found in the theoretical background section.

All samples were checked for stability against HF before carrying out autodeposition and all samples were found to be HF stable (at the given bath concentration).

- **Autodeposition tests:**

In a typical autodeposition process a total of 8 steps take place³⁹:

Step 1: Alkaline spray clean;

Step 2: Alkaline immersion clean;

Step 3: Tap water rinse;

Step 4: DI water rinse;

Step 5: Autodeposition coating;

Step 6: Tap water rinse;

Step 7: Reaction rinse;

Step 8: Curing.

Three of the above mentioned steps are of concern to this coating procedure: step 5, the autodeposition coating, step 7, the reaction rinse and step 8, the curing. Details on the individual steps are given in theoretical background section.

This process was also modified to serve our testing purpose. All miniemulsion samples that were prepared were used to prepare the autodeposition coatings bath. If the miniemulsion used contained zinc phosphate, no reaction rinse was used (step 7), but rather a deionized water rinse at 60 °C was used. Reason for this 60 °C bath will be explained hereunder.

Control samples that were prepared without any zinc phosphate samples were either prepared without a reaction rinse but with a 60 °C deionized water rinse, to serve as a blank control. Or, they were prepared with a reaction rinse to serve as a comparison to current anticorrosion protection systems currently used in industry.

Typically, the dipping time in each bath is about 2 min. For the autodeposition bath, the coating time for control samples were also 2 min. Dipping time for all other samples was adjusted to result in same film thickness.

In all experiments, curing was carried out at 180 °C for about 30 - 40 min.

- **Salt spray tests:**

Salt spray tests were carried out according to DIN EN ISO 9227 NSS. Test conditions of salt spray tests are outlined in the theoretical background.

Corrosion was evaluated according to DIN EN ISO 4628-8 in terms of corrosion propagation and delamination of the coatings film, both evaluated along the scribe, as well as according to DIN EN ISO 4628-2 in terms of degree of blistering. The degree of blistering is given using the nomenclature used in DIN EN ISO 4628-2 typically: X(SY),

where X refers to the quantity of blisters and Y refers to the size of the blisters according to the standards defined in DIN EN ISO 4628-2.

Typically, salt spray tests are carried out for 21 days. In this work, we have devised a modification to serve judging corrosion already at an early stage. Instead of the typical single scribe made in the coatings film, two were made. Salt spray test was carried out at first for 10 days where both scribes are exposed to salt spray. After those 10 days, one of the scribes was covered with a transparent adhesive tape and served as a reference to how corrosion took place for first 10 days. The sample is placed again in salt spray chamber for further 11 days where only the second scribe in this case is exposed to salt spray, making up a total of 21 days of exposure but only for one of the scribes.

- **First autodeposition coating ever from hybrid inorganic-polymer miniemulsions – adjusting coatings process' parameters:**

Two samples were used to coat steel panels: a sample prepared with 10 wt% Fortegra 100 and a zinc phosphate loading of 2.5 wt% to the organic content, as well as a control sample prepared with no zinc phosphate and no Fortegra 100. The latter was prepared using the same polymerizable phase used, containing also latent curing agent, but was prepared using a single step direct miniemulsion, followed by polymerization.

Carrying out autodeposition from the sample containing 2.5 wt% zinc phosphate was successful and is thus considered, to our knowledge, as first autodeposition coating process ever to be carried out from hybrid inorganic-polymer miniemulsions.

On a first trial (autodeposition set 1), both samples were used to coat steel panels, by using only the prepared miniemulsion in the autodeposition bath followed by tap water rinse and curing (step 5, 6 and 8, with complete elimination of step 7). The two panels coated as such are shown in Figure 30 a) and b) for the control and zinc phosphate containing sample, respectively.

On the second trial (autodeposition set 2), both samples were again used with replacing step 7 by a 60 °C deionized water bath. Photos of those panels are shown in Figure 30 c) and d) for the control and zinc phosphate containing sample, respectively.

- Autodeposition set 1: Elimination of step 7 (reaction rinse)

There are two significant observations that could be made from the pictures:

- 1) Film appearance: in the case of the control sample (Figure 30 a), the picture shows that no film was formed but rather rough appearance could be seen. In the case of sample containing zinc phosphate and Fortegra 100, a film formation could be seen, though not of a homogeneous appearance (see red arrows, Figure 30 b). Having a film formed under those conditions indicates that the sample containing zinc phosphate and Fortegra 100 has a minimum film forming temperature lower than that of the control sample.
 - 2) Film thickness: Both metal panels were dipped in the autodeposition bath for 2 min. For the control sample, the film thickness was 13 – 14 μm while for the sample containing zinc phosphate and Fortegra 100 the film thickness was found to be 6 – 7 μm . Only half the destabilized polymer was deposited when the sample contained zinc phosphate and Fortegra 100. This signifies an increased stability for the sample containing zinc phosphate and Fortegra 100, which leads to a more difficult destabilization. One very possible explanation, which will be proven with further tests, is that indeed Fortegra 100 does lie at the water / polymer interface increasing particle stability against the increased ionic strength of the bath. Previously, we have shown through DLS analysis that with increased Fortegra 100 content, an increase in mean droplet diameter also occurred. This information, together with lower film thickness proves that Fortegra 100 lies predominantly inside the droplet (hence the increased mean droplet diameter) but not entirely. The portion that lies at the particle interface is thus responsible for the increased stability.
- Autodeposition set 2: Step 7 replaced by DI water at 60 °C
 - 1) Film appearance: in this set, both samples (Figure 30 c and d) show film formation on the metal panels. The control sample film looks homogeneous while the sample prepared with zinc phosphate and Fortegra 100 again shows regions of inhomogeneity (see red arrows in Figure 30 d).
 - 2) Film thickness: in this set, the time of dipping of the metal panels was adjusted so that both resulted in a film thickness of 6-8 μm .

For the sake of process standardization, all samples from that point on were prepared using 60 °C deionized water instead of step 7, unless step 7 was used to prepare a control with reaction rinse.

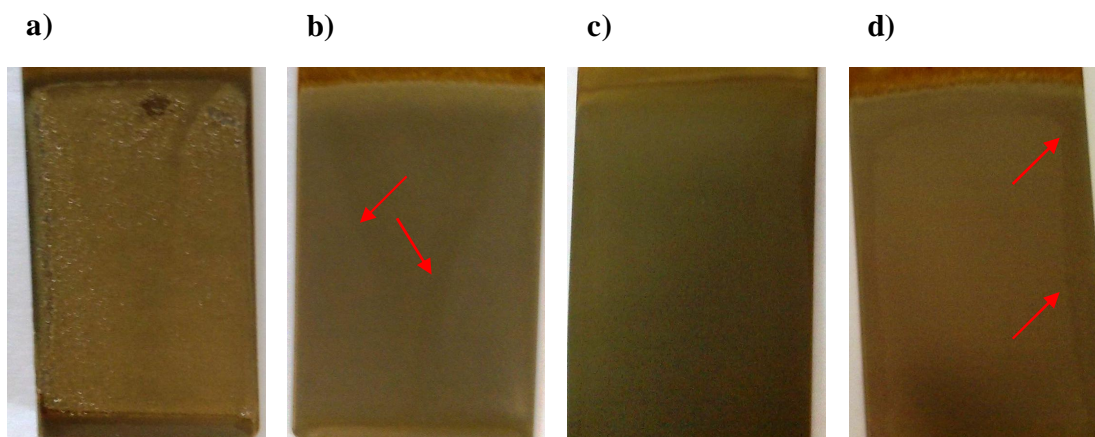


Figure 30 Metal panels autodeposited with:

- a) control sample. Panel not dipped in 60 °C deionized water bath; film thickness: 13 – 14 μm .
 - b) sample prepared with 2.5 wt% zinc phosphate loading and 10 wt% Fortegra 100. Panel not dipped in 60 °C deionized water bath; film thickness: 6 – 7 μm .
 - c) same sample as in a) but panel was dipped in 60 °C deionized water bath after autodeposition; film thickness: 6 – 8 μm .
 - d) same sample as in b) but panel was dipped in 60 °C deionized water bath after autodeposition; film thickness: 6 – 8 μm .
- Red arrows point to regions of inhomogeneities in the films formed.

One important remark on the autodeposition bath carried out using the zinc phosphate containing sample is that it showed some signs of bath instability. An instability in this case does not refer to an interaction with HF but rather the formation of flocculates in the bath over time. This is a plausible reason why the films prepared from this sample show inhomogeneity (Figure 30 b) and d)).

Several samples were then tested to check if also flocculation would occur within the coatings bath: samples prepared with 10 wt% Fortegra 100 (1 wt%, 2.5 wt% and 5 wt% zinc phosphate loading) and samples prepared with 7.5 wt% Fortegra 100 (2.5 wt% and 5 wt% zinc phosphate loading). Of all those samples, two samples showed less flocculation formation in the coating bath:

- the sample prepared with 10 wt% Fortegra 100 and a loading of 1 wt% zinc phosphate, and

- the sample prepared with 7.5 wt% Fortegra 100 and a loading of 2.5 wt% zinc phosphate.

For this reason, for the first salt spray testing run, the sample prepared with 7.5 wt% Fortegra 100 was used, since it carried a higher zinc phosphate loading and also showed acceptable autodeposition bath stability.

4.2.3. First salt spray testing run

The samples used for the coating and the corresponding coating process, whether treated with reaction rinse or only with DI water bath, are shown in Table 10. Basically, three samples have been tested:

- 1) A control sample containing no zinc phosphate was prepared with the same polymerizable phase via a single direct miniemulsion step, post-dipped in 60 °C deionized water bath at step 7. This serves as a blank control sample (sample 1 and 2).
- 2) Control sample was prepared as above mentioned, but post-dipped in reaction rinse. This serves as a comparison to current anti-corrosion protection system (sample 3 and 4).
- 3) Sample was prepared with the 7.5 wt% Fortegra 100 and 2.5 wt% zinc phosphate with post-dipping the panels in 60 °C deionized water bath at step 7 (sample 5 and 6).

Two metal panels were prepared for each of the above samples in order to check for reproducibility of results.

Table 10 Samples prepared for the first salt spray testing run, their respective constituents and coating process.

Sample	Constituents	Coating process
Sample 1 & 2	Control sample containing no zinc phosphate or Fortegra 100	Step 7: 60 °C deionized water
Sample 3 & 4	Control sample containing no zinc phosphate or Fortegra 100	Step 7: reaction rinse
Sample 5 & 6	Sample prepared with 7.5 wt% Fortegra 100 and 2.5 wt% zinc phosphate loading	Step 7: 60 °C deionized water

Figure 31 shows a picture of the 6 metal panels after 21 days of salt spray test. The scratch shown on the left which is covered with transparent adhesive tape corresponds to results after 10 days, as previously explained.

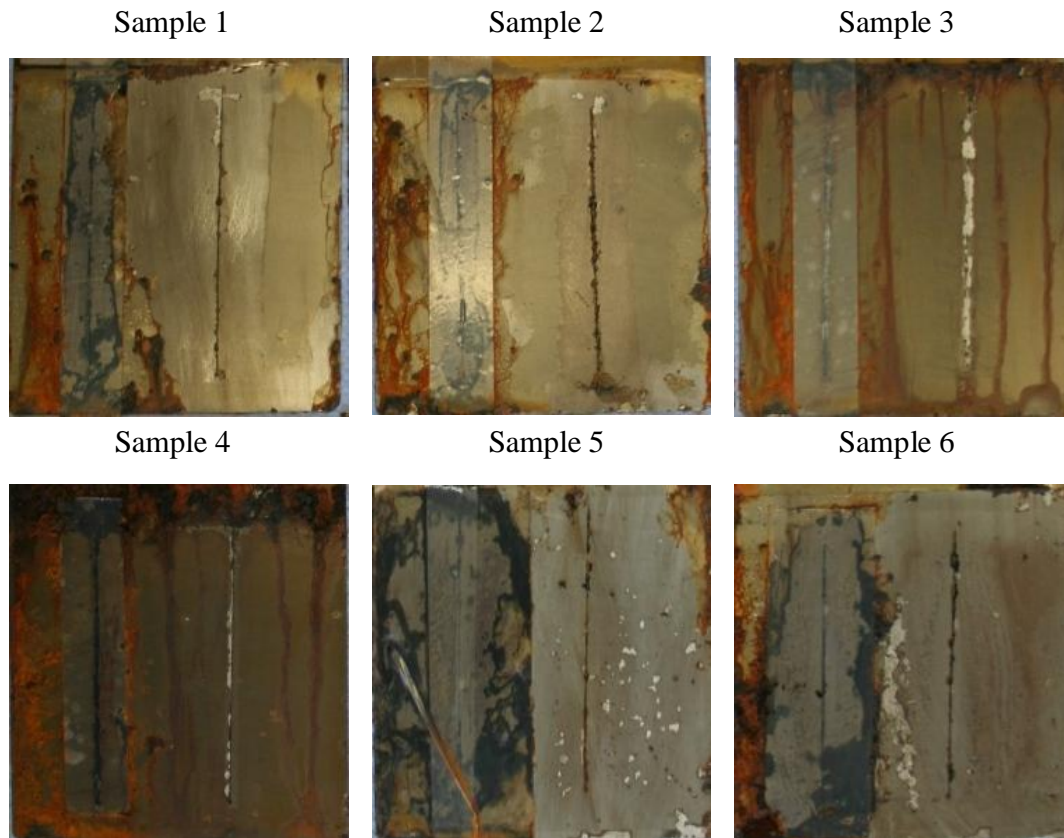


Figure 31 Cold rolled steel panels coated via autodeposition with the miniemulsion samples as follows: top left and middle: blank control sample (sample 1 & 2), top right & bottom left: control treated with reaction rinse (sample 3 & 4), bottom middle & right: sample prepared with 7.5 wt% Fortegra 100 and 2.5 wt% zinc phosphate loading (sample 5 & 6). For each panel, scratch on right shows corrosion propagation after 10 days and that on left shows corrosion propagation after 21 days.

Table 11 shows the results of the salt spray test after 10 and 21 days in terms of propagation of corrosion along the pre-made scribe (in mm), the film delamination also along scribe (in mm) and the degree of blistering, as well as, the film thickness of each sample.

A first remark on the data shown in Table 11 is that the values obtained from the panel pairs of each sample are somehow similar, though not the same – which is still acceptable. According to the corrosion propagation results after 10 days, sample 5 and 6 (zinc phosphate containing sample) show a similar corrosion propagation to the blank control

sample (sample 1 and 2), both showing lower corrosion propagation than the control prepared with reaction rinse (sample 3 and 4). This was quite surprising, till the values after 21 days were obtained. Corrosion propagation for the blank control sample and zinc phosphate containing samples (samples 1 and 2; samples 5 and 6) show almost double the values after further 11 days of exposure, while the sample treated with reaction rinse show almost no change in corrosion propagation after the same exposure time. The values of the latter though were still higher than the other two samples.

There are still two critical points for corrosion evaluation: delamination and degree of blistering, both are also an indication of corrosion, as explained in the theoretical background.

As for the degree of blistering, the sample containing the zinc phosphate and Fortegra 100 shows the most blistering coverage (quantity is represented by the first number) though the size of the blisters are all in the same range (represented by the number in brackets). This same sample set (5 and 6) show complete delamination after 21 days of the salt spray exposure, which is a sign of poor wet adhesion. One highly probable explanation for this is the presence of Fortegra 100 in a high concentration. In a study made by Charneau et al.¹²², an investigation of latex film adhesion was made on glass and poly(ethylene terephthalate) films, using different latex films and different surfactants. One of the main results was that surfactants were always available at the loci of failure.

Results and discussion

Table 11 Results for the first salt spray testing run in terms of corrosion propagation and delamination along the scribe, as well as degree of blistering after 10 days and after 21 days. Film thickness is also given for each sample.

Sample	Film thickness (μm)	Evaluated after	Corrosion propagation* (mm)	Delamination* (mm)	Degree of blistering**
Sample 1	11	10 days	0.2	7.3	2(S3-S5)
		21 days	0.3	14.2	1(S3-S5)
Sample 2	9	10 days	0.3	5.2	1(S2)
		21 days	0.5	10.3	1(S2)
Sample 3	11	10 days	0.7	0.7	2(S2)
		21 days	0.8	1.0	1(S2)
Sample 4	10	10 days	0.6	0.6	1(S2)
		21 days	0.7	1.5	1(S2)
Sample 5	9	10 days	0.2	13.6	4(S2)
		21 days	0.5	n.a.	4(S2)
Sample 6	11	10 days	0.2	11.1	4(S2)
		21 days	0.5	n.a.	4(S2)

* Corrosion propagation and delamination are measured along the scribe according to DIN EN ISO 4628-8.

** Degree of blistering is evaluated according to DIN EN ISO 4628-2.

n.a.: not applicable: due to complete delamination, degree of blistering cannot be determined.

4.2.4. Second salt spray testing run

The aim of this salt spray testing run is to identify the reason of the failure for the first run or to confirm that it is indeed due to the high Fortegra 100 concentration.

Table 12 lists all the samples that were prepared for this run:

- Sample 1 is prepared only with Fortegra 100 without any zinc phosphate. In other words, this sample will have one constituent different (i.e. Fortegra 100) than the blank control sample and the zinc phosphate containing samples. The synthesis process for this sample was somehow tricky. In a first attempt, Fortegra 100 was dissolved in the polymerizable phase and added directly to the ALS-33 solution, followed by homogenization, i.e. a single direct miniemulsion method was used. This sample had completely coagulated during polymerization. The second attempt, which was the successful synthesis route, was a mimic of the multiple miniemulsion process: deionized water was used to form the dispersed phase of an inverse miniemulsion stabilized with Fortegra 100, followed by addition of

Results and discussion

ALS-33 solution with further homogenization and formation of direct miniemulsion.

- Samples 2, 3 and 4 are all prepared with different combinations of zinc phosphate and Fortegra 100.
- Sample 5 and 6 are the blank controls. Sample 5 was dipped in the autodeposition coatings bath for 2 min, resulting in a coatings film of 30 μm (typical film thickness); while sample 6 was adjusted in order to result in a film thickness comparable to the Fortegra 100 containing samples (11 μm).

All miniemulsions were prepared with a high pressure homogenizer, as a convenient, quick method to synthesize larger scale samples. Moreover, XRF was used to confirm almost the 100% availability of zinc and phosphorus in the prepared miniemulsion, in comparison to the theoretical values. None of the coated panels was treated with a reaction rinse, but only post-dipped in the 60 °C deionized water bath.

Table 12 List of samples prepared for second salt spray testing run, including film thickness of the autodeposited coating. All samples were prepared with a post-dipping step in a 60 °C deionized water bath.

Sample	Constituents	Film thickness (μm)
Sample 1	10 wt% Fortegra 100 without any zinc phosphate	11
Sample 2	10 wt% Fortegra 100 and 2.5 wt% zinc phosphate	5
Sample 3	7.5 wt% Fortegra 100 and 2.5 wt% zinc phosphate	8
Sample 4	7.5 wt% Fortegra 100 and 5 wt% zinc phosphate	10
Sample 5	Control samples containing no zinc phosphate or Fortegra 100	30
Sample 6		11

Photos of the coated panels taken after 10 days are shown in Figure 32. Due to their extreme corrosion, the test was discontinued and no evaluation could be made, in terms of propagation of corrosion or delamination along the scribe or according to the degree of blistering. Yet, there are a few observations that could still be made:

- All four samples that show extreme corrosion (Figure 32, samples 1 \rightarrow 4) contain Fortegra 100 with either 7.5 wt% or 10 wt%.
- One of those four samples does not contain zinc phosphate (Figure 32, sample 1). Comparing the one without zinc phosphate with the other three containing zinc

phosphate, no corrosion difference could be observed – they all corroded in the same manner.

- Only the blank control samples (Figure 32, samples 5 and 6) show corrosion along the scribe and no significant delamination.

Even though this salt spray testing run was not successful, an important conclusion could still be made. The fact that the non-containing Fortegra 100 did not corrode as significantly as the other containing Fortegra 100 (with or without zinc phosphate) may strongly indicate that Fortegra 100 play an important role in corrosion. As previously mentioned, this might be due to the delamination or poor wet adhesion that takes place in the film in the presence of Fortegra 100.

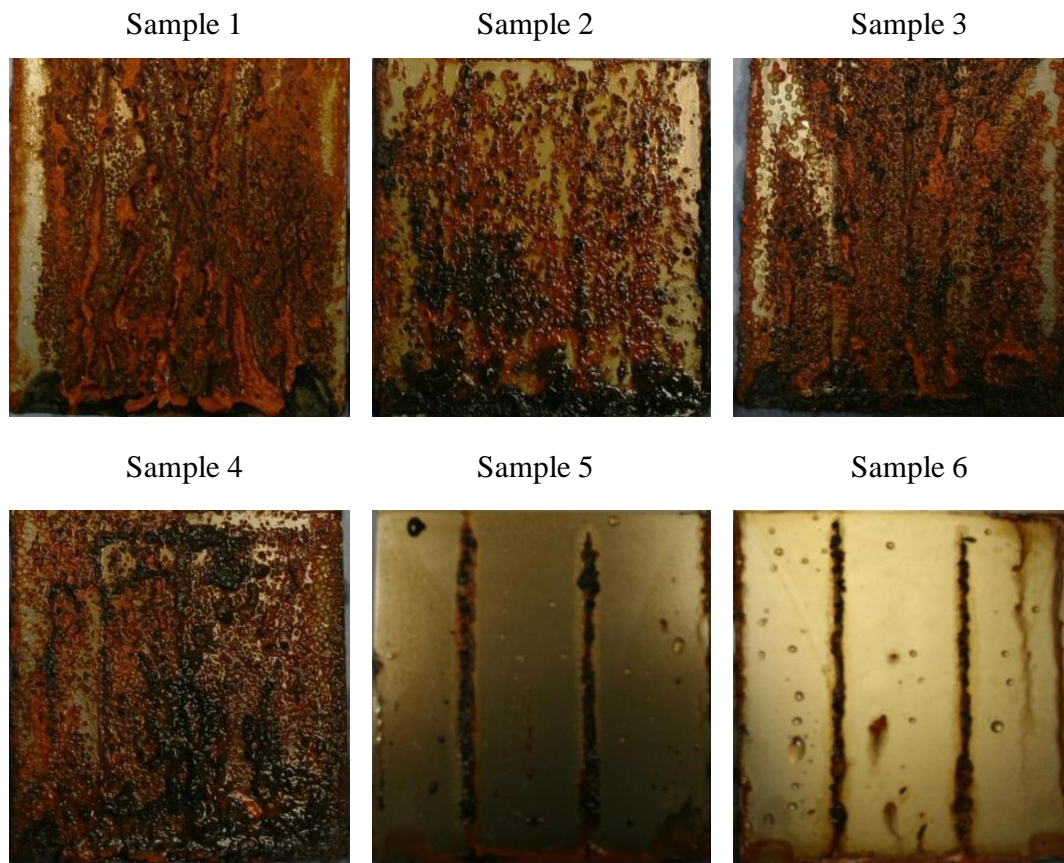


Figure 32 Cold rolled steel panels coated via autodeposition with the miniemulsion samples as follows: sample 1 prepared with 10 wt% Fortegra 100 without any zinc phosphate, sample 2 prepared with 10 wt% Fortegra 100 and 2.5 wt% zinc phosphate, sample 3 prepared with 7.5 wt% Fortegra 100 and 2.5 wt% zinc phosphate, sample 4 prepared with 7.5 wt% Fortegra 100 and 5 wt% zinc phosphate and sample 5 & 6 prepared without any Fortegra 100 or zinc phosphate. Panels show results after only 10 days of salt spray exposure.

4.2.5. Third salt spray testing run

4.2.5.1. Working on a modified formulation

Since it was clear that the problem is related to Fortegra 100 and consequently related to wet adhesion, the formulation needed to be modified in order to accommodate the presence and effect of a higher surfactant concentration than in normal latex films.

- Main changes targeted:
 - Higher concentration of epoxy: increased epoxy in the formulations show enhanced corrosion protection. Target: ideally up to 50%.
 - Substitute compatibilizers with more hydrophobic ones and increase concentration when possible in order to increase the crosslinking.
 - Use alternatives to Fortegra 100 as well as a reduction of the w/o surfactant concentration to a minimal level.

The result of this modified formulation is shown in Table 13, in comparison with the formulation that has been used so far in the previous salt spray testing runs. All failed changes made to the formulation will not be discussed. Those attempts mainly involved the evaluation of other epoxy resins and epoxy resin diluents.

- To what extent were the targets met?
 - Epoxy concentration: was raised from 35% to 40% by substitution of D.E.R. 664 with D.E.R. 671. The lower EEW of the latter will allow a higher crosslinking.
 - Substitution of compatibilizers: methacrylic acid was kept without changes. 2-Hydroxyethyl methacrylate was replaced with a mixture of the more hydrophobic hydroxylpropyl methacrylate and glycidyl methacrylate. Concentrations were kept almost unchanged. As such, also higher crosslinking could be achieved between styrene / acrylic polymers and epoxy network through glycidyl methacrylate.
 - Fortegra 100 was used with a concentration of 1.25 wt% to the dispersed phase. Other alternatives were also used: Isolan PDI, Isolan GPS, and Grindsted PGPR 90. Those surfactants were successful in preparing inverse miniemulsions, as shown in 4.1.2.5 “ *Choice of nonionic*

surfactant for inverse miniemulsions". Chemical structures are also given in that section.

All those changes, whether by increasing crosslinking in the film, increasing epoxy content or lowering the w/o surfactant concentrations, should improve wet adhesion of the film.

Table 13 List of polymerizable phase components and their concentrations used to prepare the samples for the first two salt spray testing runs, as well as the modified formulation used for the third salt spray testing run.

	Previously salt-spray tested formulation	Modified formulation
D.E.R. 664 ^{iv}	35 wt%	-
D.E.R. 671 ^v	-	40 wt%
Butyl acrylate	19.4 wt%	17.9 wt%
Methacrylic acid	1.1 wt%	1.0 wt%
Methyl methacrylate	20.7 wt%	19.1 wt%
2-hydroxyethyl methacrylate	2.4 wt%	-
Styrene	21.4 wt%	19.8 wt%
Hydroxypropyl methacrylate	-	1.1 wt%
Glycidyl methacrylate	-	1.1 wt%
Vestagon B1530 ^{vi}	4.4*	8.5*

* wt% for 100% monomer/epoxy

For the corrosion test, six miniemulsion samples were prepared using ultrasonication: the control sample containing no zinc phosphate and no Fortegra 100. All other five samples contain 2.5 wt% zinc phosphate loading but different surfactants and surfactant concentrations: 1.25 wt% Fortegra 100, 7.5 wt% Fortegra 100, 1.25 wt% Isolan PDI, 1.25 wt% Isolan GPS, and 1.25 wt% Grindsted PGPR 90. All prepared miniemulsions were investigated using DLS, as well as characterized using XRF and ICP-OES. The results are shown in Table 14.

Two main observations can be made from the DLS results. 1) The control sample has the smallest mean diameter. This is expected since in all the other samples, additional constituents are added to the droplet: a w/o surfactant and zinc phosphate; 2) both Isolan surfactants include isostearate groups, resulting in same mean droplet diameter. It is

^{iv} D.E.R. 664 is a medium molecular weight solid bisphenol-A diglycidyl ether epoxy resin based with an epoxy equivalent weight (EEW) value of 875 – 955 g/eq.

^v D.E.R. 671 is a low molecular weight solid bisphenol-A diglycidyl ether epoxy resin based with EEW values of 475 – 550 g/eq.

^{vi} latent epoxy curing agent based on isophorone diisocyanate blocked with ϵ -caprolactam.

worth mentioning here about the Isolan surfactants that they include OH group along their structure which can also react during polymerization or take part in crosslinking; 3) comparing the mean particle diameters for both samples prepared with Fortegra 100, it is found that a mean particle diameter of the sample prepared with 7.5 wt% is larger than that prepared with only 1.25 wt%. This is again in line with previous DLS experiments that showed an increased mean diameter with increased Fortegra 100 concentration. It was not investigated though, if the same relation will be obtained also with the other surfactants.

From the elemental analysis performed with XRF, there are also few observations that can be made: 1) in all samples, only 50 wt% of the theoretical values for zinc were detected and 2) for phosphorus, since this was not the case, this might imply a presence of mixed zinc phosphates (stoichiometry in this case has been disrupted and does not match that of hopeite).

As for elemental analysis obtained from ICP-OES, there is a general agreement with the XRF results obtained: almost 50% of Zn was found and almost 100% of P was found. Also, as was previously the case, the ICP-OES results show a similar or lower detection than that performed by XRF. The reason for this has been assigned to the mechanism by which the analysis is made. In XRF, samples are freeze-dried resulting in average elemental detection in the sample. In case of ICP-OES, only particles reaching the flame are analyzed. Another reason could be related to the sensitivity of the method, in XRF, only an accuracy of one decimal place is obtained on a weight percent basis, which makes the analysis not very sensitive to changes, while for ICP-OES detection it is in the range of $\mu\text{g/l}$. Worth mentioning is that the values given for the sample prepared with Grindsted PGPR 90 are unreliable since during polymerization a partial coagulation has occurred which would then deem the percentage achieved erroneously due to the loss in organic content as well.

Table 14 Mean particle diameter as measured by DLS for the miniemulsions after polymerization, as well as elemental analysis results as measured by XRF and ICP-OES for the different samples.

Sample ^a	Mean particle diameter (nm) ^b	XRF Analysis ^c		ICP-OES Analysis ^c	
		Zn	P	Zn	P
7.5% F100	219.6	50%	100%	50.1%	94.4%
1.25% F100	211.7	50%	50%	46.0%	88.7%
1.25% I-PDI	174.7	50%	100%	51.2%	94.5%
1.25% I-GPS	174.8	50%	50%	48.0%	88.9%
1.25% PGPR	194.4	50%	50%	54.9%	96.4%
Control	132.8	n.a. ^d	n.a. ^d	n.a. ^d	n.a. ^d

^a Zinc phosphate containing samples are referred to using the inverse surfactant and its concentration (wt% in ratio to dispersed phase).

^b Mean particle diameters are based on Gaussian distribution, volume weighted.

^c Elemental analysis are reported as wt% achieved experimental value from theoretical value.

^d not applicable: control sample is prepared without zinc phosphate.

4.2.5.2. Autodeposition and salt spray test with modified formulation

In total, eight panels were coated from miniemulsions via autodeposition as shown in Table 15. Sample 1 serves as a blank control, where no zinc phosphate is used, sample 7 & 8 are control samples treated with reaction rinse in order to serve as a comparison to current corrosion protection systems. Two panels were used in this case to confirm the reproducibility for those control samples. All other samples contained 2.5 wt% zinc phosphate loading, but different w/o surfactants. Samples 2, 4, 5 and 6 were prepared with Fortegra 100, Isolan PDI, Isolan GPS and Grindsted PGPR 90, all with a concentration of 1.25 wt% to the dispersed phase. Only one sample, sample 3, was prepared with 7.5 wt% Fortegra 100. Through this sample, a modified formulation could be evaluated by the comparison of the result to a previously salt sprayed sample from the first run of salt spray tests (old formulation).

During autodeposition, compared to the former samples previously tested for corrosion, the film thickness could be increased with all the samples prepared with 1.25% of the w/o surfactant (except sample prepared with Grindsted PGPR 90). Also, for the same film thickness, a lower substrate dipping time was required. Those two observations strongly suggest that in those samples the probability that the inverse surfactant lies at the droplet/water interface is much lower than the previously tested samples, leading to an easier ionic destabilization of the system. This was an indication that this might give

Results and discussion

better film properties in terms of blistering and delamination. The film thickness of each coated panel is shown in the second column of Table 16.

Table 15 Samples prepared for the third salt spray testing run, their respective constituents and coating process.

Sample	Constituents	Coating process
Sample 1	Control sample containing no zinc phosphate or w/o surfactant	Step 7: 60 °C deionized water
Sample 2	2.5 wt% zinc phosphate and 1.25 wt% Fortegra 100	Step 7: 60 °C deionized water
Sample 3	2.5 wt% zinc phosphate and 7.5 wt% Fortegra 100	Step 7: 60 °C deionized water
Sample 4	2.5 wt% zinc phosphate and 1.25 wt% Isolan PDI	Step 7: 60 °C deionized water
Sample 5	2.5 wt% zinc phosphate and 1.25 wt% Isolan GPS	Step 7: 60 °C deionized water
Sample 6	2.5 wt% zinc phosphate and 1.25 wt% Grindsted PGPR 90	Step 7: 60 °C deionized water
Sample 7 & 8	Control sample containing no zinc phosphate or w/o surfactant	Step 7: reaction rinse

Table 16 show the results of the salt spray test after 10 days and 21 days of exposure, in terms of the corrosion propagation and the delamination along the scribe, as well as the degree of blistering.

By examination of the data after 10 days of exposure, a few observations can be made. All samples containing zinc phosphate show a similar corrosion propagation along the scribe (samples 2 → 6), also the blank control (sample 1) shows the same value of corrosion propagation. Only samples prepared with reaction rinse (samples 7 & 8) show higher corrosion propagation, almost double propagation.

In terms of delamination, the blank control as well as all zinc phosphate containing samples show similar delamination values (samples 1 → 5), except for the sample prepared with Grindsted PGPR 90 (sample 6), which showed a high extent of delamination, while the controls prepared with reaction rinse (samples 7 & 8) showed minimum delamination.

In terms of degree of blistering, three samples show no signs of blisters after those 10 days of exposure: the Isolan PDI sample (sample 4) and the controls prepared with reaction rinse (samples 7 & 8).

After 21 days of salt spray exposure, the panels are once more evaluated. Data are also shown in Table 16 while photos of the panels are shown in Figure 33.

Following observations can be made:

- Sample 6 showed the worst corrosion protection in terms of the highest corrosion propagation values, high extent of delamination that lead to difficulty in determination of degree of blistering. This result though was not surprising since the sample showed a high coagulation during polymerization as well as difficulty in the autodeposition coating, resulting in only a 10 μm thick film.
- Comparing sample 3 with the corresponding sample from the first salt spray test run (using old polymerizable phase formulation) shows a comparable corrosion propagation but a clear improvement in the delamination. This clearly indicates that the modified polymerizable phase formulation with its higher epoxy content and crosslinking density did improve wet adhesion of the film, despite the same surfactant concentration.
- Comparing sample 2 and 3 (both with Fortegra 100, former with 1.25 wt% and latter with 7.5 wt% concentration) show that delamination of sample 3 is double that of sample 2. This also indicates that the high surfactant concentration affects the delamination extent, i.e. wet adhesion.
- Samples 2, 4 and 5 show similar corrosion propagation, which surprisingly also is similar to that of the blank control sample (sample 1), but lower than the sample with reaction rinse.
- Samples 7 and 8 show highest corrosion propagation but lowest delamination. This could be due to the reaction rinse composition which is optimized for good film properties.

To sum up, sample 4 seems to have shown best corrosion protection performance. It shows the lowest corrosion propagation and no signs of blistering. Although delamination does occur, this could still be worked on by further modification of the formulation. This sample was prepared with Isolan PDI, which have OH group along its structure, as shown in Table 5 in section 4.1.2.5 “*Choice of nonionic surfactant for inverse miniemulsions*”. As previously stated, this OH groups may take part in polymerization and crosslinking,

Results and discussion

which may have improved thus adhesion to substrate and consequently improved corrosion resistance.

Table 16 Results for third salt spray testing run in terms of corrosion propagation and delamination along the scribe, as well as degree of blistering after 10 days and after 21 days. Film thickness is also given for each sample.

Sample	Film thickness (μm)	Evaluated after	Corrosion propagation* (mm)	Delamination* (mm)	Degree of blistering**
Sample 1	25	10 days	0.2	5.0	1(S2)
		21 days	0.6	11.4	1(S5)
Sample 2	21	10 days	0.2	7.6	1(S2)
		21 days	0.7	7.6	1(S3)
Sample 3	20	10 days	0.2	8.0	1(S2)
		21 days	0.6	15.1	1(S2)
Sample 4	27	10 days	0.4	5.8	0(S0)
		21 days	0.5	10.8	0(S0)
Sample 5	27	10 days	0.2	6.7	1(S2)
		21 days	0.7	13.8	1(S5)
Sample 6	10	10 days	0.2	13.7	1(S2)
		21 days	1.4	20.3	n.a.
Sample 7	27	10 days	0.8	0.8	0(S0)
		21 days	1.0	3.9	2(S2)
Sample 8	27	10 days	0.9	0.9	0(S0)
		21 days	1.3	4.1	2(S3)

* Corrosion propagation and delamination are measured along the scribe according to DIN EN ISO 4628-8.

** Degree of blistering is evaluated according to DIN EN ISO 4628-2.

n.a.: not applicable: due to high degree of delamination, degree of blistering cannot be determined.

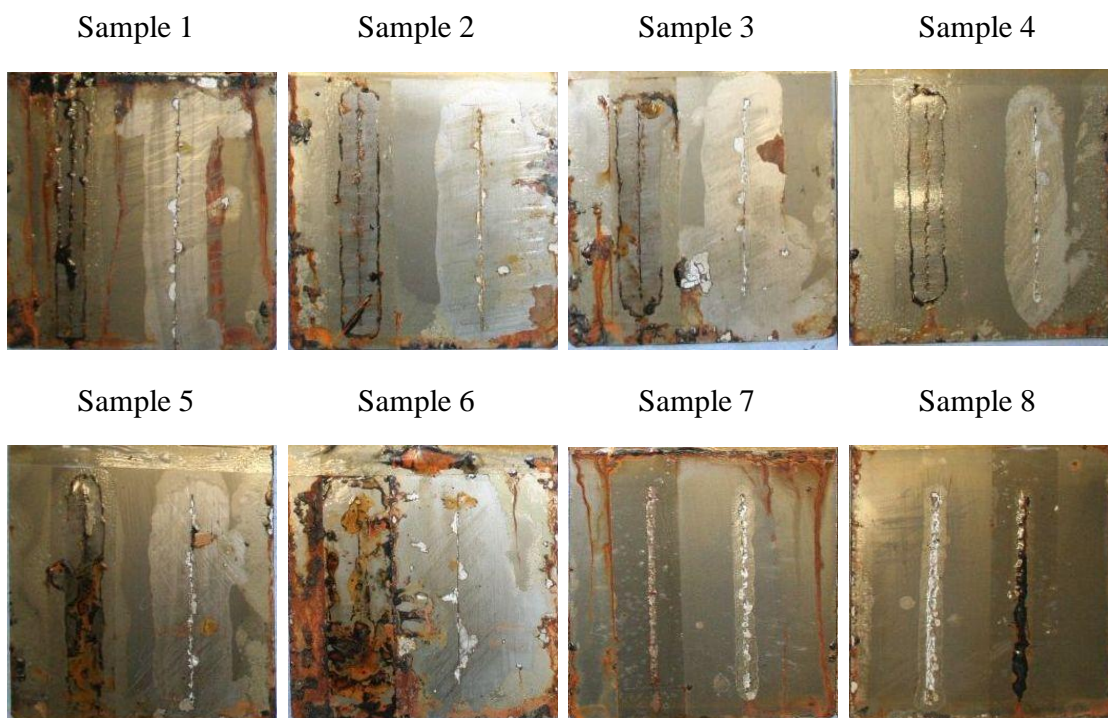


Figure 33 Cold rolled steel panels coated via autodeposition with the miniemulsion samples as listed in Table 15. Scribes at left hand side show results after 10 days of salt spray exposure, while scribes at the right hand side display results after 21 days of exposure.

4.2.6. Proposed corrosion protection mechanism

As shown in the results presented above, the hybrid zinc phosphate – polymer miniemulsion was able to impart a corrosion protection when applied as a coating on steel. The question that remained was: by what mechanism did this take place? In order to answer this, SEM coupled with EDX investigation was carried out, which will be presented hereunder.

First, the investigation of the miniemulsions prepared using the modified polymerizable phase formulation was carried out to check if the particles and zinc phosphate morphology was the same. Figure 34 shows SEM images taken for samples prepared with 1.25 wt% Fortegra 100 and 1.25 wt% Isolan PDI, both with a zinc phosphate loading of 2.5 wt%. Indeed the morphology did not change despite the modification in the polymerizable phase: zinc phosphate particles (brighter ones) appear still onto the polymeric particles.

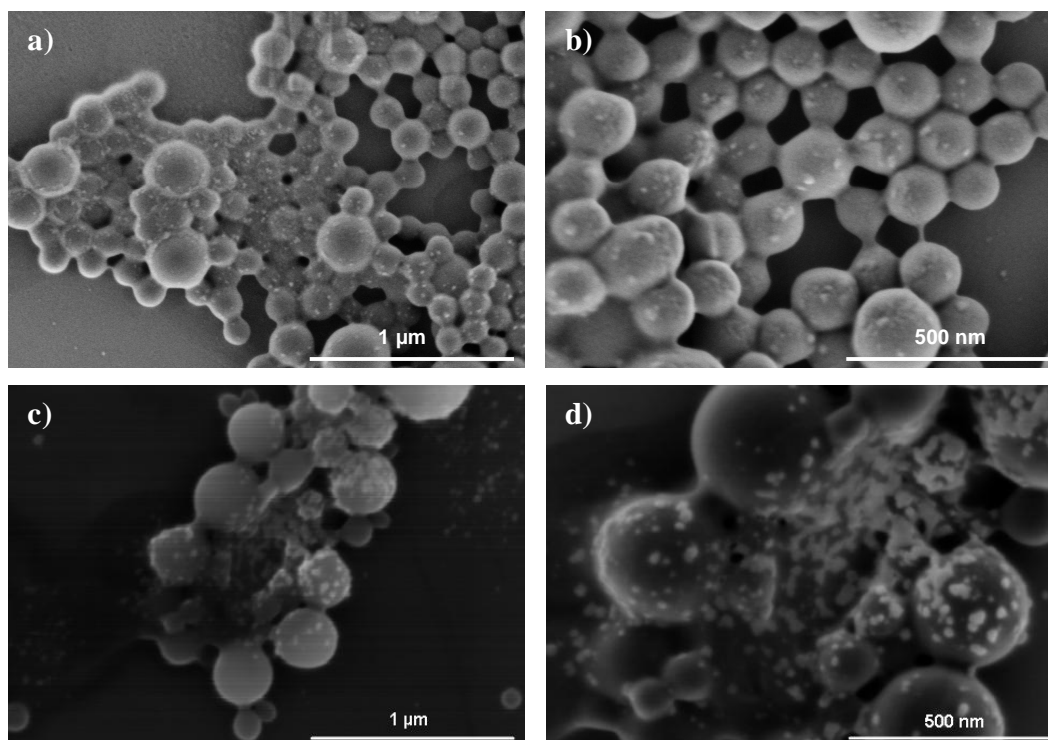


Figure 34 SEM^{vii} images for miniemulsion particles prepared with 2.5 wt% zinc phosphate loading and a) and b) 1.25 wt% Fortegra 100; and c) and d) 1.25 wt% Isolan PDI.

As a second step, it was important to examine the film cross section. To do this, a film was prepared by drop casting directly from miniemulsion onto silicon (Si) wafer, pre-cured at 105 °C for 12 h. The substrate with the film was broken at room temperature then investigated. Figure 35 shows a film cross section containing 1.25 wt% Fortegra 100 and 2.5 wt% zinc phosphate loading. By comparison to miniemulsion particles shown in Figure 34, it can be deduced that those brighter small particulates shown in Figure 35 throughout the film are zinc phosphate particulates. Unfortunately, due to the very low zinc and phosphorus concentration versus organic content, the EDX analysis could not confirm their presence.

^{vii} SEM used: Hitachi SU8000 equipped with a Bruker Quanta 400 energy dispersive X-ray (EDX) analysis system. Accelerating voltages used are as follows: a), b) and d) 0.7 kV; c) 5.0 kV. All samples were diluted and placed on Si wafer.

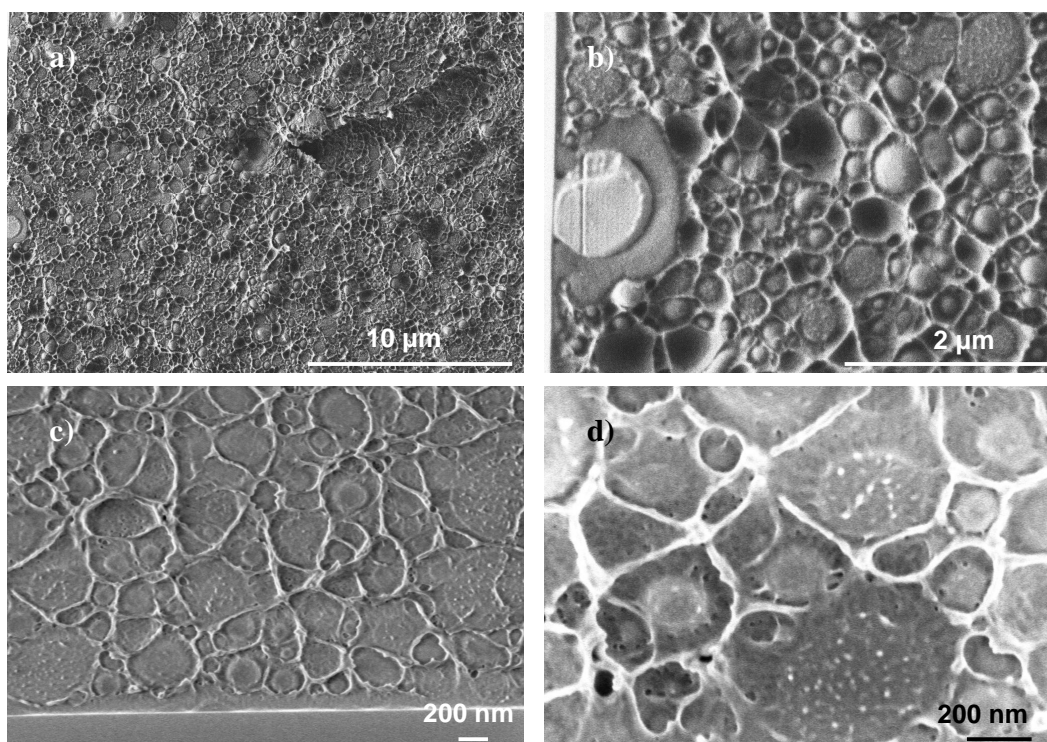


Figure 35 SEM^{viii} images taken for film cross section prepared from a miniemulsion containing 2.5 wt% zinc phosphate loading and 1.25 wt% Fortegra 100. Film was added to Si wafer by drop casting, followed by pre-curing at 105 °C for 12 hours. Cross section was prepared by Si wafer breaking at room temperature.

But to understand the corrosion protection mechanism, the cross section of the coatings film on a metal substrate has to be examined, ideally before and after complete curing.

In a first attempt, cold rolled steel panels with film autodeposited from miniemulsions were used. The steel panels were cut using a microtome with a tungsten carbide knife. The surface of the cross section were neither abraded nor polished to avoid any surface morphology changes induced by abrasion or polishing. The problem was, as such, the cross section was not smooth enough to allow reliable imaging.

In a second attempt, a model was devised that would replicate the coating process but would also be suitable for SEM imaging conditions: about 100 nm aluminium (Al) was sputtered on Si wafer. Aluminium in this case acted as the metal substrate, but was thin enough to allow breaking along with the Si wafer at room temperature. Si wafer was not used as a substrate since it was important to have the film formed on a metal to check if

^{viii} Images a) and b) taken with Hitachi SU8000 equipped with a Bruker Quanta 400 energy dispersive X-ray (EDX) analysis system. Images c) and d) taken with Zeiss 1530 Gemini. Accelerating voltage for all images is 0.7 kV.

metal – coating / zinc phosphate interactions were essential. The miniemulsion (containing 2.5 wt% zinc phosphate and 1.25 wt% Isolan PDI, i.e. the sample with highest performance during salt spray test) was added directly without dilution by drop casting forming a film of about 20 μm . Two heat treatments were carried out: pre-cure at 105 °C for 12 h, followed by full curing at 180 °C. After each heat treatment, the cross section was examined with SEM, as shown in Figure 36.

Figure 36 a) shows the cross-section of the pre-cured coating film. Fine, bright dots indicate the presence of zinc phosphate throughout the coating, in agreement with the previous film formed only on a Si wafer in Figure 35. Additionally, an interlayer can be seen between the aluminium thin film and the polymeric coating, as indicated by the white arrows in Figure 36 a) and b). The fully cured samples, the final coating form, also exhibited this same interlayer as shown in Figure 36 c). The fully cured film though did not show the tiny zinc phosphate particulates throughout the film as it was apparent after pre-curing. In order to be able to identify or locate zinc phosphate in the film in this case, the back scattered electron mode was used. As shown in Figure 36 d), the back scattered electron image indicates the presence of larger aggregates of bright particles, i.e. regions of high atomic number elements.

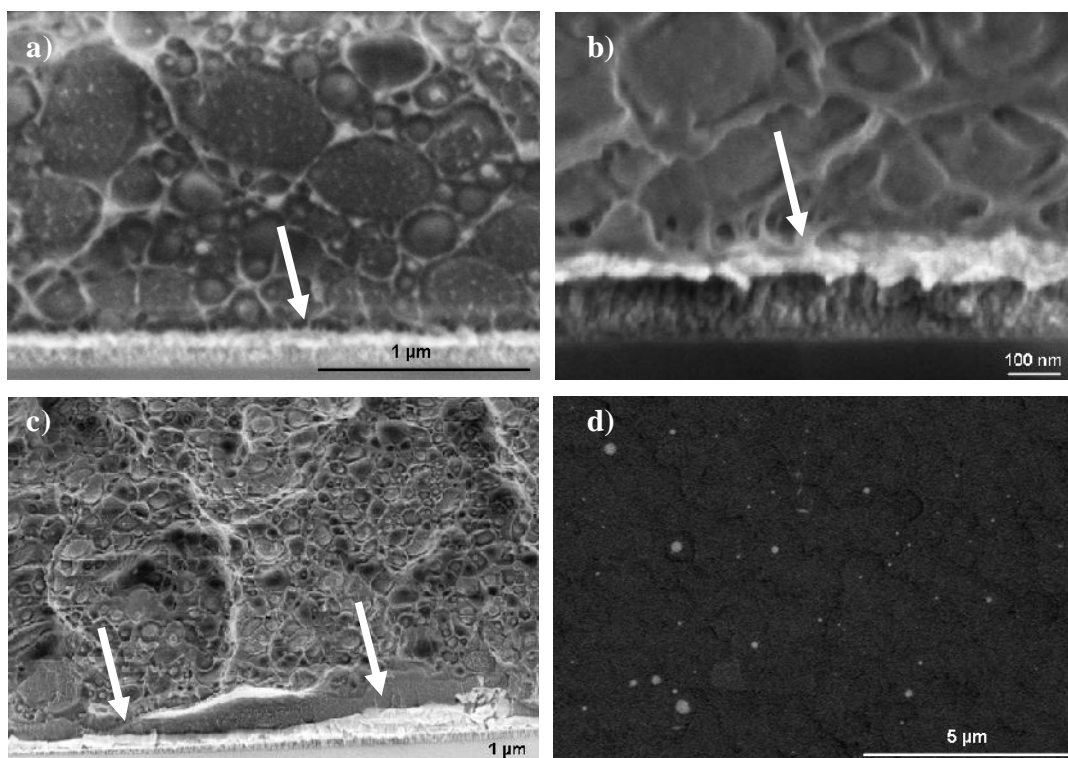


Figure 36 a) and b) SEM^{ix} cross section film prepared with 1.25 wt% Isolan PDI, after pre-curing at 105 °C for 12 hours; c) after complete curing at 180 °C for 40 minutes and d) backscattered electron image taken after full curing at 180 °C for 40 min. The film is formed on ca. 100 nm Al thin film, over Si wafer, broken at room temperature.

It was then suspected that both the interlayer and the aggregates are zinc phosphate. To investigate this, a line scan using EDX was used across the aluminium film, the interlayer and the organic film, passing through two of the aggregates, believed to be zinc phosphate, which was indicated previously via backscattered electron modes. The path of the line scan is shown in Figure 37 a). Indeed, the EDX analysis confirms the presence of zinc, phosphorus, and oxygen in those three distinctive regions and low carbon content, as well, indicating a low concentration of organic compounds where zinc phosphate aggregates are present. Combining those results with the SEM micrographs indicate that zinc phosphate particles have diffused through the organic layer, promoted by the high temperature during pre-curing at 105 °C and during full curing at 180 °C, thus showing a strong attractive interaction between the metal substrate and the zinc phosphate particles.

^{ix} Images a) and d) were taken with Hitachi SU8000 equipped with a Bruker Quanta 400 energy dispersive X-ray (EDX) analysis system, at an accelerating voltage of 0.7 kV. Images b) and c) were taken with Zeiss 1530 Gemini, also with an accelerating voltage of 0.7 kV.

Moreover, a further mobility of zinc phosphate particles took place at the curing temperature of 180 °C within the organic film, leading to the formation of aggregates.

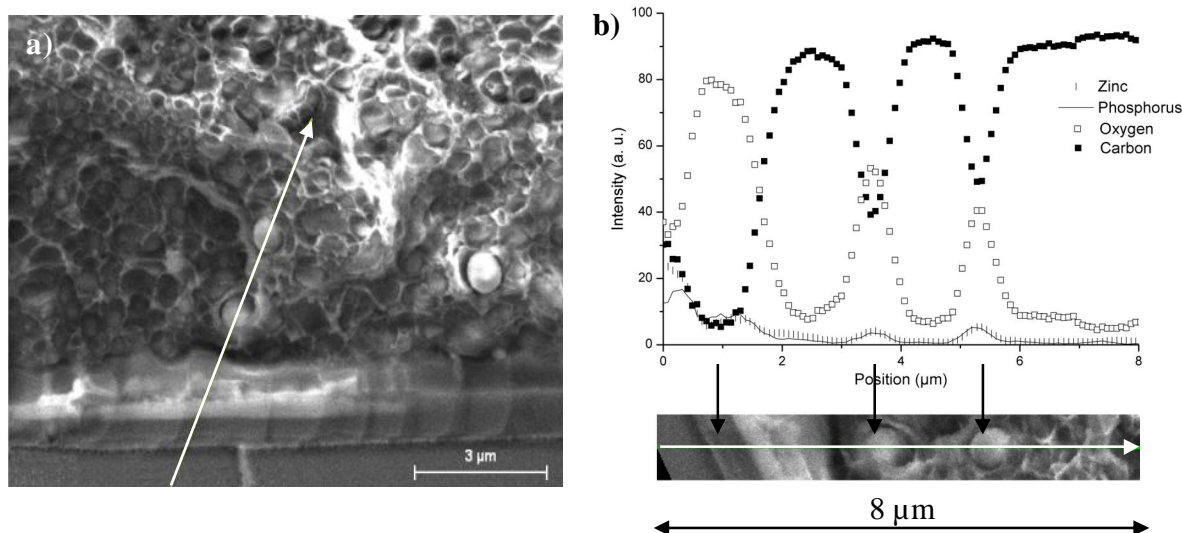


Figure 37 a) SEM^x image indicating where the EDX line scan in b) was performed: across the aluminium thin film, the zinc phosphate layer and the polymer/zinc phosphate coating containing zinc phosphate aggregates. Zinc is represented by (|), phosphorus by (—), oxygen by (□) and carbon by (■).

So what does this result reveal about the mechanism of corrosion protection? As previously mentioned, in a conventional phosphate conversion coating pretreatment using zinc phosphate, a layer of hopeite is normally formed directly on the metal surface, which protects the metal surface and on which the organic coating is afterwards applied³⁶. In the case of autodeposition followed by an immersion of the wet film in a reaction rinse, it is believed that the inorganic salts are able to interact directly with the metal surface⁴⁷, although no proof in literature could be found. In this work, it was shown that zinc phosphate show mobility through the organic film during drying at 105 °C and further during curing at 180 °C and show also affinity to the metallic substrate. Therefore, it is plausible that also in this case, the corrosion protection mechanism is related to a direct interaction between the zinc phosphate and the metal substrate.

^x SEM image and EDX line scan were performed with Hitachi SU8000 equipped with a Bruker Quanta 400 energy dispersive X-ray (EDX) analysis system.

4.3. Synthesis of water-based titanium dioxide - polymer particles via a single miniemulsion

4.3.1. Introduction

The aim of this project was to synthesize also hybrid inorganic-organic particles, namely water-based titanium dioxide-polymeric particles, via a single miniemulsion process. This miniemulsion should serve as a white pigment containing polymeric miniemulsion that would act directly as a coating, without any need for further pigmentation.

The attempt had encountered many bottle neck points, which were overcome, reaching the target – titanium dioxide-polymeric water-based miniemulsion, but unfortunately did not result in the ideal target miniemulsion and required application. For this reason, the main effort of this work was allocated to the multiple miniemulsion project. In the following sections, the main results and trials will be presented.

4.3.2. Designing the synthetic route

The idea was to synthesize titanium dioxide in-situ via the following process: a titanium dioxide precursor, miscible with the monomeric dispersed phase, was used. This titanium dioxide precursor should remain stable within the dispersed phase constituents as well as during miniemulsion formation. If this condition was not met, titanium dioxide particles will form before the miniemulsion droplet formation, i.e. before creation of our nanoreactors, disrupting as such the main advantages of having a miniemulsion with a possible miniemulsion polymerization. Once the direct miniemulsion was formed containing the titanium dioxide precursor and vinylic monomers in its dispersed phase, either titanium dioxide formation will take place spontaneously with time via a sol-gel process due to excess water in the continuous phase, or can be induced via pH changes after polymerization. A schematic diagram illustrating the synthetic routes is shown in Figure 38.

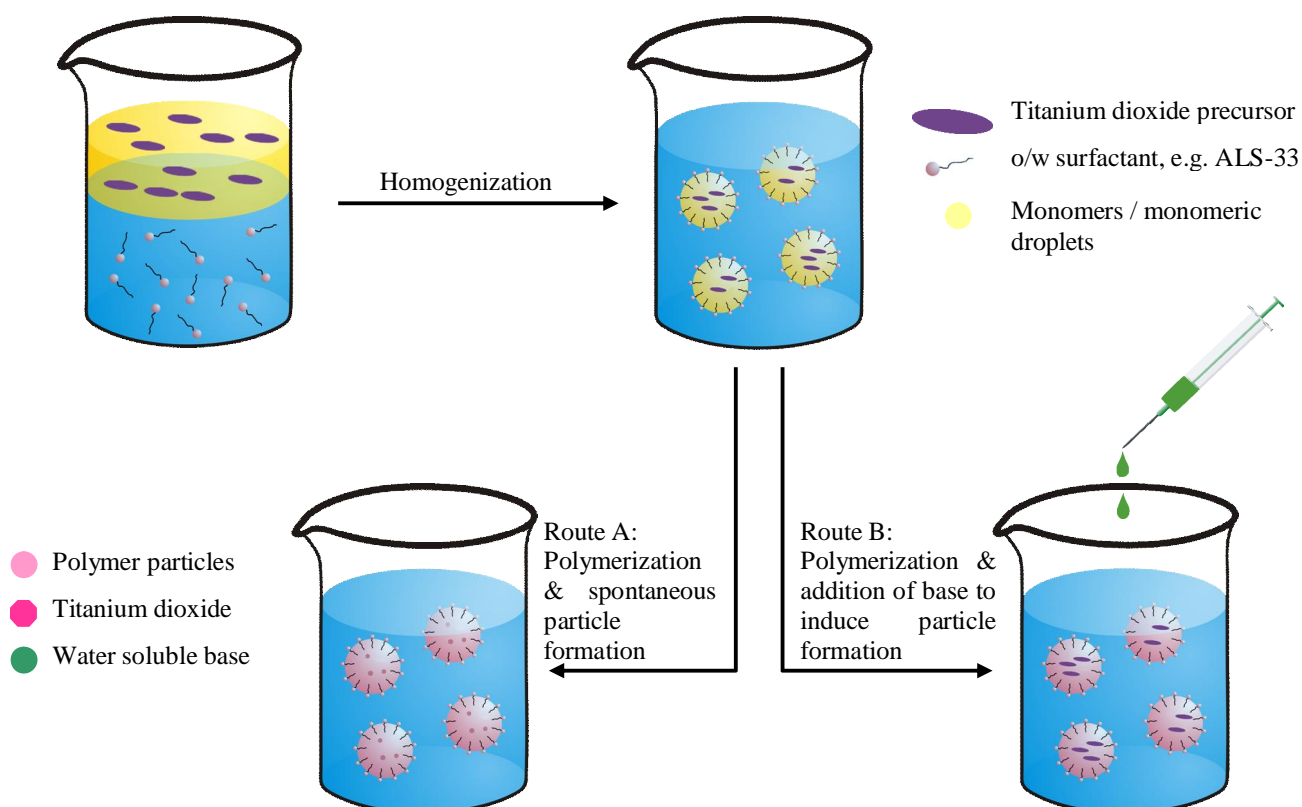


Figure 38 Schematic diagram illustrating the synthetic route. From upper left corner: titanium dioxide precursor dissolved in vinylic monomers is mixed with o/w surfactant solution, followed by homogenization and formation of direct miniemulsion and subsequent polymerization. Either titanium dioxide particles are formed spontaneously with time (route A) or is induced via addition of a water soluble base (route B).

4.3.3. Finding a stable precursor / precursor system

In order to dissolve the titanium dioxide precursor in the monomeric dispersed phase, the use of an organic precursor is inevitable, which must be stable, as previously mentioned, till the direct miniemulsion is formed. On a lab scale, a minimum of 15 min are sufficient, while on an industrial scale, 8 – 9 h of stability are necessary. Several approaches have been tested to achieve this goal, which will be presented in the following sections.

4.3.3.1. Alkoxide precursors and their corresponding alcohol – effect of pH changes

The idea was to add a mixture of titanium alkoxide and its corresponding alcohol to excess water at different pH values and visually determine at which pH is the hydrolysis reaction slowest. In total four alkoxide precursors were evaluated.

Table 17 summarizes the results.

Of all the tested precursors, isopropoxide precursor showed the highest stability till a pH < 1, for a time span of ~ 1 week, followed by ethoxide and butoxide where they both showed a stability only at a pH = 0.3 for a time span of ~ 5 and 3 days respectively. Only the 2-ethylhexyl oxide precursor did not show sufficient stability for a miniemulsion to be formed.

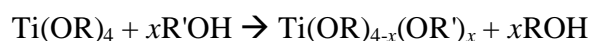
Table 17 Summary of stability trials using titanium (IV) alkoxides and their corresponding alcohol in the presence of excess water, across the pH range.

Alkoxide / alcohol pair	pH range of stability	Stability period
Titanium (IV) ethoxide / ethanol	at pH = 0.3	ca. 5 days
Titanium (IV) isopropoxide / isopropanol	at pH = 0.3 - 1	ca. 1 week
Titanium (IV) butoxide / n-butanol	at pH = 0.3	ca. 3 days
Titanium (IV) 2-ethylhexyl oxide / 2-ethylhexanol	n.a.	n.a.

n.a.: no stability shown throughout the pH range

This conclusion contradicted our expectation as it was expected that with an increased number of carbons and/or branching of the chains, the stability of the precursor will be higher, more so for the branching, due to steric hindrance effects, as in the case of the 2-ethylhexyl oxide precursor whose both the number of carbons and the extent of branching is much higher than the preceding precursors used. This signifies that there is another factor that is also affecting the instability of the precursors in aqueous solutions – the ease of removal of the alkoxy group of the precursor, i.e. electronic effects should be considered.

When an alkoxide is mixed with an alcohol, an exchange reaction is expected between the alkoxy group and the alcohol group¹²³, given by:



This exchange reaction will be highly dependent on the electronic structure of both the alcohol being used and the alkoxy group, favoring the use of a high Lewis acidity of the titanium or the high Lewis basicity of the alcohol¹²³. Considering the Lewis acidity of the titanium metal in titanium (IV) 2-ethylhexyl oxide in this case would be the lowest in Lewis acidity, affecting the exchange reaction, while the ethoxide precursor would be the

highest in terms of Lewis acidity (though lowest in terms of steric hindrance). In this case, it seems that both the extent of the Lewis acidity (electronic effects) and the steric hindrance effects given by the branching play a mutual role and give the optimum stability of the isopropoxide (in this case, highest at pH = 1).

Even though several systems have been found to be suitable for performing a miniemulsion on a lab scale, working with an extremely low pH is not favorable on an industrial scale to avoid extra precautions regarding corrosion and therefore, other stability means were sought.

4.3.3.2. Carboxylic acids as ligands

- **Oleic acid**

Several works have shown that the use of oleic acid^{124, 125}, in specific, and carboxylic acids^{123, 126, 127} in general, would significantly retard the reactivity of titanium alkoxy precursors, where the carboxylic acid would form a complex with the precursor, and therefore, less alkoxy groups would be exposed to the water phase for hydrolysis, affecting the usual vigorous hydrolysis and condensation.

Titanium (IV) isopropoxide was used since it showed the highest stability in the previous experiments. A molar ratio of 1 : 31.5 titanium (IV) isopropoxide : oleic acid was used to check the stability in excess water across the pH range. Results showed high stability from pH 0.3 to ~ pH 10 with a stability more than one week especially for pH range 1 to 10.

As such, the molar ratio was varied and tested only with excess distilled water. Molar ratios of 1 : 25, 20, 15, 10, 5 and 1 were evaluated. As of molar ratio 1 : 10 stability of only 1 day was achieved while a molar ratio of 1 : 1 showed no stability and titania particles were formed instantaneously.

The stability obtained can be explained as follows: the reaction of carboxylic acids with titanium alkoxides forms a new precursor, in our case, titanium oleate, whose rate of hydrolysis is much slower than that of the alkoxide precursors¹²³:



But the system does not seem to be that simple. Schubert¹²³ explains several possibilities and side reactions that can take place, where a continuous competition between them

exist. For example, an esterification reaction can take place between the liberated alcohol and any free carboxylic acid present, resulting in the formation of water. The latter would though be insignificant due to the excess of water already present in the system.

Despite the very satisfying stability results obtained with oleic acid, the interest was then moved to find a polymerizable ligand that would be able to stabilize the titanium alkoxide precursor but also take part in the polymerization of vinylic monomers that will be available later on in the dispersed phase of the miniemulsion.

▪ Acrylic acid and methacrylic acid

The combination of acrylic acid and a titanium oxide precursor to affect the reactivity of the alkoxide was mentioned in few works, for example by Méndez-Vivar et al.¹²⁸ and Zhang et al.¹²⁹, while even more studies were made on the complexation of titanium alkoxide precursors with methacrylic acid^{123, 128, 130, 131}. Both, acrylic acid and methacrylic acid are bidentate ligands¹²⁸, coordinating with both oxygens in the carboxylic acid group.

Each was added to titanium (IV) isopropoxide with a molar ratio of 1 : 10 and 1 : 31.5 titanium (IV) isopropoxide : acrylic acid or methacrylic acid and were tested for stability in excess water in the pH range between 1 and 7. Both showed the same results: instantaneous precipitate was formed upon addition of excess water. One possible explanation for this instability could be the miscibility of acrylic acid and methacrylic acid with water; it does not seem to give enough protection or enough hydrophobizing effect to the precursor in the presence of excess water, as was the case with the highly hydrophobic oleic acid.

▪ Using an amine to drive hydrolysis

So far, the oleic acid has shown the highest stability against hydrolysis. The question remaining was: how to induce titania formation from the highly stable titanium oleate precursor in case it was the chosen route? The answer was provided by Cozzoli et al.¹²⁴, Rammal et al.¹²⁶ and Zhang et al.¹²⁵, who have shown that titania was produced from titanium isopropoxide in oleic acid using an amine (namely, trimethyl amine¹²⁴, trimethylamino-*N*-oxide¹²⁴, tetramethylammonium hydroxide^{124, 126}, tetrabutylammonium

hydroxide¹²⁴, oleylamine¹²⁵ and octylamine¹²⁵). Zhang et al.¹²⁵ explain that an aminolysis reaction takes place where the amine group attacks the carbonyl group. This was the main idea to induce titania formation in case of carboxylic acid assisted stability.

4.3.3.3. β -ketoesters and β -diketones as ligands

- **2-(Acetoacetoxy)ethyl methacrylate (AAEMA)**

AAEMA was used as an example of β -ketoesters. The presence of an acetylacetone group would act as a ligand providing possibly a stable titanium alkoxide complex, while also providing a polymerizable group. Moreover, it acts as an adhesion promoter for various materials¹³², which would therefore be ideal for coatings application. The idea of evaluating AAEMA was inspired by few works that have used AAEMA and titanium alkoxides to produce titania-organic polymer networks¹³³⁻¹³⁹. In the same manner, a molar ratio of 1 : 10 of titanium (IV) isopropoxide to AAEMA was used and added to excess water at different pH values. At pH lower than 3.2, precipitation occurred instantaneously. At the pH range of ~ 3.2 to ~ 5.4, no precipitation occurred but instead a high dense gel was formed after two hours of phase mixing. To confirm if this is also titania or a sol-gel process related phenomena, IR was used to investigate pure AAEMA, AAEMA-titanium (IV) isopropoxide mixture and the dense gel occurring after excess water addition. Results show that the latter possesses no Ti-O-C bond which highly indicates that disruption of the complex and subsequent occurrence of sol-gel process took place.

- **Acetylacetone**

Acetylacetone is an example of β -diketones and has been described to be a strong chelating ligand¹⁴⁰ and was used in many works to modify the hydrolysis rate of titanium alkoxides¹⁴⁰⁻¹⁴⁴, just to name a few. Even though acetylacetone does not contain a polymerizable group, it may still be useful in coatings applications as it is known to improve adhesion properties¹⁴¹. Also in this case, instability was found as a precipitate was instantaneously formed. A molar ratio of 1 : 10 was used.

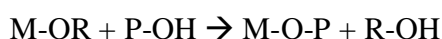
4.3.3.4. Further ligands

- **Methacryloyloxyethyl succinate (GR-80) and phosphate of caprolactone modified 2-hydroxyethyl methacrylate (PM-21)**

GR-80 and PM-21 were evaluated as being generally used in coatings industry, especially the latter, since phosphate functional (meth)acrylate esters improve coatings adhesion of acrylic latex¹⁴⁵. Both were unfortunately found to be instable in the presence of excess water.

- **N-octylphosphonic acid and diethyl vinylphosphonate**

The work done by Errington et al.¹⁴⁶ and Guerrero et al.¹⁴⁷ discuss the formation of titanium alkoxides modified by organophosphonates. Mehring et al.¹⁴⁸ explain that phosphonic acids, like carboxylic acids, upon the reaction with titanium alkoxides would liberate alcohols¹⁴⁹:



Normally, with a carboxylic acid, the liberated alcohol may react with the excess carboxylic acid available in the system creating water molecules. In the case of phosphonic, this esterification reaction by the liberated alcohol does not occur¹⁴⁸ (or is very difficult to occur¹²³) and thus the produced complex remains stable and was able to be isolated and studied by several groups¹⁴⁶⁻¹⁵⁰. This stability is, unfortunately, not available in a medium of excess water.

4.3.3.5. General remark on hydrolytic stability

The problem that we have faced so far was that all research work on hydrolytic stability of precursors has been carried out in a limited amount of water while in order to form a direct miniemulsion, excess water is present in our system as the continuous phase. Several works on sol-gel chemistry confirm that the amount of water available is influential. For example, Hoebbel et al.¹⁴⁴ have expressed the amount of water used for hydrolysis in molar ratio to the –OR groups available in the alkoxide – “h = H₂O:OR”. Similarly, Blanchard et al.¹⁴³ have introduced the variation of amount of water in molar reference to titanium – “H = [H₂O]/[Ti]”. In general, the hydrolytic stability decreases with the increase of either “h” or “H”, i.e. the water content. Therefore, it was hard to

judge the stability of the precursor modifier based on literature or previous research work done in this field.

4.3.3.6. Hydrolytic stability within vinylic monomers mixture

On a further step, now that oleic acid has shown so far the highest hydrolytic stability obtained, oleic acid was added to a mixture of three vinylic monomers that are mainly used in coatings application: butyl acrylate, methyl methacrylate and styrene, with compositions given in Table 18.

A molar ratio of 1 : 10 of titanium (IV) isopropoxide to oleic acid was used which showed a high hydrolytic stability as was the case with pure oleic acid. The molar ratio was then reduced to 1 : 4 and the same stability was also observed. Hence, with this formulation, a miniemulsion was ready to be carried out and eventually followed by polymerization.

Table 18 Weight percent of the monomer mixture containing oleic acid as the ligand.

Constituent	Weight percent
Butyl acrylate	27.8
Methyl methacrylate	30.5
Styrene	29.1
Oleic acid	12.6

Two additional monomer mixtures were also evaluated. A monomer mixture containing butyl acrylate, methyl methacrylate, styrene, methacrylic acid and 2-hydroxyethyl methacrylate was evaluated to check if this would retard rates of hydrolysis. No research work was found on this but the idea was just to check stability in typical vinylic monomers used in coatings applications. Additionally, AAEMA was mixed with butyl acrylate, methyl methacrylate, and styrene, since AAEMA did show hydrolytic stability for two hours before undergoing hydrolysis. Unfortunately, both monomer mixtures with ligands and titanium (IV) isopropoxide showed instantaneous precipitation formation once excess water was added.

4.3.4. Formation of miniemulsions

4.3.4.1. Using oleic acid

Miniemulsions were prepared using titanium alkoxide with pure oleic acid with a molar ratio of 1 : 10 using 2.5 wt% of ALS-33 to the dispersed phase. The aim was to optimize the miniemulsion in terms of two main variables: titanium alkoxide precursors and pH of aqueous continuous phase. The miniemulsions were evaluated using DLS measurements. The pH was fixed by using distilled water while four different titanium alkoxide precursors were used. All other parameters remained unchanged. The evaluated precursors were: titanium (IV) ethoxide, titanium (IV) isopropoxide, titanium (IV) n-butoxide, and titanium (IV) 2-ethylhexyl oxide. Additionally, a blank miniemulsion was prepared that contained only oleic acid as the dispersed phase without titanium alkoxide precursor. Both control sample and ethoxide based sample showed a bimodal droplet size distributions, while with the more hydrophobic precursors, a monomodal distribution was observed.

In order to test for the pH effect, titanium (IV) 2-ethylhexyl oxide was used being the most hydrophobic, based on above-mentioned results. Four samples were prepared: besides one with distilled water, also at pH of 2.3, 4.5 and 9.15. Both samples prepared with distilled water and at a pH of 9.15 showed stable miniemulsion with monomodal droplet size distributions. The miniemulsion prepared with an aqueous phase at pH of 2.3 showed phase separation while that prepared with pH of 4.5 showed a bimodal distribution. One explanation for this could be the presence of H^+ may result in the presence of oleic acid mainly in a protonated form. This may have then affected the degree of complexation.

On a different extension of miniemulsion formations, a miniemulsion using titanium (IV) isopropoxide was prepared with AAEMA as the ligand with a molar ratio of 1 : 10, in order to check if those two hours of stability is enough to form stable miniemulsions. Unfortunately, the miniemulsions formed underwent a phase separation. AAEMA was, therefore, not used in further experiments.

4.3.4.2. Using oleic acid within vinylic monomers mixture

- **First results**

Two miniemulsions were performed using the monomer / oleic acid mixture shown in Table 18, each with a different Ti to oleic acid molar ratio, namely 1 : 10 and 1 : 4. Even though the previous hydrolytic stability tests were performed using titanium (IV) isopropoxide, those miniemulsions were prepared with titanium (IV) 2-ethylhexyl oxide based on the results obtained from oleic acids miniemulsions, as above mentioned.

Investigation of the miniemulsions with DLS measurements showed bimodal droplet size distributions for both samples. Since no significant difference was available, it was decided that polymerization would be pursued with samples using 1 : 4 Ti to oleic acid molar ratios to avoid an unnecessary presence of oleic acid. Polymerization was then carried out using KPS and AIBN. Only with the latter did polymerization proceed to completion. To check if TiO₂ can be induced, a quick test was performed where the miniemulsion was treated with ethylene diamine, diethylamine or triethylamine. In all three cases, the miniemulsion phase separated while titanium dioxide precipitated. As a concept check, it was successful, but modification of the process was still required so that miniemulsion would remain stable. No further fine-tuning was done at this stage, since increase in TiO₂ loading was still necessary.

- **Increasing TiO₂ loading**

Assuming a full condensation of the TiO₂-precursor to TiO₂, we would have only a TiO₂ loading of 1.6 wt% in the miniemulsion, as above prepared. Therefore, one main target is to increase the loading of TiO₂ to about 5 wt% of the miniemulsion. To do this, one should increase the amount of the TiO₂-precursor in the formulation which consequently means increasing the oleic acid content in the formulation.

First changes were made to achieve this higher loading by changing the alkoxide precursor from titanium (IV) 2-ethylhexyl oxide to titanium (IV) n-butoxide. This was done for a couple of reasons: with an n-butoxide based precursor, we have lower weight in the dispersed phase to induce the same amount of TiO₂; also when oleic acid caps the titanium (IV) n-butoxide, n-butanol is then released which has more water solubility and can thus be released from the droplet or even act as phase compatibilizer. The result of several trials showed that the lowest oleic acid content used to stabilize the higher loading

was found to be a Ti to oleic acid molar ratio of 7 : 10. Table 19 shows the modified monomer mixture with increased oleic acid content.

Table 19 Weight percent of the monomer mix containing oleic acid as the ligand after titanium alkoxide precursor loading increase.

Constituent	Weight percent
Butyl acrylate	24.7
Methyl methacrylate	27.1
Styrene	25.9
Oleic acid	22.3

Another variable that was changed was the ALS-33 content. So far, in all experiments, ALS-33 concentration of 2.5 wt% to dispersed phase has been used. The target was to reduce the ALS-33 concentration so that the mean droplet diameter would reach about 350 nm, so that titanium dioxide particles that would eventually be generated inside the particles would not be too small, i.e. so that white pigment properties would remain. As a result of several experiments, it was found that a mean droplet diameter of about 340 nm before polymerization was obtained with an ALS-33 amount of 0.25 wt% at a solid content of 20 wt%.

▪ Polymerization of the high TiO₂-loaded miniemulsions

A few attempts to polymerize the above sample using AIBN or KPS have failed due to coagulation of the miniemulsion. Heating up the miniemulsion without any initiator has shown that the miniemulsion prepared was not stable at high temperatures and phase separation always resulted at temperatures above 45 °C. This meant that low temperature polymerization was necessary to keep the miniemulsion identity. A lot of work has been done in this respect using UV initiators, redox initiators, as well as low temperature thermal initiators. The best result was obtained using a mixture of V-70 and AIBN, both oil soluble azo-based thermal initiators, with ten hour half life time of 30 °C and 65 °C in toluene, respectively. The miniemulsion was first heated to 30 °C for about fourteen hours bringing the solid content to 13 wt%, followed by increasing the temperature to 65 °C for six hours brought the polymerization to completion without any coagulates.

There were two main remarks at this point: 1) the color of the miniemulsion had changed to white (from pink) during the process, which was a first indication that the Ti-oleic acid complex has been disrupted. 2) DLS measurements, shown in Figure 39, demonstrate the

formation of bimodal particle size distribution but after polymerization with V-70 which persists with post polymerization using AIBN.

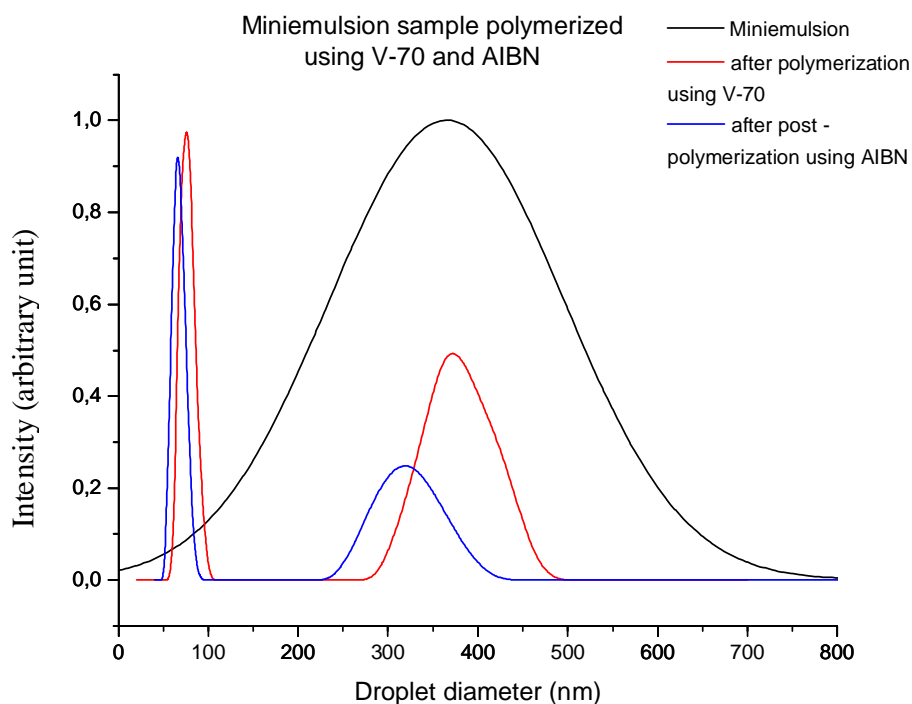


Figure 39 DLS results showing droplet diameters for the miniemulsion after preparation, after polymerization using V-70 and after post-polymerization using AIBN. Droplet diameters are based on a volume distribution based on either NICOMP or Gaussian distribution, depending on the χ^2 value. For the miniemulsion as prepared, the distribution is that of Gaussian, while after polymerization is that according to NICOMP.

▪ Discussion and conclusion

There were two main drawbacks for this system, which will be stated hereunder.

One is related to the miniemulsion properties, namely that the miniemulsion always ended up with a bimodal distribution after polymerization. Since the miniemulsions were prepared using n-hexadecane, Ostwald ripening is thus repressed. Also, since the miniemulsions were prepared with relatively hydrophobic monomers, no secondary nucleation is expected during polymerization. So what creates this bimodal distribution? One very plausible explanation is inspired by Musyanovych et al. where they also encountered in their work a bimodal particle size distribution created, as in our case, during polymerization¹⁵¹. This was attributed to a budding effect where additional stabilization was created within the growing particles during polymerization as a result of

formation of ionic polymers. Eventually, those fractions of the particles which are additionally stabilized split. Our hypothesis is that this same budding effect does take part as well, also due to the presence of additional stabilization that takes place via oleic acid. In the work done by Saygı-Arslan et al.¹⁵², they prepared emulsions using in-situ preparation of the surfactant at the water/oil interface. In their work potassium oleate (cmc = 0.22 wt%) was the surfactant produced in-situ, i.e. oleic acid was added to styrene in the oil phase while the aqueous phase contained KOH, thus producing potassium oleate and subsequently (either by sonication or stirring) an emulsion was formed. In other words, the oleate species are surface active. If oleate was created (deprotonated oleic acid) triggered for some reason during the polymerization stage, this may eventually lead to a splitting of the droplets or particles, leading to the budding effect. For example, this could be temperature-triggered since already the formation of micelles is temperature dependent, with the so-called Krafft point²³. If oleic acid is slowly consumed within the miniemulsion for the stabilization of new particles, this might also lead to a release of titanium species leading to hydrolysis and a subsequent TiO₂ formation, which actually also fits to the change in color that occurred during polymerization.

This brings us to the second main drawback, the size of TiO₂ particles and the film properties. SEM images shown in Figure 40 illustrate that TiO₂ formed particles are about 10 nm or smaller. At this size, typically sizes from 2 – 50 nm of titanium dioxide particles, become transparent as visible light is in this case transmitted. Thus they are used mainly as UV blockers as they lose any white pigment properties¹⁵³. This was indeed confirmed by forming a film on a glass substrate showing an almost transparent film. Another important property observed for this film was that it was formed at room temperature instead of usually at about 60 °C. This indicated that the minimum film formation temperature was greatly reduced due to the presence of oleic acid, which has obviously acted in the system as a softener or plasticizer. This could also be observed from SEM images shown in Figure 40 where no discrete particles were found.

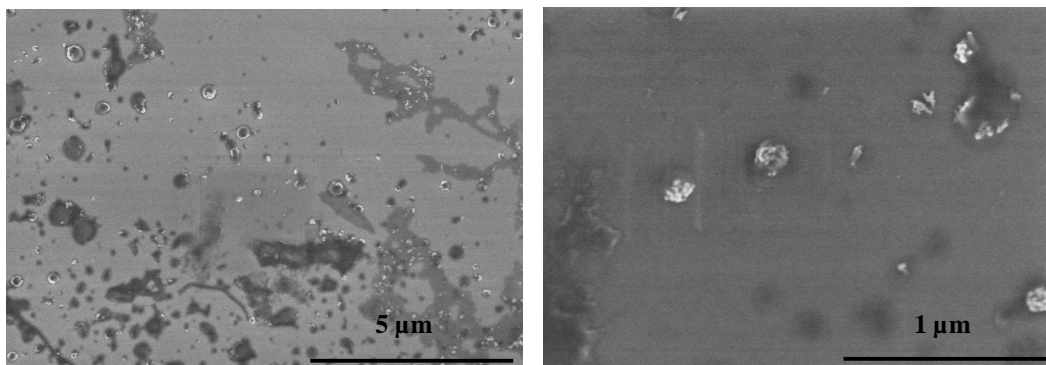


Figure 40 SEM image^{xi} for sample prepared with ca. 5 wt% TiO₂ loading after polymerization.

To sum up, the presence of oleic acid has resulted in a change in film properties and a bimodal particle size distribution. Therefore, a replacement was necessary for this system. At this point, all efforts were allocated for the multiple miniemulsion project and no further work was carried out in this one.

^{xi} SEM images were taken with Hitachi SU8000 at an accelerating voltage of 1 kV.

5. Experimental procedures

In this work, pre-homogenization was carried out using a rotor stator from Ystral, model X10/25 with 10/F shaft, with a speed of 11,000 rpm. Homogenization was carried out using ultrasound, a Branson 450 W sonifier with a ½" tip. Ultrasonication was always carried out at amplitude of 90%, with a ten seconds pulse time and five seconds pause between each pulse. During ultrasonication, the samples are placed in an ice bath to avoid heating up of the sample.

5.1. Preparation of water-based hybrid inorganic - polymer particles via multiple miniemulsions

▪ Preliminary tests for choosing inorganic ingredients

In the preliminary tests carried out to determine suitable zinc phosphate precursors, zinc precursor was dissolved in 10 ml of DI water while the surfactant PE/B-*b*-PEO (2.5 wt% to the dispersed phase) was dissolved in 25 g of cyclohexane (or Isopar M) by stirring, followed by an ultrasonication bath at 60 °C for 30 min. Both phases were then added together and pre-emulsified for two min., followed by ultrasonication for 2 min. The phosphoric acid miniemulsion was prepared from phosphoric acid solution in the same manner outlined above. Both miniemulsions were added together and ultrasonicated for four min. The amounts of each precursor used are listed in Table 20. For the XRD characterization, the resulting miniemulsion was freeze-dried in case of cyclohexane or centrifuged and left to dry at room temperature in case of Isopar M.

Table 20 Different zinc precursors used in preliminary experiments and their respective amounts.

Sample	Zn precursor	Zn precursor (mg)	Zn ²⁺ : PO ₄ ³⁻ (molar)
A	Zn(NO ₃) ₂ · 6 H ₂ O	594.98	1 : 1.05
B	Zn(NO ₃) ₂ · 6 H ₂ O	446.235	1.5 : 1
C	Zn(CH ₃ COO) ₂ · 2 H ₂ O	439.02	1 : 1.05

For the preliminary experiments of calcium carbonate and barium sulfate, precursor amounts were used as is given in Table 22 for the 5 wt% loading. The same continuous

phase and procedure was used as described above for zinc phosphate preparation with replacing the 2.5 wt% PE/B-*b*-PEO with 2.5 wt% Fortegra 100.

- **Proof of concept using styrene and zinc phosphate**

The same procedures and concentrations as outlined in the preliminary experiment were used but replacing cyclohexane with styrene. The precursor amounts are that of sample C in Table 20, 25 g of styrene and 2.5 wt% of PE/B-*b*-PEO were used.

Once the co-homogenization of the inverse miniemulsions was carried out, about 10 g of the inverse miniemulsion was added to a solution of 260 mg ALS-33 (or Lutensol AT50) dissolved in 25 g DI water followed by sonication for 4 min.

For the polymerization, 1.5 wt% to styrene of KPS or AIBN were used. KPS was added as solution after heating up the miniemulsion while AIBN was added by dissolving in the inverse miniemulsion before transferring to direct one. Polymerization was carried out at the ten hour half life time of the thermal initiator for about 18 h.

- **synthesis within polymerizable phase of butyl acrylate, methyl methacrylate and styrene**

Those set of experiments were used to evaluate the different w/o surfactants. Same procedure and components were used but only replacing the 25 g of styrene with 25 g of a mixture composed of 31.5 wt% butyl acrylate, 33.6 wt% methyl methacrylate and 34.9 wt% styrene. Additionally 4 wt% to the dispersed phase of n-hexadecane was used. The evaluated surfactants were also used at a concentration of 2.5 wt% and the precursors in an amount as in sample C (Table 20).

For transfer to direct miniemulsion, only ALS-33 was used. 10 g of the inverse miniemulsion containing zinc phosphate were added to 25 g of water containing 73.6 mg of ALS-33.

In addition to the two above mentioned thermal initiators, V-70 was evaluated which was also dissolved in the inverse miniemulsion before transfer to direct one.

- **synthesis within polymerizable phase containing mixture of vinylic monomers, epoxy and latent curing agent**

In general, the following procedure was carried out: for the preparation of the continuous phase of the inverse miniemulsions containing precursor solutions, two identical mixtures of monomer and epoxy resins, including a latent epoxy curing agent, were prepared.

Experimental procedures

Constituents and concentrations are shown in Table 21. To this mixture, one suitable w/o surfactant was used. The amount of the added surfactant was varied from 1.25 wt% to 7.5 wt%, in ratio to the dispersed phase, i.e. water and the precursor. Both D.E.R. and Vestagon B 1530, being in solid form, are allowed to dissolve in the monomer, surfactant-containing mixture overnight on a shaker or via insertion in an ultrasound bath followed by stirring, till complete dissolution.

Table 21 Polymerizable phase constituents and their concentration as a variable of epoxy resin content.

Polymerizable phase constituent	50 wt% epoxy	45 wt% epoxy	40 wt% epoxy	35 wt% epoxy
D.E.R. 664	17.82 g	16.135 g	14.43 g	12.70 g
Butyl acrylate	5.31 g	5.88 g	6.45 g	7.03 g
Methyl methacrylate	5.67 g	6.275 g	6.89 g	7.51 g
Styrene	5.88 g	6.51 g	7.14 g	7.78 g
2-hydroxyethyl methacrylate	0.67 g	0.74 g	0.81 g	0.89 g
Methacrylic acid	0.29 g	0.32 g	0.35 g	0.38 g
Vestagon B 1530	2.27 g	2.05 g	1.84 g	1.62 g

Precursor 1 for the inorganic material of interest is dissolved in 10 g of deionized water. Similarly, precursor 2 is also dissolved in 10 g of deionized water. Exact amounts of precursor 1 and precursor 2 depend on the desired loading and are given in details in Table 22.

Table 22 Composition of precursor solution 1 and precursor solution 2 for the preparation of the different zinc phosphate, calcium carbonate and barium sulfate samples.

Inorganic loading in ratio to organic content	Precursor 1 solution (dissolved in 10 g DI water)	Precursor 2 solution (dissolved in 10 g DI water)
1 wt% zinc phosphate	0.44 g zinc acetate dihydrate	242.12 mg phosphoric acid
2.5 wt% zinc phosphate	1.10 g zinc acetate dihydrate	605.29 mg phosphoric acid
5 wt% zinc phosphate	2.20 g zinc acetate dihydrate	1.21 g phosphoric acid
2.5 wt% calcium carbonate	1.71 g calcium acetate monohydrate	1.03 g sodium carbonate
5 wt% calcium carbonate	3.51 g calcium acetate monohydrate	2.11 g sodium carbonate
2.5 wt% barium sulfate	1.06 g barium acetate	0.59 g sodium sulfate
5 wt% barium sulfate	2.18 g barium acetate	1.21 g sodium sulfate

For the preparation of inverse miniemulsion 1, precursor solution 1 is added to the corresponding monomer / epoxy resin / latent curing agent mixture containing an inverse surfactant at chosen concentration based on precursor 1 solution, followed by pre-homogenization for two min. Directly afterwards, the mixture was ultrasonicated for two min. For the preparation of inverse miniemulsion 2, the same procedure carried out for inverse miniemulsion 1 is employed.

To form the inorganic pigment in-situ, both inverse miniemulsion 1 and inverse miniemulsion 2 are added together and ultrasonicated for four min.

In the meantime, 1.68 g of ALS-33 are dissolved in 110 g of deionized water. 37.91 g of the co-mini-emulsified inverse miniemulsion are added to the ALS-33 solution, followed by pre-homogenizing for 4 min. Afterwards, the mixture was ultrasonicated four min. The direct miniemulsion is then transferred to a 250 ml two neck round bottom flask, purged for 10 min with nitrogen gas and is heated up in an oil bath while stirring using a magnetic stirrer. The temperature of the miniemulsion is monitored via an inserted thermometer. When the temperature of the miniemulsion reaches 60 °C, a solution comprised of 442 mg of potassium persulfate dissolved in 10 g of deionized water, is added directly to the miniemulsion. Polymerization is carried out at 60 °C for 16 h.

5.2. Preparation of zinc phosphate - polymer miniemulsion for corrosion tests

The preparation of 1st and 3rd salt spray testing run was carried out using ultrasound as explained above. For the 2nd run, high pressure homogenization was carried out. For those set of samples, Pre-emulsification was carried out using an ultraturrax T25 basic (IKA Labortechnik) for about two min. while homogenization was carried out using Microfluidizer Processor M-110Y (Microfluidics, USA), operating at 10,000 psi outlet pressure for 3 passes. The procedure steps as well as concentrations are identical to that described above.

For the 3rd run, the polymerizable phase constituents that makes up the inverse miniemulsion for each precursor was altered to: 6.986 g D.E.R. 671, 3.122 g butyl acrylate, 0.170 g methacrylic acid, 3.334 g methyl methacrylate, 3.458 g styrene, 0.197 g hydroxypropyl methacrylate, 0.197 g glycidyl methacrylate and 1.490 g Vestagon B 1530.

All other constituents (surfactants, inorganic precursors), their concentration and procedure remain unchanged.

5.3. Preparation of water-based titanium dioxide - polymer particles via a single miniemulsion

5.3.1. Hydrolytic stability tests

- **Alkoxide precursors and their corresponding alcohols**

Two phases were prepared separately. The aqueous phase was 25 ml of water at the required pH. The whole pH range was tested with an interval of 0.3 – 0.5 pH difference. The organic phase was composed of 1 mmol of titanium (IV) alkoxide precursor in 10 ml of corresponding alcohol. Both mixtures were then added together and observed for any precipitation.

- **Use of ligands**

- Oleic acid: the same procedure was used as described above, only that 31.5 mmol of oleic acid was used instead of 10 ml of corresponding alcohol, while changing the pH. Titanium (IV) isopropoxide was used as the precursor (1 mmol). Oleic acid concentration was also changed to 25, 20, 15, 10, 5 and 1 mmol.
- Acrylic acid and methacrylic acid: 10 and 31.5 mmol were used.
- AAEMA, acetylacetone, GR-80, phosphate of caprolactone modified 2-hydroxyethyl methacrylate: only 10 mmol was used.
- N-octylphosphonic acid: 2.5 mmol of the acid in 2 ml of chloroform followed by the addition of titanium (IV) isopropoxide (0.25 mmol), so that the molar ratio of precursor:ligand is 1 : 10 were added to 6.5 ml of water.
- Diethyl vinylphosphonate: 0.5 mmol of titanium(IV) isopropoxide was added to 5 mmol of diethyl vinylphosphonate and mixed with 12.5 ml of water.

- **Mixtures of ligands and vinylic monomers**

- Mixture A: titanium (IV) isopropoxide (1 mmol and 0.4 mmol) was added to 8.3 g of mixture A so that the total mmoles of ligand available = 4 mmol, i.e. precursor to ligand molar ratio would be 1 : 4 and 1 : 10, respectively. The organic phase was then added to 25 ml of water, adjusted to required pH.

- Mixture B: exact procedure as mixture A, only 8.7 g of mixture B was used in order to keep same molar ratios to alkoxide precursor.
- Mixture C: same as above but using 9 g of mixture C.

All components and concentrations of the mixtures are given in Table 23.

Table 23 Composition and concentration of vinylic monomers and ligands used.

Constituent	Mixture A (wt%)	Mixture B (wt%)	Mixture C (wt%)	Mixture D (wt%)
Butyl acrylate	30.0	25.6	27.8	24.7
Methyl methacrylate	33.0	36.0	30.5	27.1
Styrene	31.5	33.1	29.1	25.9
Methacrylic acid	1.5	-	-	-
2-hydroxyethyl methacrylate	4.0	-	-	-
AAEMA	-	5.3	-	-
Oleic acid	-	-	12.6	22.3

5.3.2. Miniemulsions

▪ With oleic acid

Throughout all the miniemulsions prepared with pure oleic acid, the following parameters were kept constant: amount of oleic acid (10 mmol), alkoxide precursor (1 mmol), type of surfactant (ALS-33), amount of surfactant (2.5% to dispersed phase), volume of aqueous continuous phase (25 ml).

All the miniemulsions were prepared in the same manner: the dispersed phase is composed of the oleic acid and the alkoxide precursor, while the continuous phase is composed of the aqueous phase at a predetermined pH value and ALS-33. After dissolving ALS-33 in the aqueous phase, both phases were added together and stirred for one hour as a pre-mini-emulsification followed by ultrasonication for two min.

The following variables were then changed, one at a time:

- Precursor: the evaluated precursors were titanium (IV) ethoxide, titanium (IV) isopropoxide, titanium (IV) n-butoxide and titanium (IV) 2-ethylhexyl oxide. Distilled water was used for those experiments.

- pH: following pH of aqueous phase were used: besides distilled water, also solutions with a pH of 2.3, 4.5 and 9.15 were used. For those experiments, titanium (IV) 2-ethylhexyl oxide was used as precursor.

- **With AAEMA**

One single miniemulsion was prepared. Exact same procedure was used as in oleic acid. Titanium (IV) isopropoxide and distilled water were used.

- **Mixture C**

Miniemulsions were prepared with same Ti to oleic acid molar ratios stated above for mixture C, using titanium (IV) 2-ethylhexyl oxide. All other conditions kept constant.

Miniemulsions were prepared same as with pure oleic acid, with substituting stirring with one hour by pre-homogenization using the rotor stator for two min.

Polymerization was carried out for the miniemulsion prepared with a 1 : 4 molar ratio of Ti to oleic acid using KPS solution, at 70 °C for three hours under nitrogen flow. Additionally AIBN was also tried out, by dissolving it first in organic phase. Polymerization in this case was carried out at 80 °C for two and a half hours. In both cases, 1.5 wt% of thermal initiators to vinylic monomers were used.

- **Mixture D**

Miniemulsions to increase TiO₂ loading:

12.6 g of mixture D (shown in Table 23) and 2.4 g of titanium (IV) n-butoxide were used so that Ti to oleic acid ratio is 7 : 10. ALS-33 was varied from 2.5 wt% to 0.25 wt% in ratio to dispersed phase. 4 wt% to dispersed phase of n-hexadecane was dissolved in the dispersed phase. Aqueous phase volume was changed from 25 g to 120 g, dependent on solid content.

For polymerization of samples, 120 g of water and 0.25 wt% of ALS-33 were used. KPS, AIBN or V-70 and AIBN mixture were used, each with a concentration of 1.5 wt% to vinylic monomers. Details on polymerization were given in results section.

6. Conclusion

In this work, a synthetic route was designed for the incorporation of inorganic materials within water-based miniemulsions with a complex and adjustable polymer composition that would suit coatings application. The process involved co-homogenization of two inverse miniemulsions constituting precursors of the desired inorganic salt dispersed within a polymerizable continuous phase, followed by transfer to a direct miniemulsion via addition to an o/w surfactant solution with subsequent homogenization and radical polymerization. To our knowledge, this is the first work done where a polymerizable continuous phase has been used in an inverse (mini)emulsion formation followed by transfer to a direct miniemulsion, followed by polymerization, so that the result is a water-based dispersion. The versatility of the process was demonstrated by the synthesis of different inorganic pigments, but also the use of unconventional mixture of vinylic monomers and epoxy resin as the polymerizable phase (unconventional as a miniemulsion continuous phase but typical combination for coating applications). The polymerizable phase was composed of a mixture of vinylic monomers (styrene and acrylics) but also a medium molecular weight, solid epoxy resin as well as a latent epoxy curing agent. A lot of effort was dedicated to finding a suitable w/o surfactant to form the inverse miniemulsion with a polymerizable phase. For the synthesis of various inorganic pigments, an amphiphilic block copolymer surfactant under the trade name of Fortegra 100 was used as the w/o surfactant. This surfactant was chosen not only based on its performance during sample preparation, but also since it is commercially available as an epoxy toughening agent which may thus bring also toughening properties to the coatings. Furthermore, the epoxy resin content was found to be crucial in the formulation. The particle size distribution of the water-based miniemulsion was found to be dependent on the viscosity of the polymerizable phase and consequently on the content of epoxy resin. The epoxy resin content was adjusted so that particle size distribution would lie within a typical miniemulsion range, i.e. mean diameter between 50 and 500 nm.

As for the inorganic pigments, preliminary tests in cyclohexane were carried out in order to determine the resulting crystal structures, as well as the optimum precursor combination and concentration. Zinc phosphate, calcium carbonate and barium sulfate

were all successfully incorporated in the polymer-epoxy matrix. Samples were prepared with a pigment loading of up to 5 wt% to the organic content and were investigated using electron microscopy techniques (TEM and electron diffraction) as well as elemental analysis was performed using XRF and ICP-OES. Depending on the pigment type, different results in terms of pigment distribution within the polymeric-based particles were observed, indicating complex pigment-soft matter interactions. The choice of the system was based on a typical functional coatings system, but is not limited to. This system can be extended to incorporate various inorganic and further materials as long as the starting materials are water-soluble or hydrophilic.

The hybrid zinc phosphate – polymer water-based miniemulsion, containing 2.5 wt% zinc phosphate loading, prepared by the above route was then applied to steel panels using autodeposition process. This is considered the first autodeposition coatings process to be carried out from a miniemulsion system containing zinc phosphate particles. Those steel panels were then tested for corrosion protection using salt spray tests. The tests showed that the content of surfactant as well as the polymerizable phase composition affected the wet adhesion of the coating and consequently corrosion performance. Polymerizable phase formulation was thus modified all with the aim of improving adhesion to substrate. Those modifications included: 1) increasing epoxy resin content using low molecular weight, solid epoxy resin; 2) use of glycidyl methacrylate to promote crosslinking between the epoxy resin and the vinylic monomers and lastly; 3) other w/o surfactants were evaluated at reduced concentrations. Process and zinc phosphate loadings remained unchanged. Such modifications also illustrate that the synthetic route is truly versatile where adjustments in the monomers, concentrations as well as surfactants can be made in order to fit the application in question.

Salt spray tests after formulation modification showed that the hybrid particles can protect substrate from corrosion and even improve corrosion protection, compared to a control sample where corrosion protection was performed at a separate step.

Investigation of film cross section was also carried out using electron microscopy techniques (SEM and EDX). The miniemulsion was applied on an aluminium thin film which in turn is applied on a silicon wafer and heat treated with two different temperatures, pre-curing at 105 °C and full curing at 180 °C, with investigation after each

heat treatment. Those investigations show that zinc phosphate particles diffuse through the film as a result of heat treatment, with a certain affinity to be situated at the metal / coating interface, but also to aggregate at the higher temperatures. The mechanism of corrosion protection was thus suggested to be related to this mobility and consequently the presence at the metal / coating interface. In the future, it would be interesting to determine the crystal structure of zinc phosphate at the interface with a metal in general, as well as for steel in specific. Moreover, further studies on temperature controlled diffusion, at different temperatures, its behavior and effect on corrosion protection could also be of interest.

To recapitulate, this work has shown that a hybrid zinc phosphate – polymer miniemulsion applied via autodeposition coating can improve corrosion protection for steel substrates, illustrating the possibility for hybrid coatings to replace single functionality coatings. The synthetic route was designed to be flexible with the possibility of adjusting the polymerizable phase composition and inorganic precursor composition. The fact that the process was also performed completely organic-solvent free and that miniemulsions can be scaled-up using high pressure homogenizers, opens to this route vast opportunities for different industries, not only coatings applications.

7. Appendix I – Characterization methods

▪ **Dynamic light scattering (DLS)**

DLS was used to determine droplet (before polymerization) and particle (after polymerization) size distributions of the miniemulsions. It was carried out using NICOMP 380 particle sizer at a scattering angle of 90°. Measurements for direct miniemulsions were done at a temperature of 23 °C and using a laser whose wavelength is 635 nm and were highly diluted with deionized water prior to DLS measurements. Measurements for inverse miniemulsions (continuous phase of butyl acrylate, methyl methacrylate and styrene) were carried out at 20 °C using samples diluted with same continuous phase. Throughout this work, only volume average based mean diameters and distributions are given.

▪ **X-ray fluorescence (XRF)**

XRF was used in elemental analysis and was performed using an Axios (PANalytical) with an Rh tube, operating at a power of 4 kW. The samples were freeze-dried to remove the continuous aqueous phase before analysis.

▪ **Inductively coupled plasma-optical emission spectroscopy (ICP-OES)**

Also ICP-OES was used for elemental analysis. An Activa M spectrometer (Horiba Jobin Yvon, Bernsheim, Germany) equipped with a Meinhardt-type nebulizer, a cyclone chamber and controlled by ACTIVAnalyst 5.4 software was used. For analysis, the dispersions were diluted to a solid content of 0.5 wt% using a solution with 0.75 wt% SDS solution. The Argon emission line at 404.442 nm was used as reference line. Measurements were performed using four different standard concentrations. As baseline correction, a dynamic underground correction provided by the software was used. The emission lines chosen for the characterization of the respective elements were: 202.548 nm, 206.200 nm and 481.053 nm for Zn; 177.433 nm and 178.221 nm for P; 370.603 nm, 373.690 nm and 422.673 nm for Ca; 234.759 nm, 389.178 nm and 413.065 nm for Ba analysis. The measurements were performed in triplicate and averaged. The method was devised in¹⁵⁴.

▪ **Transmission electron microscopy (TEM)**

For imaging of the samples and electron diffraction, a Tecnai F20 (Fei) with an accelerating voltage of 200 kV was used. Samples were diluted and added to a carbon coated copper grid by drop casting and left to dry at room temperature.

Some samples were also investigated using a Philips CM12, with an accelerating voltage of 120 kV. Samples were diluted and placed on a Formvar coated copper grids. Samples in inverse miniemulsion form were investigated undiluted.

In the results and discussion section, the microscope used was indicated as footnotes to the images.

▪ **Scanning electron microscopy (SEM)**

With SEM, three different equipments were used to investigate the samples. A Hitachi SU8000 equipped with a Bruker Quanta 400 energy dispersive X-ray (EDX) analysis system, a Zeiss 1530 Gemini and a Philips XL30 were employed. For sample investigation using the latter, samples were sputtered with gold before imaging. All miniemulsion samples were highly diluted before sample preparation, unless the samples investigated were in inverse miniemulsion form.

For investigation of coating film cross section, either undiluted miniemulsion was added using drop casting directly on Si wafer or on a about 100 nm Al thin film applied using sputtering on a Si wafer. The condition was indicated as well as the equipment and accelerating voltage used as footnotes to the images in the results and discussion section.

▪ **X-ray Powder diffraction (XRD)**

XRD was used only to identify the inorganic pigments during preliminary experiments. Either Philips PW 1820 or Bruker AXS D5000 was employed, both using a Cu K α radiation with a wavelength of 1.54 Å.

8. Appendix II - Materials

In this work, all chemicals were used without further purification and monomers were used without distillation in order to mimic a typical industrial formulation. In all experiments deionized water was used.

8.1. *Materials used in inorganic-polymer multiple miniemulsion systems*

For the organic/polymer phase, styrene (for synthesis, Merck), methyl methacrylate (for synthesis, Merck), butyl acrylate (99%, Acros organics), methacrylic acid (99.5%, Acros organics), 2-hydroxyethyl methacrylate (97%, Acros organics), hydroxypropyl methacrylate (mixture of hydroxypropyl and hydroxyisopropyl methacrylate, 97%, Sigma-Aldrich), glycidyl methacrylate (97%, Acros organics), D.E.R. 664 (a medium molecular weight solid bisphenol-A diglycidyl ether epoxy resin based with an epoxy equivalent weight (EEW) value of 875 – 955 g/eq., Dow) or D.E.R. 671 (a low molecular weight solid epoxy resin based on bisphenol-A with EEW values of 475 – 550 g/eq., Dow), as well as Vestagon B 1530 (latent epoxy curing agent based on isophorone diisocyanate blocked with ϵ -caprolactam with an unblocking temperature over 170 °C, Evonik) were used. For the miniemulsions carried out without epoxy resin, n-hexadecane (analytical standard, Fluka) was used ultrahydrophobe.

The following surfactants were used for the preparation of inverse miniemulsions: Isolan GPS (polyglyceryl-4 diisostearate / polyhydroxystearate / sebacate, Evonik Goldschmidt), Isolan PDI (diisostearoyl polyglyceryl-3 dimer dilinoleate, Evonik Goldschmidt), Fortegra 100 (amphiphilic block copolymer, Dow) and Grinsted PGPR 90 (polyglycerol-polyricinoleate, Danisco). For the preparation of the direct miniemulsion, Disponil ALS 33 (33 wt% solution of ammonium lauryl sulfate, Cognis) was used, which was referred to in text as ALS-33.

Moreover, several surfactants have been investigated for the inverse miniemulsion synthesis, which failed to produce stable miniemulsions. Those were: amphiphilic block-copolymer poly(ethylene-co-butylene)-*b*-poly(ethylene oxide) (PE/B-*b*-PEO) with a

$M_w = 14,579.8$ g/mol), which was synthesized in our group via coupling “Kraton liquid” with ethylene oxide by anionic polymerization according to the process outlined in¹⁵⁵, Lubrizol U (poly(isobutylene-succinimide pentamine), Lubrizol France), Tween 20 (polyethylene glycol sorbitan monolaurate, Sigma-Aldrich), Span 80 (sorbitane monooleate, Sigma-Aldrich), Hostacerin DGI (diglycerol diisostearate, Clariant), Hostacerin DGMS (diglycerol monostearate, Clariant), Genapol UD 030 (nonylphenol poly(ethylene oxide) with 4 ethoxy units, Clariant), Hostaphat KL 340 D (lauryl polyethoxy phosphate ester with 4 ethoxy units, Clariant), Hostaphat KW 340 D (stearyl polyethoxy phosphate ester, with 4 ethoxy units, Clariant), Isolan IS (methyl glucose isostearate, Evonik Goldschmidt), Isolan GI 34 (polyglyceryl-4 isostearate, Evonik Goldschmidt) and last but not least Isolan GO 33 (polyglyceryl-3 oleate, Evonik Goldschmidt). Also, for the direct miniemulsion, Lutensol AT50 (alkylpolyethylene glycol ethers, with an alkyl chain of 16 or 18 units and 50 ethoxy units, BASF) was used. For the in-situ preparation of inorganic particles, the following precursors were used: phosphoric acid solution (H_3PO_4 , 85 wt%, ACS reagent, Sigma-Aldrich), zinc acetate dihydrate ($Zn(CH_3CO_2)_2 \cdot 2 H_2O$, 98+%, ACS reagent, Sigma-Aldrich), calcium acetate monohydrate ($Ca(CH_3CO_2)_2 \cdot H_2O$, $\geq 99\%$, ACS reagent, Sigma-Aldrich), sodium carbonate (Na_2CO_3 , anhydrous, analytical reagent, Riedel-de Haën), barium acetate ($Ba(CH_3CO_2)_2$, 99%, Alfa Aesar) and sodium sulfate (Na_2SO_4 , anhydrous, technical grade, Riedel-de Haën). Moreover for the preliminary experiments of inorganic synthesis, zinc nitrate hexahydrate ($Zn(NO_3)_2 \cdot 6 H_2O$, reagent grade 98%, Sigma-Aldrich), cyclohexane (for HPLC, VWR) and Isopar M (isoparaffin fluid, ExxonMobil) were also employed.

Potassium persulfate ($K_2S_2O_8$, p.a. Merck) was used for thermal initiation of the radical polymerization. Also 2,2'-Azobis(2-methylpropionitrile) (AIBN, 98%, Sigma-Aldrich), V-70 (2,2'-Azobis(4-methoxy-2.4-dimethyl valeronitrile), Wako) were also evaluated as thermal initiators.

Lastly, sodium dodecyl sulfate, (SDS, Sigma-Aldrich) was used to prepare a 0.75 wt% solution, for ICP-OES measurements, as explained in the characterization methods section.

8.2. Materials used in TiO₂-polymer single miniemulsion system

As titanium alkoxide precursors, the following were used: titanium (IV) ethoxide (purum, Sigma-Aldrich), titanium (IV) isopropoxide (purum, $\geq 97.0\%$, Sigma-Aldrich), titanium (IV) butoxide (reagent grade, 97%, Sigma-Aldrich) and titanium (IV) 2-ethylhexyloxy (95%, Sigma-Aldrich).

For the alcohols, ethanol (95%, Sigma-Aldrich), isopropanol (laboratory reagent, $\geq 99.5\%$, Sigma-Aldrich), n-butanol (ACS reagent, $\geq 99.4\%$, Sigma-Aldrich), 2-ethylhexanol ($\geq 99\%$, Sigma-Aldrich) were used.

As ligands the following were employed: oleic acid (technical grade, 90%, Sigma-Aldrich), 2-(acetoacetoxy)ethyl methacrylate (AAEMA, Lonzamon® AAEMA, Lonza), acetylacetone ($\geq 99.3\%$, Sigma-Aldrich), methacryloyloxyethyl succinate (GR-80, Henkel), phosphate of caprolactone modified 2-hydroxyethyl methacrylate (PM-21, Kayamer PM 21, Nippon Kayaku Co.) and n-octylphosphonic acid (98%, VWR), diethyl vinylphosphonate (97%, Sigma-Aldrich).

Vinyl monomers, surfactants and thermal initiators used in this work were the same ones used in multiple miniemulsion project.

9. Appendix III – List of abbreviations

AAEMA	2-(Acetoacetoxy)ethyl methacrylate
AIBN	Azobisisobutyronitrile
ALS-33	Ammonium lauryl sulfate, 33 wt% solution
BADGE	Bisphenol-A diglycidylether
cmc	Critical micelle concentration
DI water	Deionized water
DLS	Dynamic light scattering
EDX	Energy dispersive X-ray
EEW	Epoxy equivalent weight
GR-80	Methacryloyloxyethyl succinate
HR-TEM	High resolution transmission electron microscopy
ICP-OES	Inductively coupled plasma-optical emission spectroscopy
KPS	Potassium persulfate
NSS	Neutral salt spray
o/w	Oil-in-water
o/w/o	Oil-in-water-in-oil
(PE- <i>alt</i> -P)- <i>b</i> -PEO	poly(ethylene- <i>alt</i> -propylene)- <i>b</i> -poly(ethylene oxide)
PE/B- <i>b</i> -PEO	Poly(ethylene-co-butylene)- <i>b</i> -poly(ethylene oxide)
PEO	Polyethylene oxide
PM-21	phosphate of caprolactone modified 2-hydroxyethyl methacrylate
SDS	Sodium dodecyl sulfate
SEM	Scanning electron microscopy
SHE	Safety, health and environment
TEM	Transmission electron microscopy
UV	Ultraviolet
VOC	volatile organic compounds
w/o	Water-in-oil
w/o/w	Water-in-oil-in-water
XRD	X-ray diffraction
XRF	X-ray fluorescence

References

1. Kickelbick, G., *Introduction to Hybrid Materials*. Wiley-VCH Verlag GmbH & Co. KGaA: Weinheim, 2007; p 1-48.
2. Sanchez, C.; Julian, B.; Belleville, P.; Popall, M., Applications of hybrid organic-inorganic nanocomposites. *Journal of Materials Chemistry* 2005, 15 (35-36), 3559-3592.
3. Bourgeat-Lami, E.; Duguet, E., Polymer Encapsulation of Inorganic Particles. In *Functional Coatings*, Ghosh, S. K., Ed. Wiley-VCH Verlag GmbH & Co. KGaA: 2006; pp 85-152.
4. Briand, R.; Larson, G.; Procopio, L.; Rosano, W.; Smith, P., Making connections – Pigment-binder interaction enhances performance of exterior coatings. *European Coatings Journal* 2008, 10, 19-25.
5. Ghosh, S. K., *Functional Coatings and Microencapsulation: A General Perspective*. Wiley-VCH Verlag GmbH & Co. KGaA: Weinheim, 2006; p 1-28.
6. Bourgeat-Lami, E.; Lansalot, M., Organic/Inorganic Composite Latexes: The Marriage of Emulsion Polymerization and Inorganic Chemistry. In *Hybrid Latex Particles*, Springer Berlin / Heidelberg, 2011; Vol. 233, pp 53-123.
7. Rohm and Haas Avanse™ Technology: Breathing high performance environmentally advanced, low VOC coatings. In *Rohm and Haas*, 2007.
8. Landfester, K., Encapsulation Through (Mini)Emulsion Polymerization. In *Functional Coatings*, Ghosh, S. K., Ed. Wiley-VCH Verlag GmbH & Co. KGaA: 2006; pp 29-66.
9. Antonietti, M.; Landfester, K., Polyreactions in miniemulsions. *Progress in Polymer Science* 2002, 27 (4), 689-757.
10. Landfester, K.; Weiss, C., Encapsulation by Miniemulsion Polymerization. In *Advances in Polymer Science*, Springer Berlin / Heidelberg, 2010; Vol. 229, pp 1-49.
11. The Effects and Economic Impact of Corrosion. In *Corrosion: Understanding the Basics*, Davis, J. R., Ed. ASM International Ohio, 2000; pp 1-17.
12. Streitberger, H.-J., Introduction. In *Automotive Paints and Coatings*, Streitberger, H.-J.; Dössel, K.-F., Eds. Wiley-VCH Verlag GmbH & Co. KGaA: Weinheim, 2008; pp 1-11.
13. Nicholson, J. W., Polymersiation reactions. In *The Chemistry of Polymers*, 2nd ed.; The Royal Society of Chemistry: Cambridge, 1997; pp 27-46.
14. Braun, D.; Cherdron, H.; Rehahn, M.; Ritter, H.; Voit, B., Synthesis of Macromolecules by Chain Growth Polymerization. In *Polymer Synthesis: Theory and Practice*, 4th ed.; Springer Berlin Heidelberg, 2005; pp 157-262.
15. Arshady, R., Suspension, emulsion, and dispersion polymerization: A methodological survey. *Colloid Polym. Sci.* 1992, 270 (8), 717-732.
16. Nomura, M.; Tobita, H.; Suzuki, K., Emulsion Polymerization: Kinetic and Mechanistic Aspects. In *Polymer Particles*, Okubo, M., Ed. Springer Berlin / Heidelberg, 2005; Vol. 175, pp 1-128.
17. Chern, C. S., Emulsion polymerization mechanisms and kinetics. *Progress in Polymer Science* 2006, 31 (5), 443-486.

18. Antonietti, M.; Basten, R.; Lohmann, S., Polymerization in microemulsions — a new approach to ultrafine, highly functionalized polymer dispersions. *Macromolecular Chemistry and Physics* 1995, 196 (2), 441-466.
19. Crespy, D. Tuning Polymeric Latex Functionality via The Miniemulsion Technique. Doctoral dissertation, Universität Ulm, Ulm, 2006.
20. Rosen, M. J., Dispersion and Aggregation of Solids in Liquid Media by Surfactants. In *Surfactants and interfacial phenomena*, 3rd ed.; John Wiley & Sons, Inc. : New Jersey, 2004; pp 332-352.
21. Pashley, R. M.; Karaman, M. E., Charged Colloids. In *Applied Colloid and Surface Chemistry*, John Wiley & Sons Ltd.: West Sussex, 2004; pp 93-126.
22. Rosen, M. J., Adsorption of Surface-Active Agents at Interfaces: The Electrical Double Layer. In *Surfactants and interfacial phenomena*, 3rd ed.; John Wiley & Sons, Inc. : New Jersey, 2004; pp 34-104.
23. IUPAC. Compendium of Chemical Terminology, 2nd ed. (the "Gold Book"). Compiled by A. D. McNaught and A. Wilkinson. Blackwell Scientific Publications, Oxford (1997). XML on-line corrected version: <http://goldbook.iupac.org> (2006-) created by M. Nic, J. Jirat, B. Kosata; updates compiled by A. Jenkins. ISBN 0-9678550-9-8. doi:10.1351/goldbook. .
24. Tadros, T., General Principles of Colloid Stability and the Role of Surface Forces. In *Colloid Stability*, Tadros, T., Ed. Wiley-VCH: Weinheim, 2007; Vol. 1, pp 1-22.
25. Grasso, D.; Subramaniam, K.; Butkus, M.; Strevett, K.; Bergendahl, J., A review of non-DLVO interactions in environmental colloidal systems. *Reviews in Environmental Science and Biotechnology* 2002, 1 (1), 17-38.
26. Goel, A., Protection of Colloids. In *Colloidal Chemistry*, Discovery Publishing House Pvt. Ltd.: New Delhi, 2006; pp 88-91.
27. Kitchener, J. A., Principles of action of polymeric flocculants. *British Polymer Journal* 1972, 4 (3), 217-229.
28. Frelichowska, J.; Bolzinger, M.-A.; Chevalier, Y., Pickering emulsions with bare silica. *Colloids and Surfaces A: Physicochemical and Engineering Aspects* 2009, 343 (1-3), 70-74.
29. Binks, B. P., Particles as surfactants - similarities and differences. *Current Opinion in Colloid & Interface Science* 2002, 7 (1-2), 21-41.
30. Atkins, P. W., In *Physical Chemistry*, 6th ed.; Oxford University Press: Oxford, 1998; p 180.
31. Wicks, Z. W.; Jones, F. N.; Pappas, S. P.; Wicks, D. A., Corrosion protection by coatings. In *Organic coatings: science and technology*, 3rd ed.; John Wiley & Sons, Inc. : New Jersey, 2007; pp 137-158.
32. Austin, M. J., Inorganic anti-corrosive pigments. In *Paint and coating testing manual: fourteenth edition of the Gardner-Sward handbook*, Koleske, J. V., Ed. ASTM: Philadelphia, 1995.
33. Buxbaum, G.; Pfaff, G., Anticorrosive pigments. In *Industrial inorganic pigments*, 3rd ed.; Buxbaum, G.; Pfaff, G., Eds. Wiley-VCH: Weinheim, 2005; pp 207-229.
34. Pham, H. Q.; Marks, M. J., Epoxy Resins. In *Ullmann's Encyclopedia of Industrial Chemistry*, John Wiley & Sons, Inc.: 2010.

35. Kendig, M. W.; Buchheit, R. G., Corrosion inhibition of aluminum and aluminum alloys by soluble chromates, chromate coatings, and chromate-free coatings. *Corrosion* 2003, 59 (5), 379-400.
36. Gehmecker, H., Pretreatment of Multimetal Car Bodies. In *Automotive Paints and Coatings*, Streitberger, H.-J.; Dössel, K.-F., Eds. Wiley-VCH Verlag GmbH & Co. KGaA: Weinheim, 2008; pp 61-87.
37. Streitberger, H.-J., Electrodeposition Coatings. In *Automotive Paints and Coatings*, Streitberger, H.-J.; Dössel, K.-F., Eds. Wiley-VCH Verlag GmbH & Co. KGaA: Weinheim, 2008; pp 89-127.
38. Wicks, Z. W.; Jones, F. N.; Pappas, S. P.; Wicks, D. A., Electrodeposition coatings. In *Organic coatings: science and technology*, 3rd ed.; John Wiley & Sons, Inc. : New Jersey, 2007; pp 535-547.
39. Bammel, B. D., Recent developments in autodeposition coatings. *Metal Finishing* 2003, 101 (5), 38-43.
40. Bammel, B. D.; McGee, J. D., Novel autodepositing coating composition produced by mini-emulsion synthetic approach. *Polymer Preprints* 2004, 45 (2), 181-182.
41. Omar, M. A., New Concept in Automotive Manufacturing; a System-Based Manufacturing. In *New Trends and Developments in Automotive Industry*, Chiaberge, M., Ed. InTech: Rijeka, 2011; pp 177-190.
42. Hall, W. S., Autodeposition: a survey of a new water-borne coating technology. *Journal of coatings technology* 1980, 52 (663), 72-78.
43. Honda, T. K.-k., JP), Naito, Kazuhisa (Kanagawa-ken, JP) Autodeposition coating composition. US 5,646,211 1997.
44. McGee, J. D. T., MI, US); Bammel, B. D. R. H., MI, US); Yang, Z. T., MI, US) Corrosion resistant films based on ethylenically unsaturated monomer modified epoxy emulsions. US 7,138,444 B2, 2006.
45. Autodeposition process. <http://www.henkel.com/autodeposition-process-12740.htm> (accessed 29th June 2011).
46. Steinbrecher, L.; Dollman, D. Y.; Buczkowski, D. E.; Harrison, J. W. Method and apparatus for measuring fluoride activity. 3329587, 1967.
47. Agarwal, R. K. B., MI), Brown, Douglas (San Francisco, CA), Fristad, William E. (Rochester Hills, MI), Butcher, Graham (Buckingham, GB), Iqbal, Zafar (Batley, GB) Protective reaction rinse for autodeposition coatings. US 6,613,387 B2, 2003.
48. Bandau, A. H., Chemical resistance. In *Paint and Coating Testing Manual: Fourteenth Edition of the Gardner-Sward Handbook (Astm Manual Series)*, Koleske, J. V., Ed. ASTM: Philadelphia, 1995; pp 662-666.
49. Bos, T. Prediction of coating durability: early detection using electrochemical methods. Doctoral dissertation, Delft University of Technology, Delft, 2008.
50. Folta-Stogniew, E. J., Macromolecular Interactions: Light Scattering. In *Encyclopedia of Life Sciences*, John Wiley & Sons, Ltd: 2001.
51. Schärftl, W., Fundamental Concepts. In *Light scattering from polymer solutions and nanoparticle dispersions*, Pasch, H., Ed. Springer-Verlag: Berlin Heidelberg, 2007; pp 1-24.
52. Dynamic light scattering: an introduction in 30 minutes. Malvern Instruments Ltd.: Worcestershire, p 8.

53. Sperling, L. H., *Introduction to physical polymer science*. John Wiley & Sons, Inc. : New York, 2001.
54. Nicomp 380 DLS - User manual. Particle Sizing Systems, Inc. : Santa Barbara, 2006.
55. Lagaly, G.; Schulz, O.; Zimehl, R., *Dispersionen und Emulsionen - Einführung in die Kolloidik feinverteilter Stoffe einschliesslich der Tonminerale*. Dr. Dietrich Steinkopff Verlag, GmbH & Co. KG: Darmstadt, 1997.
56. Brouwer, P., *Theory of XRF: Getting acquainted with the principles*. 2nd ed.; PANalytical B.V.: Almelo, 2006.
57. Jenkins, R., X-Ray Fluorescence Spectrometry. In *Handbook of Analytical Techniques*, Günzler, H.; Williams, A., Eds. Wiley-VCH Verlag GmbH: Weinheim, 2001; Vol. 2, pp 753-766.
58. Goodhew, P. J.; Humphreys, F. J.; Beanland, R., Electron diffraction. In *Electron microscopy and analysis*, 3rd ed.; Taylor & Francis: London, 2001; pp 40-65.
59. Varnes, A., Inductively coupled plasma atomic emission spectroscopy. In *Handbook of instrumental techniques for analytical chemistry*, Settle, F. A., Ed. Prentice Hall: New Jersey, 1997; pp 395-418.
60. Nölte, J., *ICP Emission Spectrometry: A Practical Guide*. Wiley-VCH Verlag GmbH & Co. KGaA: Weinheim, 2003.
61. Zhou, W., Transmission Electron Microscopy. In *Metal Oxide Catalysis*, Wiley-VCH Verlag GmbH & Co. KGaA: 2009; pp 443-485.
62. Goodhew, P. J.; Humphreys, F. J.; Beanland, R., The transmission electron microscope. In *Electron microscopy and analysis*, 3rd ed.; Taylor & Francis: London, 2001; pp 66-121.
63. Smith, D. J., Characterisation of Nanomaterials Using Transmission Electron Microscopy. In *Nanocharacterisation*, Kirkland, A. I.; Hutchison, J. L., Eds. The Royal Society of Chemistry: Cambridge, 2007; pp 1-27.
64. Reichelt, R., Scanning electron microscopy. In *Science of microscopy*, Hawkes, P. W.; Spence, J. C. H., Eds. Springer Science+Business Media, LLC: New York, 2007; Vol. 1, pp 133-272.
65. Goodhew, P. J.; Humphreys, F. J.; Beanland, R., The scanning electron microscope. In *Electron microscopy and analysis*, 3rd ed.; Taylor & Francis: London, 2001; pp 122-168.
66. Michler, G. H., Scanning Electron Microscopy (SEM). In *Electron Microscopy of Polymers*, Springer Verlag: Berlin Heidelberg, 2008; pp 87-120.
67. Brydson, R., Electron Energy-loss Spectroscopy and Energy Dispersive X-Ray Analysis. In *Nanocharacterisation*, Kirkland, A. I.; Hutchison, J. L., Eds. The Royal Society of Chemistry: Cambridge, 2007; pp 94-137.
68. Schneider, R., Energy-dispersive X-ray Spectroscopy (EDXS). In *Surface and thin film analysis: principles, instrumentation, applications*, Bubert, H.; Jenett, H., Eds. Wiley-VCH: Weinheim, 2002; pp 194-208.
69. Landfester, K., The generation of nanoparticles in miniemulsions. *Advanced Materials* 2001, 13 (10), 765-768.
70. Landfester, K., Synthesis of colloidal particles in miniemulsion. *Annual Review of Materials Research* 2006, 36, 231-279.

71. Ramírez, L. P.; Landfester, K., Magnetic Polystyrene Nanoparticles with a High Magnetite Content Obtained by Miniemulsion Processes. *Macromolecular Chemistry and Physics* 2003, 204 (1), 22-31.
72. Tiarks, F.; Landfester, K.; Antonietti, M., Encapsulation of Carbon Black by Miniemulsion Polymerization. *Macromolecular Chemistry and Physics* 2001, 202 (1), 51-60.
73. Gan, L. M.; Chew, C. H., Polymerization in the transparent water-in-oil solutions (I). methyl methacrylate and the copolymerizable cosurfactant. *Journal of Dispersion Science and Technology* 1983, 4 (3), 291-312.
74. Palkovits, R.; Althues, H.; Rumpelcker, A.; Tesche, B.; Dreier, A.; Holle, U.; Fink, G.; Cheng, C. H.; Shantz, D. F.; Kaskel, S., Polymerization of w/o microemulsions for the preparation of transparent SiO₂/PMMA nanocomposites. *Langmuir* 2005, 21 (13), 6048-6053.
75. Abbasian, Z.; Moghbeli, M. R., Preparation of highly open porous styrene/acrylonitrile and styrene/acrylonitrile/organoclay polymerized high internal phase emulsion (PolyHIPE) foams via emulsion templating. *J. Appl. Polym. Sci.* 2010, 119 (6), 3728-3738.
76. Menner, A.; Powell, R.; Bismarck, A., Open Porous Polymer Foams via Inverse Emulsion Polymerization: Should the Definition of High Internal Phase (Ratio) Emulsions Be Extended? *Macromolecules* 2006, 39 (6), 2034-2035.
77. Menner, A.; Salgueiro, M.; Shaffer, M. S. P.; Bismarck, A., Nanocomposite foams obtained by polymerization of high internal phase emulsions. *J. Polym. Sci. Pol. Chem.* 2008, 46 (16), 5708-5714.
78. Bennett, D. J.; Burford, R. P.; Davis, T. P.; Tilley, H. J., Synthesis of porous hydrogel structures by polymerizing the continuous phase of a microemulsion. *Polymer International* 1995, 36 (3), 219-226.
79. Menger, F. M.; Tsuno, T.; Hammond, G. S., Crosslinked polystyrene incorporating water pools. *J. Am. Chem. Soc.* 1990, 112 (3), 1263-1264.
80. Seifriz, W., Studies in Emulsions. III-V. *The Journal of Physical Chemistry* 1925, 29 (6), 738-749.
81. Garti, N., Double emulsions - scope, limitations and new achievements. *Colloids and Surfaces A: Physicochemical and Engineering Aspects* 1997, 123-124, 233-246.
82. Matsumoto, S., W/o/w - type multiple emulsions with a view to possible food applications. *Journal of Texture Studies* 1986, 17 (2), 141-159.
83. Boutti, S.; Bourgeat-Lami, E.; Zydowicz, N., Silica/Polyamide Nanocomposite Synthesis via an Original Double Emulsification Process in Miniemulsion. *Macromol. Rapid Commun.* 2005, 26 (23), 1860-1865.
84. Landfester, K.; Bechthold, N.; Tiarks, F.; Antonietti, M., Formulation and Stability Mechanisms of Polymerizable Miniemulsions. *Macromolecules* 1999, 32 (16), 5222-5228.
85. Wicks, Z. W.; Jones, F. N.; Pappas, S. P.; Wicks, D. A., Epoxy and phenolic resins. In *Organic coatings: science and technology*, 3rd ed.; John Wiley & Sons, Inc. : New Jersey, 2007; pp 271-294.
86. Hegedus, C.; Pepe, F.; Dickenson, J.; Walker, F., Waterborne acrylic-epoxy coatings. *Journal of coatings technology* 2002, 74 (927), 31-39.

87. Tiarks, F.; Landfester, K.; Antonietti, M., Preparation of Polymeric Nanocapsules by Miniemulsion Polymerization. *Langmuir* 2001, 17 (3), 908-918.
88. Kojima, S.; Watanabe, Y., Development of high performance, waterborne coatings. Part I: Emulsification of epoxy resin. *Polymer Engineering & Science* 1993, 33 (5), 253-259.
89. Pan, G.; Wu, L.; Zhang, Z.; Li, D., Synthesis and characterization of epoxy-acrylate composite latex. *J. Appl. Polym. Sci.* 2002, 83 (8), 1736-1743.
90. Guy, A.; Marrion, A., Coatings components beyond binders. In *The Chemistry and Physics of Coatings*, The Royal Society of Chemistry: 2004; Vol. 1, pp 267-316.
91. Wicks, Z. W.; Jones, F. N.; Pappas, S. P.; Wicks, D. A., Inert pigments. In *Organic coatings: science and technology*, 3rd ed.; John Wiley & Sons, Inc. : New Jersey, 2007; pp 430-431.
92. Kresse, R.; Baudis, U.; Jäger, P.; Riechers, H. H.; Wagner, H.; Winkler, J.; Wolf, H. U., Barium and Barium Compounds. In *Ullmann's Encyclopedia of Industrial Chemistry*, Wiley-VCH Verlag GmbH & Co. KGaA: Weinheim, 2000.
93. Köhler, K.; Simmendinger, P.; Roelle, W.; Scholz, W.; Valet, A.; Slongo, M., Paints and Coatings, 4. Pigments, Extenders, and Additives. In *Ullmann's Encyclopedia of Industrial Chemistry*, Wiley-VCH Verlag GmbH & Co. KGaA: Weinheim, 2000.
94. Knovel Critical Tables (2nd Edition). Knovel: 2008.
95. Montemor, M. F.; Simões, A. M. P.; Ferreira, M. G. S., Chloride-induced corrosion on reinforcing steel: from the fundamentals to the monitoring techniques. *Cement & Concrete Composites* 2003, 25, 491-502.
96. Herschke, L.; Rottstegge, J.; Lieberwirth, I.; Wegner, G., Zinc phosphate as versatile material for potential biomedical applications Part 1. *Journal of Materials Science-Materials in Medicine* 2006, 17 (1), 81-94.
97. Marella, P.; Claverie, J. P., Nanoparticles of zinc phosphate: Preparation and dispersion in epoxy coatings: Applications to corrosion protection. *Polymeric Materials: Science & Engineering* 2005, 93, 452-453.
98. Castellano, M.; Matijevic, E., Uniform colloidal zinc compounds of various morphologies. *Chemistry of Materials* 1989, 1 (1), 78-82.
99. Parhi, P.; Manivannan, V.; Kohli, S.; McCurdy, P., Room temperature metathetic synthesis and characterization of [alpha]-hopeite, $Zn_3(PO_4)_2 \cdot 4H_2O$. *Materials Research Bulletin* 2008, 43 (7), 1836-1841.
100. Grzmil, B.; Kic, B.; Lubkowski, K., Studies on obtaining of zinc phosphate nanomaterials. *Reviews on Advanced Materials Science* 2007, 14 (1), 46-48.
101. Sziklai, G.; Szucs, I.; Megyerikanya, E., Preparation of Zinc Phosphate Pigments. *Hung. J. Ind. Chem.* 1982, 10 (2), 215-221.
102. Roming, M.; Feldmann, C.; Avadhut, Y. S.; auf der Gunne, J. S., Characterization of noncrystalline nanomaterials: NMR of zinc phosphate as a case study. *Chemistry of Materials* 2008, 20 (18), 5787-5795.
103. Herschke, L.; Enkelmann, V.; Lieberwirth, I.; Wegner, G., The role of hydrogen bonding in the crystal structures of zinc phosphate hydrates. *Chem.-Eur. J.* 2004, 10 (11), 2795-2803.
104. Pawlig, O.; Trettin, R., Synthesis and characterization of [alpha]-hopeite, $Zn_3(PO_4)_2 \cdot 4H_2O$. *Materials Research Bulletin* 1999, 34 (12-13), 1959-1966.

References

105. Al-Maydama, H. M. A.; Gardner, P. J.; McAra, I. W., The standard enthalpies of formation of zinc orthophosphate and its hydrates. *Thermochimica Acta* 1992, *194*, 117-127.
106. Frost, R. L., An infrared and Raman spectroscopic study of natural zinc phosphates. *Spectrochimica Acta Part A: Molecular and Biomolecular Spectroscopy* 2004, *60* (7), 1439-1445.
107. Dickie, R. A., Paint adhesion, corrosion protection, and interfacial chemistry. *Progress in Organic Coatings* 1994, *25* (1), 3-22.
108. Willert, M.; Rothe, R.; Landfester, K.; Antonietti, M., Synthesis of Inorganic and Metallic Nanoparticles by Miniemulsification of Molten Salts and Metals. *Chemistry of Materials* 2001, *13* (12), 4681-4685.
109. Pai, R. K.; Pillai, S., Nanoparticles of amorphous calcium carbonate by miniemulsion: synthesis and mechanism. *Crystengcomm* 2008, *10* (7), 865-872.
110. Thomas, I. M.; Weller, M. T., Synthesis, structure and thermal properties of phosphophyllite, $Zn_2Fe(PO_4)_2 \cdot 4H_2O$. *Journal of Materials Chemistry* 1992, *2* (11), 1123-1126.
111. Perez-Navarro, M.; Pera, G.; Haro, M.; Gascon, I.; Lafuente, C., Refractive Indices of the Ternary Mixtures Butanol plus n-Hexane+1-Chlorobutane. *Journal of Solution Chemistry* 2008, *37* (11), 1499-1510.
112. Grindstedt® PGPR Polyglycerol Polyricinoleate. http://www.danisco.com/products/product_range/emulsifiers/grindstedt_pgpr/ (accessed 9th July 2011).
113. Meyer, J.; Allef, P.; Fötsch, H., A Novel PEG-free Emulsifier Designed for Formulating W/O Lotions with a Light Skin Feel. *SÖFW-Journal* 2005, *131* (11), 20-28.
114. Bates, F. S. S. L. P., MN, US), Hahn, Stephen F. (Midland, MI, US) Amphiphilic block copolymer-toughened epoxy resins. US 2009/0082486 A1, 2009.
115. Fream, A.; Magnet, S., Low VOC, high performance coating formulation using surfactant-free latex blends. *Surface Coatings International Part B: Coatings Transactions* 2000, *83* (9), 447-454.
116. Landfester, K., Quantitative considerations for the formulation of miniemulsions. In *Adsorption and Nanostructures*, Dekany, I., Ed. 2002; Vol. 117, pp 101-103.
117. Nabih, N.; Schiller, R.; Lieberwirth, I.; Kockrick, E.; Frind, R.; Kaskel, S.; Weiss, C. K.; Landfester, K., Mesoporous CeO_2 nanoparticles synthesized by an inverse miniemulsion technique and their catalytic properties in methane oxidation. *Nanotechnology* 2011, *22* (135606).
118. Liu, J.; Sue, H.-J.; Thompson, Z. J.; Bates, F. S.; Dettloff, M.; Jacob, G.; Verghese, N.; Pham, H., Strain rate effect on toughening of nano-sized PEP-PEO block copolymer modified epoxy. *Acta Materialia* 2009, *57* (9), 2691-2701.
119. Thompson, Z. J.; Hillmyer, M. A.; Liu, J.; Sue, H. J.; Dettloff, M.; Bates, F. S., Block Copolymer Toughened Epoxy: Role of Cross-Link Density. *Macromolecules* 2009, *42* (7), 2333-2335.
120. Ni, M.; Ratner, B. D., Differentiating calcium carbonate polymorphs by surface analysis techniques—an XPS and TOF-SIMS study. *Surface and Interface Analysis* 2008, *40* (10), 1356-1361.

121. Thomer, K. W., Materials and Concepts in Body Construction. In *Automotive Paints and Coatings*, Streitberger, H.-J.; Dössel, K.-F., Eds. Wiley-VCH Verlag GmbH & Co. KGaA: Weinheim, 2008; pp 13-60.
122. Charneau, J. Y.; Kientz, E.; Holl, Y., Adhesion of latex films; influence of surfactants. *Progress in Organic Coatings* 27 (1-4), 87-93.
123. Schubert, U., Chemical modification of titanium alkoxides for sol-gel processing. *J. Mater. Chem.* 2005, 15 (35-36), 3701-3715.
124. Cozzoli, P. D.; Kornowski, A.; Weller, H., Low-temperature synthesis of soluble and processable organic-capped anatase TiO₂ nanorods. *J. Am. Chem. Soc.* 2003, 125 (47), 14539-14548.
125. Zhang, Z. H.; Zhong, X. H.; Liu, S. H.; Li, D. F.; Han, M. Y., Aminolysis route to monodisperse titania nanorods with tunable aspect ratio. *Angew. Chem.-Int. Edit.* 2005, 44 (22), 3466-3470.
126. Rammal, A.; Brisach, F.; Henry, M., Hydrothermal synthesis of TiO₂ anatase nanocrystals using hexaprismatic-shaped oxo-carboxylate complexes. *C. R. Chim.* 2002, 5 (1), 59-66.
127. Sui, R. H.; Thangadurai, V.; Berlinguette, C. P., Simple protocol for generating TiO₂ nanofibers in organic media. *Chem. Mat.* 2008, 20 (22), 7022-7030.
128. Mendez-Vivar, J.; Bosch, P.; Lara, V. H., Synthesis and spectroscopic study of mixed metal clusters using methacrylate and acrylate ligands. *J. Non-Cryst. Solids* 2005, 351 (24-26), 1949-1957.
129. Zhang, J.; Luo, S. C.; Gui, L. L., Poly(methyl methacrylate)-titania hybrid materials by sol-gel processing. *J. Mater. Sci.* 1997, 32 (6), 1469-1472.
130. Sayilkan, H.; Senre, S.; Sener, E.; Arpac, E., New metal alkoxides: Synthesis and hydrolysis-condensation reactions; some adsorption features of the hydrolysis-condensation products. *J. Mater. Sci.* 1999, 34 (21), 5325-5330.
131. Schubert, U.; Arpac, E.; Glaubitt, W.; Helmerich, A.; Chau, C., Primary hydrolysis products of methacrylate-modified titanium and zirconium alkoxides. *Chem. Mat.* 1992, 4 (2), 291-295.
132. Chen, H. J.; Wang, L. Y.; Chiu, W. Y.; Don, T. M., Synthesis of nanosized PAA/titania hybrid composites - Experiment and modeling. *Ceram. Int.* 2008, 34 (3), 467-477.
133. Miele-Pajot, N.; Hubert-Pfalzgraf, L. G.; Papiernik, R.; Vaissermann, J.; Collier, R., Synthesis and molecular structure of [Ti-4(OPri)(8)(mu,eta(2)-OCH₂CH = CHCH₂O)(2)(mu(3),eta(2)-OCH₂CH = CHCH₂O)(2)]. Application to the elaboration of low density, microcellular, doped organic materials. *J. Mater. Chem.* 1999, 9 (12), 3027-3033.
134. Franc, J.; Blanc, D.; Zerroukhi, A.; Chalamet, Y.; Last, A.; Destouches, N., Organo-silica-titania nanocomposite elaborated by sol-gel processing with tunable optical properties. *Mater. Sci. Eng. B-Solid State Mater. Adv. Technol.* 2006, 129 (1-3), 180-185.
135. Guerrero, D. J.; Flaim, T. D., Photosensitive titania polymers. *Journal of Photopolymer Science and Technology* 2002, 15 (3), 447-451.
136. Segawa, H.; Abrams, N.; Mallouk, T. E.; Divliansky, I.; Mayer, T. S., Fabrication of TiO₂-Organic hybrid dot arrays using nanosecond laser interference lithography. *J. Am. Ceram. Soc.* 2006, 89 (11), 3507-3510.

137. Gbureck, U.; Probst, J.; Thull, R., Polymerization behaviour of organically modified titanium alkoxides in solution. *J. Sol-Gel Sci. Technol.* 2003, 27 (2), 157-162.
138. Mendez-Vivar, J.; Bosch, P.; Lara, V. H.; Mendoza-Serna, R., The role of 2-(methacryloyloxy) ethyl acetoacetate in the polymerization of hybrid multicomponent (Si, Ti, Zr) sols. *J. Sol-Gel Sci. Technol.* 2002, 25 (3), 249-254.
139. Cauro-Gamet, L. C.; Hubert-Pfalzgraf, L. G.; Lecocq, S., Syntheses and molecular structures of titanium derivatives with polymerizable ligands. Toward extended arrays. *Zeitschrift Fur Anorganische Und Allgemeine Chemie* 2004, 630 (12), 2071-2077.
140. Sanchez, C.; Livage, J.; Henry, M.; Babonneau, F., Chemical modification of alkoxide precursors. *J. Non-Cryst. Solids* 1988, 100 (1-3), 65-76.
141. Yang, J.-H.; Han, Y.-S.; Choy, J.-H., TiO₂ thin-films on polymer substrates and their photocatalytic activity. *Thin Solid Films* 2006, 495 (1-2), 266-271.
142. Jung, M. W.; Oh, H. J.; Yang, J. C.; Shul, Y. G., Structural investigation of the hydrolysis-condensation process of modified titanium isopropoxide. *Bull. Korean Chem. Soc.* 1999, 20 (12), 1394-1398.
143. Blanchard, J.; Ribot, F.; Sanchez, C.; Bellot, P.-V.; Trokiner, A., Structural characterization of titanium-oxo-polymers synthesized in the presence of protons or complexing ligands as inhibitors. *J. Non-Cryst. Solids* 2000, 265 (1-2), 83-97.
144. Hoebbel, D.; Reinert, T.; Schmidt, H.; Arpac, E., On the hydrolytic stability of organic ligands in Al-, Ti- and Zr-alkoxide complexes. *Journal of Sol-Gel Science and Technology* 1997, 10 (2), 115-126.
145. Wicks, Z. W.; Jones, F. N.; Pappas, S. P.; Wicks, D. A., Adhesion. In *Organic coatings: science and technology*, 3rd ed.; John Wiley & Sons, Inc. : New Jersey, 2007; pp 121-136.
146. Errington, R. J.; Ridland, J.; Willett, K. J.; Clegg, W.; Coxall, R. A.; Heath, S. L., Organophosphonate derivatives of titanium and niobium alkoxoanions. *Journal of Organometallic Chemistry* 1998, 550 (1-2), 473-476.
147. Guerrero, G.; Mehring, M.; Mutin, P. H.; Dahan, F.; Vioux, A., Syntheses and single-crystal structures of novel soluble phosphonato- and phosphinato-bridged titanium oxo alkoxides. *Journal of the Chemical Society-Dalton Transactions* 1999, (10), 1537-1538.
148. Mehring, M.; Guerrero, G.; Dahan, F.; Mutin, P. H.; Vioux, A., Syntheses, characterizations, and single-crystal X-ray structures of soluble titanium alkoxide phosphonates. *Inorganic Chemistry* 2000, 39 (15), 3325-3332.
149. Guerrero, G.; Mutin, P. H.; Vioux, A., Mixed nonhydrolytic/hydrolytic sol-gel routes to novel metal oxide/phosphonate hybrids. *Chemistry of Materials* 2000, 12 (5), 1268-1272.
150. Mehring, M.; Lafond, V.; Mutin, P. H.; Vioux, A. In *New sol-gel routes to organic-inorganic hybrid materials: Modification of metal alkoxide by phosphonic or phosphinic acids*, Abano Terme, Italy, Sep 16-21; Abano Terme, Italy, 2001; pp 99-102.
151. Musyanovych, A.; Rossmannith, R.; Tontsch, C.; Landfester, K., Effect of hydrophilic comonomer and surfactant type on the colloidal stability and size distribution of carboxyl- and amino-functionalized polystyrene particles prepared by miniemulsion polymerization. *Langmuir* 2007, 23 (10), 5367-5376.

References

152. Sayg, Ö.; inodot; -Arslan; Sudol, E. D.; Daniels, E. S.; El-Aasser, M. S.; Klein, A., *In situ* surfactant generation as a means of miniemulsification? *J. Appl. Polym. Sci.* 2009, *111* (2), 735-745.
153. Allen, N. S.; Edge, M.; Ortega, A.; Liauw, C. M.; Stratton, J.; McIntyre, R. B., Behaviour of nanoparticle (ultrafine) titanium dioxide pigments and stabilisers on the photooxidative stability of water based acrylic and isocyanate based acrylic coatings. *Polymer Degradation and Stability* 2002, *78* (3), 467-478.
154. Vogel, N.; Hauser, C. P.; Schuller, K.; Landfester, K.; Weiss, C. K., Accurate Elemental Analysis of Metal-Containing Polymer Latexes Using ICP-Optical Emission Spectrometry. *Macromolecular Chemistry and Physics* 2010, *211* (12), 1355-1368.
155. Thomas, A.; Schlaad, H.; Smarsly, B.; Antonietti, M., Replication of Lyotropic Block Copolymer Mesophases into Porous Silica by Nanocasting: Learning about Finer Details of Polymer Self-Assembly. *Langmuir* 2003, *19* (10), 4455-4459.







List of publications

Publications based on this work:

Nabih, N.; Landfester, K.; Taden, A., Water-based inorganic – polymer hybrid particles prepared via a multiple miniemulsion process, accepted for publication in *Journal of Polymer Science Part A: Polymer Chemistry*.

Nabih, N.; Herrmann, U.; Glasser, G.; Lieberwirth, I.; Landfester, K.; Taden, A., Water-based hybrid zinc phosphate – polymer miniemulsion as anticorrosive coating, submitted.

Patent, Pigmenthaltige Lackdispersionen sowie W/O Emulsionen als Präkursor für die Bereitstellung der Lackdispersion (Pigment containing coating dispersions, as well as w/o emulsions as precursors for coating dispersions), submitted on 18th March 2011 to the European Patent Office.

Other publications:

Nabih, N.; Schiller, R.; Lieberwirth, I.; Kockrick, E.; Frind, R.; Kaskel, S.; Weiss, C. K.; Landfester, K., Mesoporous CeO₂ nanoparticles synthesized by an inverse miniemulsion technique and their catalytic properties in methane oxidation. *Nanotechnology* 2011, 22 (13), 135606.